UNIVERSITÀ
DEGLI STUDI
DI PADOVA

DIPARTIMENTO DI INGEGNERIA INDUSTRIALE

SCUOLA DI DOTTORATO DI RICERCA IN INGEGNERIA INDUSTRIALE
INDIRIZZO IN INGEGNERIA CHIMICA DEI MATERIALI E DELLA PRODUZIONE
CICLO XVIII

Dense and Porous Glass and Glass Ceramics from Natural and Waste Raw Materials

Direttore della Scuola: Ch.mo Prof. Paolo Colombo
Coordinatore d'indirizzo: Ch.mo Prof. Enrico Savio
Supervisore: Ch.mo Prof. Paolo Colombo
Co-supervisore: Prof. Enrico Bernardo

Dottorando: Mauro Marangoni

Sommario

Il principale obiettivo delle attività di ricerca qui presentate riguardano lo sviluppo di nuovi processi e materiali per applicazioni in edilizia adattate alle esigenze dell'Arabia Saudita in base alle informazioni scambiate con i partner di KACST (King Abdulaziz City of Science and Technology).

L'attività di ricerca è stata focalizzata sullo sviluppo di una vasta gamma di componenti ceramici mediante sintercristallizzazione di vetri prodotti da rifiuti (ceneri volanti e scorie) con o senza l'aggiunta di fondenti come rottame di vetro o silicati. Le materie prime sono state miscelate in rapporti adeguati alla produzione di composizioni ceramiche adatte all'utilizzo in edilizia; ad esempio piastrelle vetroceramiche, pannelli alleggeriti e aggregati leggeri.

Vetroceramiche e ceramiche, dense e porose, sono state realizzate come sostituti alle pietre naturali e ai ceramici tradizionali. Vetroceramici densi presentano proprietà eccezionali (durezza, resistenza meccanica, durabilità), mentre vetroceramiche porose presentano ridotte densità e conducibilità termica. Inoltre sinterizzando fritte vetrose sono stati ottenuti smalti altamente riflettenti con bianchezza corrispondente al marmo di Thassos. Tutti i materiali sviluppati sono basati sull'utilizzo di risorse naturali o materiali di scarto provenienti dall'Arabia Saudita. Inoltre, sono state sviluppate diverse tecniche per la schiumatura diretta di vetroceramiche, portando alla realizzazione di materiali altamente porosi con celle principalmente chiuse. Utilizzando tecniche alternative sono state invece sviluppate vetroceramiche con una prevalenza di celle aperte.

Abstract

The main goal of the herewith presented research activities was to develop innovative processes and materials for building applications adapted to the needs of Saudi Arabia according to the information exchanged with the partners from KACST (King Abdulaziz City of Science and Technology).

The research activity focused on the development of a wide range of ceramic components via sinter-crystallization of glasses produced from waste (fly ash, slag, sludge) with or without the addition of vitrification aids, such as cullet or silicates. The raw materials have been mixed in the appropriate ratios to yield ceramic compositions that could be used in the building industry (e.g glass ceramic tiles, porous panels, lightweight aggregates). Monolithic, porous or dense, sintered glass ceramics and ceramics were manufactured as substitutes for natural stones or traditional ceramics. Dense glass ceramics have outstanding properties (hardness, mechanical strength, durability), while porous glass ceramics provide low density and thermal conductivity. Furthermore highly reflective glazes, also matching the whiteness of Thassos marble, were manufacture sintering glass frits.

All the developed materials are based on the use of natural resources or waste materials from Saudi Arabia. Moreover, several techniques for direct foaming of glass ceramics have been developed, leading to highly porous ceramics with mainly closed cells. Alternative techniques have been developed for the production of open-celled ceramics.

General Introduction

I – Dense and Porous Waste Derived Glass and Glass Ceramics

Melting several types of inorganic waste into glasses ("waste glasses") is a well-known technique for immobilizing pollutants.[1] Although recommended for highly hazardous residues, like radioactive waste, the vitrification method is currently rather discouraged, due to the high energy consumption, so that less expensive treatments such as disposal in landfills or immobilization in cement matrices may become more attractive [2-4].

The realization of marketable products from waste glasses may counterbalance their intrinsic processing costs and glass ceramics manufactured sintering powdered glasses is one of the most interesting application [5-7]. If the parent glass is not refined, prior to be finely ground, the costs and the duration of vitrification may be drastically reduced. Firstly, shortening the melting treatments the volatilization of heavy metals from the glass melt are limited, with an improved sealing of hazardous pollutants. Secondly, sintered glass ceramics are based on surface crystallization (sintering with concurrent crystallization, i.e. "sinter-crystallization"), largely favored for small glass granules (free glass surfaces are preferred sites for devitrification) [8-10]: catalysts in the glass formulation or long nucleation/crystal growth treatments are not needed and crystallization is achieved in very short times [11], even in the case of crystal phases which are hardly obtained by conventional nucleation and crystal growth treatments (e.g. feldspar and feldspathoid crystals) [12-13].

A proper balance of viscous flow sintering and crystallization is pivotal for the obtainment of dense glass ceramics. In fact, an intense surface crystallization of glass powders may hinder the densification, leading to very porous materials. A possible solution is provided adopting a sintering temperature well above the crystallization temperature, by applying high heating rates and forcing the glass to sinter before extensive crystallization [14]. A more economically convenient alternative is the "co-sintering" with a secondary glass not prone to crystalliza-

tion acting as sintering aid, i.e. common soda-lime scrap, or recycled pharmaceutical borosilicate glass etc., may improve the densification and also promote the chemical inertia of the obtained glass ceramics [15].

Glass ceramics tiles from waste, obtained by conventional nucleation-and-growth mechanisms [16-20] or by sinter-crystallization [21-27], have been produced by several research groups. Also stoneware-based tiles containing waste-derived glass have been produced [28-30].

Although dense glass and glass ceramics posses remarkable strength and optical properties, glass and glass ceramic foams were sintered for thermal and acoustical insulation [31-35].

Glass foams are produced in limited quantities due to high processing costs, and are used in substitution for organic foams when high mechanical strength, incombustibility, thermal and chemical stability are required. Furthermore when the foams are produced with a closed cell structure the material is watertight and an efficient barrier against humidity. The production of glass foams may follow two distinct processes: the first, dating back to the 1930s, consists of the direct fluxing of gases into molten glass; the second one, less expensive, is based on the viscous flow sintering of fine glass powders, which creates a pyroplastic mass which is foamed by the action of specific powder additives, foaming agents, owing to decomposition or oxidation reactions. The decomposition reactions involve carbonates and sulfates, while oxidation reactions are due to the interaction of carbon-containing species (C, SiC) and polyvalent ions (Fe, Mn, Ce) with oxygen, coming mainly from the atmosphere of the sintering furnace. The adoption of a sintering approach paved the way for the use of glass not specifically designed for foam production; significantly, the sintering approach led to the extensive use of cullet for this application. Soda-lime glass is a common raw material; however, a number of recent investigations showed that it is possible to fabricate foams using other glasses, such as cathode-ray tube glass (CRT) [36]. The low characteristic temperature of these glasses enables foaming at particularly low temperature (even below 750°C), through the decomposition of added calcium carbonate.

The foaming of waste-derived glasses is more complicated by the previously discussed tendency of these glasses to crystallize upon heating. The high specific

surface of the foam enhances the surface nucleation and growth of crystals during the foaming process, originating problems in the homogeneity and reproducibility of the overall foam morphology. This issue may be overcome by using a combined approach, i.e. by foaming mixtures of soda-lime glass and the glass undergoing crystallization [37], or again of soda-lime glass and selected wastes [38]. In this case the crystallization may actually be useful, since it enhances the mechanical properties. A similar situation is found when using mixtures of soda-lime glasses with cullet more difficultly recycled but quite prone to crystallization, e.g. glass residue from the manufacturing of glass fibers, having a CaO-Al_2O_3-SiO_2 composition similar to that of many waste glasses used for the preparation of glass ceramics [39].

The effective crystallization of waste glasses may be even advantageous when foams characterized by an open porosity are desired, e.g. for filtering applications. Open-celled glass ceramics may be obtained by mixing glass powders with polymeric microspheres or by the infiltration of slurries onto polyurethane sponges, followed by the burn-out of the sacrificial polymers and sinter-crystallization [40].

II – Waste Derived Glass Ceramics Belonging to the CaO-Al_2O_3-SiO_2 System

Most waste-based glass ceramics belong to the CaO-Al_2O_3-SiO_2 system [8, 41] due to the chemical composition of the most relevant types of inorganic waste: metallurgical slags, fly ashes from municipal solid waste incineration or from coal combustion and contaminated sediments.

To limit the costs for the realization of waste derived glass to be used to form sintered glass ceramics the following conditions should be fulfilled:

- Maximization of “waste absorption”. The glass should be produced minimizing the contents of valuable raw materials and consequently recycling the highest content of waste. By combining different types of wastes is possible to limit the employment of mineral. Furthermore, combining several types of waste can provide a way to control possible fluctuations of the chemical composition of the waste materials.

- Relatively low characteristic temperatures of the glass.
- Glass composition suitable for fast sinter crystallization.
- Formation of crystal phases leading to good mechanical properties, e.g. needle-like silicate crystals, mutually interlocked.
- Control of secondary features, e.g. the present work frequently focused on a combination of waste leading to an overall composition with a relatively low amount of coloring oxides, such as Fe_2O_3 or Cr_2O_3;

Predictions about characteristic temperatures and crystals formation after sintering are quite complex. A good solution may be referring to the literature; more specifically to compositions similar to those for Russian "Slag-sitalls", i.e. waste derived glass ceramics [see ref. 1, 2] well known to be used as building materials. Slag-sitalls crystallize effectively when the starting glass is heated at about 1000°C, developing wollastonite ($CaO{\cdot}SiO_2$) as the main crystalline phase, coupled with alumino-silicates such as anorthite ($CaO{\cdot}Al_2O_3{\cdot}2SiO_2$) and gehlenite ($2CaO{\cdot}Al_2O_3{\cdot}SiO_2$). Interestingly, the compositions for Slag-sitalls are quite similar to those for other very important glass ceramics for architectural purposes, e.g. Japanese "Neoparies" [8]. Neoparies are the most remarkable industrial glass ceramics manufactured by the "sinter-crystallization" approach: glass is fabricated in the form of granules, subsequently viscous flow sintered with concurrent crystallization. The fabrication of glass granules is very easy and very advantageous when using waste raw materials, since they can be obtained by pouring a glass melt in water, just after homogenization, without expensive refining step; in addition, crystallization may be obtained very rapidly (in 1h or less, at an adequate sintering temperature), on the basis of surface nucleation, even in the presence of glasses with a very low amount of oxides that could act as nucleating agents (i.e. oxides with a poor solubility in glass, such as TiO_2, ZrO_2 etc.).

III – Raw materials provided

The raw materials provided by KACST were the following (see **Tab. 1**):

Tab. 1: List of raw materials to be used in the experiments

No.	Name of Raw Materials
01	Steel plant fly ash
02	Slag
03	Basalt scoria
04	Clay A
05	Clay E
06	Cement Fly Ash 02
07	Cement Fly Ash 03 /04
08	Cement Fly Ash 05
09	Cement Fly Ash 06
10	Cement Fly Ash 07
11	Stainless steel waste
12	Tiles ceramics waste
13	Clay Pipe waste
14	Bricks waste
15	Limestone ($CaCO_3$)
16	Air Pollution Control (APC) residues
17	Coal waste
18	Cullet (glass waste)
19	Municipal burned paper waste
20	Building waste
21	Silica sand
22	White clay
23	Dolomite
24	Magnesia

Of these materials only a part was used for the experiments.

IV – Thesis summary

The present investigations were divided into 6 main topics and are fully described in the next Chapters.

Chapter 1. The main topic of this chapter refers to the development of porous glass ceramics for building applications (light weight aggregates and insulating panels). The investigations focused on a self-foaming mixture of waste glass and a basalt rock discarded from the cement industry. The influence of composition, particle dimension, firing temperature and heating rate were studied in order to manufacture samples with different porosity and mechanical

strength according to the designed application. Moreover the self-foaming mechanism was investigated in accordance with micro-structural studies (XRD, chemical titration, DTA, TGA, porosities determination, μ-CT).

The produced cellular glass ceramics were produced in larger amounts to investigate a possible application as lightweight aggregates for the realization of lightweight structural concrete.

This topic was finalized with a publication [42] and a patent application [43].

Chapter 2. In spite of environmental issues hydraulic fracturing was widely used in the US for the extraction of oil using proppants. At this purpose, the development of a method for the realization of lightweight ceramic proppants for fracking applications is described. Glass ceramic proppants were obtained firing natural basalt in oxidizing or reducing atmosphere. Furthermore a minor, but interesting effort is represented by the realization of black glass ceramics based on sintered natural basalt scoria.

Chapter 3. Describes the results achieved to fabricate monolithic sintered glass ceramics as substitute for natural stones or traditional ceramics. In particular a composition and method were designed for manufacturing a white glaze and a substrate glass ceramics for building applications (ceramic tiles) using waste and natural materials. Firstly, a waste derived frit with a controlled amount of iron oxide (low content - high content), to be applied as a glass ceramic glaze, was produced. Secondly, a ceramic substrate with a composition suitable for a single step process at a low firing temperature (1150°C) was produced. The match between the coefficients of thermal expansion of the substrate and the glaze was achieved by mixing the glaze with additives and whitening agents.

This topics were finalized with a scientific publication [44] and two patent applications [45, 46].

Chapter 4. In this chapter is described a method for manufacturing a white glass ceramic composite and a colored glass ceramic composite mixing whitening additives and waste glass.

The proposed method was successfully finalized with a patent [47].

Chapter 5. In order to provide a thermal barrier in an arid environment, highly reflective coatings were deposited on porous substrates made of natural raw materials from Saudi Arabia. Although highly reflective coatings inhibit heat

absorption from the incoming sunlight, the body of conventional ceramic tiles warms up to environmental temperature through conduction, convection and radiation. A strategy to reduce the penetration of this heat into the building is to use a highly porous substrate, which reduces the thermal conductivity of the tile, coupled with a highly reflective glaze. The approach leads to the concept of "cool" tiles, which should improve the thermal efficiency of buildings.

Chapter 6. Realization of glass ceramics from low cost natural raw materials with a specific interest in the obtainment of samples resembling the color of Thassos marble.

Bibliography

1 U.S. Environmental Protection Agency. Handbook on vitrification technologies for treatment of hazardous and radioactive waste. Office of Research and Development, Washington DC, Report EPA/625/R-92/002 edition, MAY 1992.
2 P. Colombo et al., Document Inertization and reuse of waste materials by vitrification and fabrication of glass-based products, Curr. Opin. Solid State Mat. Sci. 7 (2003) 225
3 P.A. Bingham, R.J. Hand, Adv. Appl. Ceram. 105 (2006) 21
4 E. Gomez et al., J Haz Mat 161 (2008) 614-626
5 R.D. Rawlings et al., J. Mat. Sci. 41 (2006) 733
6 A. Boccaccini et al. Materials World, May:16-18 (2002)
7 A.A. Francis et al., J Mater Sci Lett 21 (2002)975-980
8 W. Höland, G. Beall, "Glass ceramic Technology", The American Ceramic Society, Westerville OH (2002)
9 T.J. Clark, J.S. Reed, J. Am. Ceram. Soc., 69 (1986) 837
10 R.D. Rawlings et al. J Mater Sci 41 (2006) 733-761
11 E. Bernardo, J. Non Cryst. Sol. 354 (2008) 3486
12 E. Bernardo et al., J. Eur. Ceram. Soc. 26 (2006) 3335
13 E. Bernardo et al., J. Am. Ceram. Soc. 88 (2005) 1886
14 E. Bernardo et al., J. Am. Ceram. Soc. 92 (2009) 528-30
15 E. Bernardo et al., Ceram. Int. 36 (2010) 1675-1680
16 AR Boccaccini et al, Ceram Int (1995) 21:231-235
17 M. Romero et al, Mat Res Bull 36 (2001) 383-395
18 ML Öveçoglu et al., J Eur Ceram Soc 18 (1998) 161-168
19 S Suzuki et al., J Mat Sci 32 (1997) 1775-1779
20 F. Peng et al., Fuel 84 (2005) 341-346
21 A. Karamanov et al., Glastech Ber Glass Sci Technol 67 (1994) 227-230
22 E. Bernardo et al., J Am Ceram Soc 92 (2009) 528-530
23 E. Bernardo, J Non-Cryst Sol 354 (2008) 3486-3490
24 A. Karamanov et al., J Am Ceram Soc 83 (2000) 3153-57
25 A. Karamanov et al., J Eur Ceram Soc 23 (2003) 827-32
26 A. Karamanov et al., J Eur Ceram Soc 25 (2005) 1531-1540
27 AA Francis et al.; J Mater Sci Lett 21 (2002) 975-980
28 E. Bernardo et al. Adv Appl Ceram 108 (2009)2-8
29 L. Barbieri et al., Waste Manag 22 (2002) 859-63
30 E. Bernardo et al., J Am Ceram Soc 91 (2008) 2156-2162
31 E. Bernardo et al., Glass Sci Technol 78 (2005) 7-11
32 E. Bernardo et al., Ceram Int 33 (2007) 963-968
33 HR Fernandes et al., Adv Appl Ceram 108 (2009) 9-13
34 E. Bernardo J Eur Ceram Soc 27 (2007) 2415-2422
35 G. Scarinci et al. in "Cellular Ceramics. Structure, Manufacturing, Properties and Applications", Ed. M. Scheffler, P. Colombo Wiley-VCH, Weinheim, Germany (2005)
36 E. Bernardo, F. Albertini, Ceram. Int. 32 (2006) 603-608
37 D.U. Tulyaganov et al., J. Por. Mater. 13 (2006) 133-139

38 J.P. Wu et al., Adv. Appl. Ceram. 105 (2006) 32-39
39 Bernardo et al., J. Por. Mat. 17 (2010) 359-365
40 E. Bernardo, J. Eur. Ceram. Soc. 27 (2007) 2415-2422
41 Z. Strnad, "Glass ceramic Materials", Elsevier Science Publishers, Amsterdam (1986).
42 M. Marangoni, M. Secco, M. Parisatto, G. Artioli, E. Bernardo, P. Colombo, H. Altlasi, M. Binmajed, M. Binhussain. Cellular glass–ceramics from a self foaming mixture of glass and basalt scoria Journal of Non-Crystalline Solids 403 (2014) 38–46
43 Patent application 13162767.1-1354 A porous glass ceramic composition and method for manufacturing the same
44 M.A. Binhussain, M. Marangoni, E. Bernardo, P. Colombo, Sintered and glazed glass ceramics from natural and waste raw materials, Ceram. Int. 40 (2014) 3543-3551.
45 Patent application 13162770.5-1354 A glaze composition, method for manufacturing the glaze composition and methods for glazing.
46 Patent application A glass ceramic composition and method for manufacturing the same.
47 M. Binhussain, P. Colombo, E. Bernardo, M. Binmajed, M. Marangoni, H. H. Altalsi, A. M. Alajimi and A. Altamimi, Method for manufacturing glass-ceramic composite, EP 2752394, US 2014191448, Filed 4 March 2013.

Part II – Experimental

Chapter 1 – Cellular Waste Derived Glass Ceramics

1.1 Introduction

1.1.1 Glass Ceramic Foams a General Introduction

Glass foams are appreciated for their lightness and capacity of thermal and acoustic insulation combined with good mechanical properties, far superior than those of polymeric foams. Moreover, as they are incombustible and waterproof [1], they are increasingly considered for use as lightweight filling or insulating materials in civil engineering.

The production of glass foams commonly relies on the viscous flow sintering of fine glass powders, which creates a pyroplastic mass in turn foamed by the action of specific powder additives (foaming agents), when heating at 850-1000°C. Foaming occurs because of the release of CO, CO_2 or SO_3 gases, generated from the decomposition or oxidation of the additives. Decomposition reactions typically derive from the presence of carbonates or sulphates, whereas oxidation reactions are associated to the interaction of carbon-containing species (C, SiC) with oxygen, mainly derived from the atmosphere within the sintering furnace [1]. In all cases, the gases may represent an environmental problem (toxicity, greenhouse effect, etc.), in clear contradiction with the "green character" of glass foams, associated to the use of many different types of crushed recycled glass, including glasses deriving from the vitrification of inorganic waste [2-7].

1.1.2 Glass Ceramic Foams Studied in Laboratory

After preliminary studies fundamental for determining the sintering conditions (firing temperature and powder size) and experimental set-up determination, we researched self foaming cellular glass ceramics obtained by sintering mixtures of *basalt scoria* and *soda lime cullet* for 15 min at 1050 and 1100°C. The effect of polyvalent ions (Fe^{3+}/Fe^{2+}) on porosity (from 53 to 86 vol%) and crystallization was studied for different mixtures subjected to different thermal treatments. Due to the range of mechanical strength values (crushing strength from 2 to 50 MPa) and total

porosity achieved, these porous glass ceramics could be applied as building materials, as lightweight aggregate for concrete or as lightweight panels. The study focused on the development of glass-based foams from mixtures exploiting oxygen as foaming gas instead of greenhouse gases. The release of oxygen, caused by the reduction of ferric oxide into ferrous oxide, has been already reported as effective for the development of expanded materials [8-9]; the present work greatly extends previous investigations and provides evidence for the significant tunability of the approach, which leads to partially crystallized products with total porosity and crushing strength varying in a wide range of values, depending on the balance between glass and scoria or on the sintering conditions.

1.1.4 Glass Ceramic Foams as Light Weight Aggregates (LWA)

The large demand of concrete in the building industry originated products with a very high strength, resistance to highly corrosive environments and also with improved specific strength when lightness and high strength are required. Lightweight concrete (LWC) was developed both for structural and thermal insulating applications and can be manufactured according to very different processes. Cellular concrete is an example of foamed LWC used mostly for non- and semi-structural applications [10].

Differently from cellular concrete, LWA are used in concrete to substitute traditional aggregates and to form lightweight aggregate concrete (LWAC). In literature there are many LWAC used for the realization of structural concrete, in fact the structural efficiency (specific strength) is more important than a mere consideration of absolute strength. A decreased density for the same strength level reduces the self-weight, foundation size, and construction costs. Some LWACs were realized using organic precast aggregates of styrene–butadiene rubber [11], or even oil palm shells [12]. However most frequently LWAs are inorganic lightweight rocks like pumice [13], or expanded materials like perlite [14] and clay.

1.1.5 Light Weight Concrete using Cellular Glass Ceramics

In the present chapter is also described the process to manufacture a relatively large amount of cellular glass ceramics using a pilot scale tunnel furnace at SASIL (Biella) in collaboration with personnel from CIRCE (Centro Interdipartimentale di Ricerca per lo Studio dei Materiali Cementizi e dei Leganti Idraulici). We then realized tradi-

tional concrete samples to be compared with LWAC substituting 30 vol% of the traditional aggregates with cellular glass ceramics. The investigation of the properties of the LWAC is at a preliminary stage and only limited amount of data are available for comments and interpretation of the results. However the results obtained were valuable and herewith presented.

1.2 Materials and Methods

1.2.3 Selection of Compositions and Thermal Treatments

A simple notation is used for the definition of the proportions of raw materials in each composition: for example, instead of writing 40 wt% of cullet and 60 wt% of basalt, we will use the sample label: C4B6. The compositions, C4B6, C5B5, and C6B4 were selected in order to explore a reasonably wide variation of the proportions between cullet and basalt. For these compositions the samples were heated by direct firing, DF, for a soaking time of 15 minutes, at either 1050°C or 1100°C.

The heating rate strongly affects the characteristics of the final components, therefore, for composition C5B5 the effect of four different heating rates was investigated. For composition C5B5 the firing of samples was performed in two distinct ways. In the first case, glass/scoria samples were treated at 1050-1100°C by direct insertion in a muffle furnace, with a holding time of 15 min. At the end of the holding time, the samples were rapidly cooled, at approximately 60°C/min, below 900°C (with the muffle switched off and muffle door partially open), and then naturally cooled to room temperature (inside the muffle). In the second case, for a selected formulation, the samples were fired at 1100°C for 15 min operating with 3 different heating rates (10°C/min, 20°C/min and 40°C/min); the cooling was performed in the same conditions.

We should observe that that the DF procedure is suitable for the production of light weight aggregates, LWA, while the progressive heating is suitable for the production of insulating panels, IP.

Tab. 2 – Chemical analysis (oxide contents in wt% and mol%) of the waste glass cullet, basalt scoria and mixtures C4B6, C5B5 and C6B4.

	Cullet		Basalt Scoria		C4B6	C5B5	C6B4
	Wt%	Mol%	Wt%	Mol%	Wt%	Wt%	Wt%
SiO_2	71.7	71.2	47.1	52.9	57.3	59.8	62.3
TiO_2	0.1	0.1	1.9	1.6	1.2	1.0	0.8
Al_2O_3	0.7	0.4	14.7	10.5	9.1	7.7	6.3
Fe_2O_3	0.1	0.0	12.3	4.8	7.5	6.2	5.0
MnO	0.0	0.0	0.2	0.2	0.1	0.1	0.1
MgO	3.3	4.9	11.0	16.1	7.9	7.2	6.4
CaO	10.1	10.7	7.7	9.2	8.7	8.9	9.2
Na_2O	13.2	12.7	3.2	3.7	7.3	8.3	9.3
K_2O	0.1	0.0	1.0	0.7	0.6	0.5	0.4
P_2O_5	0.0	0.0	0.5	0.3	0.3	0.3	0.2
SO_3	0.22	0.2	0.03	0.0	0.1	0.1	0.1
L.O.I.	0.5		0.9		-	-	-

1.2.2 Starting Materials

Tab. 2 reports the chemical compositions of the starting materials, inferred from X-ray fluorescence analysis (XRF, Philips PW2400, Eindhoven, The Netherlands). Both soda-lime glass cullet (C) and basalt scoria (B) were considered after ball milling and sieving to a size below 90 μm. Both powders were subjected to differential thermal analysis (DTA-TGA, DSC 404, Netzsch Gerätebau GmbH, Selb, Germany, 10°C/min heating rate).

1.2.3 Experimental Set Up

The raw materials were subjected to X-ray powder diffraction (XRPD) using a Bragg–Brentano θ-2θ diffractometer equipped with a real time multiple strip (RTMS) detector (PANalytical X'Pert PRO, Almelo, The Netherlands), employing CuKα radiation (0.15418 nm) and working at 40 kV and 40 mA. Data acquisition was performed by operating a continuous scan from 3.01° [2θ] to 79.99° [2θ], with a virtual step scan of 0.02° [2θ]. The diffraction patterns were analyzed by means of the X'Pert HighScore Plus 3.0 software (PANalytical), using data from the PDF-4 database (International Centre for Diffraction Data – ICDD, Newtown Square, PA, USA). Mineralogical quantitative phase analysis (QPA), based on the Rietveld method [15],

was performed using the TOPAS software (Bruker AXS, Karlsruhe, Germany). The contents of crystalline and amorphous phases were determined using the combined Rietveld–RIR method [16]. The observed patterns were modeled through a pseudo-Voigt function, fitting the background by 14 Chebyshev polynomials. For each phase, the lattice parameters, Lorentzian crystal sizes and scale factors were refined and residual preferred orientation effects were modeled with the March Dollase algorithm [17].

Furthermore, the basalt scoria was microstructurally and microchemically characterized by Scanning Electron Microscopy coupled with energy dispersive X-rays fluorescence microanalysis (SEM-EDS), using an instrument equipped with a LaB_6 cathode, a four quadrant solid state BSE detector for imaging and a LEAP+ Si(Li) detector for microanalysis (CamScan MX2500, Waterbeach, UK; EDAX, Mahwah, NJ, USA). The analytical conditions were: accelerating voltage: 20 kV; filament current: 1.80 A; emission current: 20 μA; aperture current: 300 nA; working distance: 20-30 mm. Qualitative interpretation of spectra and semiquantitative chemical analyses were performed through SEM Quant Phizaf software (EDAX, Mahwah, NJ, USA).

1.2.4 Green Bodies Preparation

In order to execute the experiments in the most reproducible way possible, about 200 ml of basalt were ball milled (250 ml is the volume of the jar) and employed for all the experiments. In spite of the fact that the cullet employed is more homogenous than basalt, a similar procedure was used to produce about 100 grams of powdered cullet. All the ground raw materials were sieved and the fraction larger than 90 μm was further ground until was fine enough to be sieved. Cullet (C) and basalt scoria (B) powders were first dry mixed at 300 rpm in a ball milling jar for 30 minutes in different proportions, as reported in **Tab. 2** (C:B equal to 4:6, 5:5 and 6:4), and then added with 7 wt% distilled water without any binder. For each formulation, powders were uniaxially cold pressed in a rectangular die (50 mm × 34 mm) at 30 MPa. The resulting green bodies were cut into square pellets, dried at 80°C overnight. Only for the mixture C5B5, additional rectangular bars were prepared and dried overnight.

For the DF experiments, the green body was cut into about 15 (about 1 cm^2) squared pieces and dried at 80°C overnight. For the progressive heating experi-

ments, one green body of composition C5B5, was cut into about 15 (about 1 cm^2) squared pieces and dried at 80°C overnight. For the progressive heating experiments, one green body (17 cm^2) was also kept intact and dried at 80°C overnight.

1.2.5 Firing

The direct firing experiments were carried out for all the compositions C4B6, C5B5, and C6B4 at two different firing temperature, 1050°C and 1100°C, following this procedure:

- 15 sample (1 cm^2) were placed on a cordierite honeycomb refractory.
- The muffle was heated at the firing temperature and hold for 30/60 minutes in order to heat effectively the refractories of the oven and thus limiting the drop in temperature during the insertion of the samples.
- The samples were directly inserted into the muffle.
- After 15 minutes the door of the muffle was opened letting the temperature drop until 900°C with a rate approximately of 60°C/min.
- The oven was then naturally cooled until room temperature.

The progressive heating experiments were carried out only for composition C5B5, firing the specimens at 1100°C for 15 minutes at 3 different heating rate (10°C/min, 20°C/min, and 40°C/min), following this procedure:

- The green body tile (17 cm^2) and 5 samples (1 cm^2) were placed on a cordierite honeycomb refractory and inserted into the muffle at room temperature.
- The muffle was heated applying the selected heating rate.
- The firing temperature was hold for 15 minutes.
- The door of the muffle was opened letting the temperature drop until 900°C with a rate approximately of 60°C/min.
- The oven was then naturally cooled until room temperature.

1.2.6 Oxidation Tests and Firing

The oxidation of basalt scoria powders was studied on pellets obtained by uniaxial pressing (at 40 MPa) fine powders, with no glass addition, in a cylindrical mold (diameter of 13 mm). The pellets were fired for 30 minutes at 4 different temperatures

(1050-1200°C) and quenched in air. The FeO content was determined after dissolution of the samples in a solution of sulphuric acid (32%) and hydrofluoric acid (13.3%), and subsequent titration with potassium permanganate; Fe_2O_3 was obtained by difference to the total content of iron oxide measured by XRF (Fe_2O_3 tot).

1.2.7 Characterization Techniques

Water absorption, W_{AB}, was determined using the boiling method, according to the UNI EN ISO10545-3 standard protocol. The geometric or bulk density, ρ_b, was obtained by considering the mass to volume ratio for 3–6 selected cellular glass ceramics; the apparent density, ρ_a, and density of the solid, or true density, ρ_t, were evaluated by means of a gas pycnometer (Micromeritics AccuPyc 1330, Norcross, GA), employing glass ceramic samples “as fired” or crushed into fine powder, respectively. The three density values were used to compute the amounts of open and closed porosity.

Some pellets were investigated using a high resolution X-ray micro-computed tomography scanner (Bruker microCT-Skyscan 1172) operating at 66 kV and 149 μA. To scan the entire object volume, preserving at the same time a sufficient level of spatial resolution, the acquisitions of radiographs were carried out for each pellet in two separate scans (upper and lower) that were then automatically connected by the instrument software. The nominal spatial resolution (pixel size) was 5.59 μm for all the investigated samples. A total number of 1800 radiographs per scan were acquired over a 360° rotation (angular step 0.2°, exposure time ranging from 930 to 975 ms). At each angular position, 8 frames were collected and averaged together in order to improve the recorded signal-to-noise ratio. The reconstruction of cross-sectional slices from 2D X-ray projections was carried out using a modified FDK algorithm [18] for cone-beam geometry, implemented in the Skyscan NRecon software. Corrections for the beam hardening effect and ring artifacts (i.e. circular features in the slices caused by anomalous responses from some pixels of the detector) were also applied during the reconstruction process in order to improve image quality [19-20].

Crushing and four-point bending (40 mm outer span, 20 mm inner span) tests were performed using an Instron 1121 UTM (Instron, Danvers, MA, crosshead speed of 1 mm/min) on pellets (10 mm × 10 mm × 8 mm) and bars (4 mm × 5 mm × 50

mm) cut from tile samples, respectively. Before bending tests, the bars were used for the determination of the elastic modulus, by means of the dynamic resonance method (GrindoSonic Mk5, Leuven, B).

Finally, the mineralogical composition was determined on ground samples by XRD and Rietveld quantitative phase analysis, adopting the same analytical procedure used for the characterization of the raw materials.

1.2.8 Lightweight Aggregates Manufacturing Using a Pilot Scale Tunnel Furnace

To investigate the application of the studied cellular glass ceramics in lightweight concrete a relatively large amount of aggregates was produced using a pilot scale tunnel furnace (Nanetti ER-15 S) at SASIL (Biella). The aggregates were produced using basalt scoria (<90 μm) from Saudi Arabia and glass cullet (<90 μm) processed at SASIL. The glass cullet employed was the fraction discarded from the recycling process due to the large contamination of inorganic impurities. The quantitative XRD analysis performed on the cullet powders, **Fig. 1**, shows that crystalline impurities are in the order of 9 wt%.

Composition C6B4 was selected and the powders were mixed in plastic bags adding 0.2 wt% of graphite, to increase the reducing conditions, and 7 wt% of water to increase the plasticity of the mixture.

The powders were uniaxially pressed applying a load of 0.5 MPa, the green body was then cut in fragments of about 1-3 cm^2 and placed on top of inox plates (18/10) coated with a thin layer of alumina powders. The samples were then fast fired holding the samples at 1100°C for about 10 min.

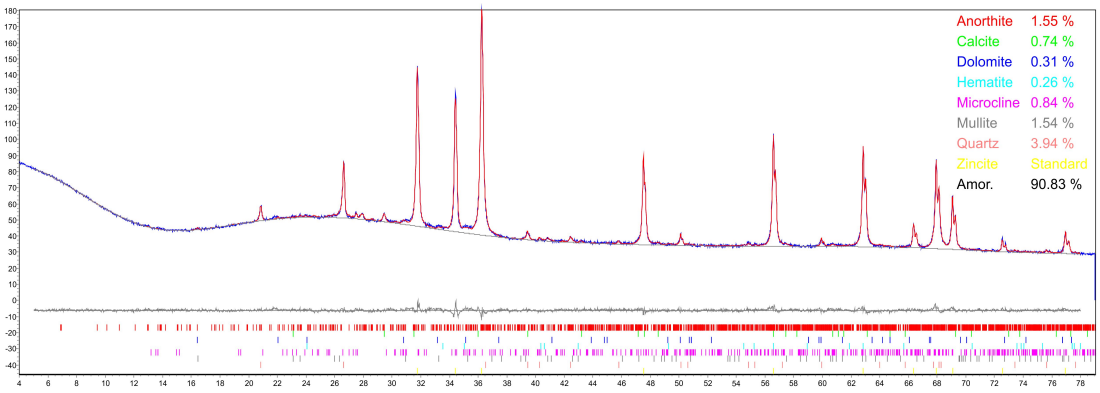

Fig. 1 – Quantitative XRD analysis on the cullet powders showing the high percentage of impurities. The most intense peaks are originated by the internal standard employed.

1.2.9 Lightweight Aggregates Concrete

The mix design of the traditional aggregates (carbonates gravel from local quarries) was realized according the Bolomey's curve, whereas the LWAs were used to substitute 30 vol% of the larger fraction of the aggregates. Aggregates with a maximum diameter of 25mm were introduced in a concrete mixer adding 2aII 425r Portland cement (300 kg/m^3) using a ratio water/cement of 0.58.

According to the standard EN-12390, 6 cylindrical samples (L=200 mm, Ø=100 mm) both using traditional and lightweight aggregates were realized to characterize the mechanical properties. The capping was performed using a mixture of cement and sand 1:1. After 1 day of curing the samples were placed in water for 27 days (pH ~13) to keep the samples hydrated. After 28 day the samples were left in open air for the determination of the mass and density, successively the elastic modulus and compressive strength were evaluated on 3 samples per set according to the EN 12390-13 and EN 12390-3 respectively using a Galdabini SUN 60. The tensile strength was then evaluated by means of the Brazilian test (EN 12390-6) using a hydraulic press (full scale 12 tons).

1.3 Results and Discussion

1.3.1 Starting Materials Characterization

The DTA and TGA analysis of cullet, shown in **Fig. 2**, revealed an exothermic peak at about 300°C and a slight mass loss attributed to the decomposition of organic impurities present in the starting scraps. From the DTA curve (**Fig. 2a**), the T_G of glass cullet was determined to be ~560°C; the broad exothermic peak at 740°C is attributed to the sintering of fine powders (since crystallization of soda lime glass powders upon heating is not effective).

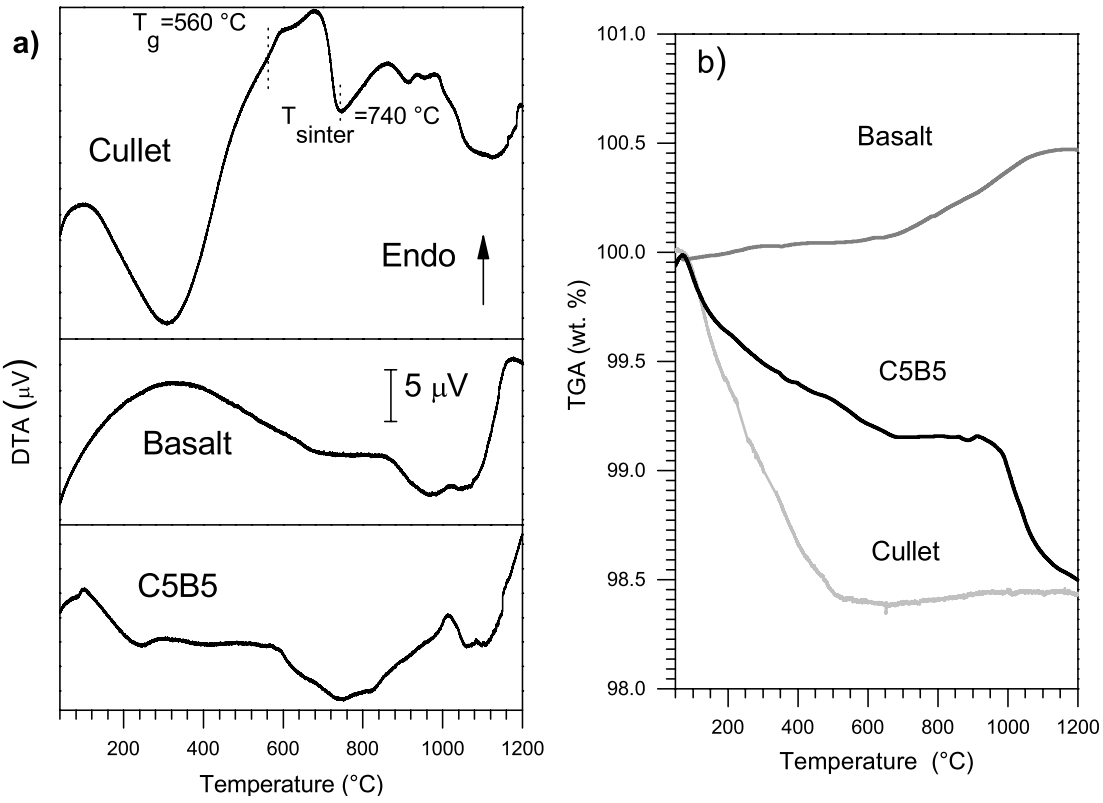

Fig. 2 – DTA (a) and TGA (b) curves for basalt, cullet and B5C5 mixture

Tab. 3 – Mineralogical quantitative phase analysis of the basalt scoria at room temperature and after firing at increasing temperature (wt%), obtained by full profile fitting of the experimental XRD patterns according to the Rietveld method (R_{wp}, R-factor of the weighted profile for each refined pattern is reported). FeO concentration (wt%), Fe^{2+}/Fe^{3+} ratio and forsterite unit cell volume (Å^3) for each temperature is also reported.

		Room T	1050°C	1100°C	1150°C	1200°C
R_{wp}		4.22	4.34	4.22	2.70	2.75
Amorphous	wt%	32.01	14.06	21.86	35.71	78.52
Andesine	wt%	39.94	50.62	47.67	36.39	12.09
Augite	wt%	10.67	12.45	11.54	4.39	-
Forsterite	wt%	15.14	13.76	9.65	13.08	3.54
Spinel	wt%	2.25	1.14	0.81	-	-
Hematite	wt%	-	7.20	7.54	8.51	1.32
Maghemite	wt%	-	0.76	0.92	1.84	4.53
FeO	wt%	6.64	1.08	1.11	1.75	1.89
Fe^{2+}/Fe^{3+}	-	1.50	0.11	0.11	0.19	0.21
Forsterite cell volume	Å^3	294.60	290.92	290.46	290.77	290.80

As determined by mineralogical quantitative phase analysis (Rietveld refinements), shown in **Tab. 3**, the basalt scoria mainly consisted of plagioclase (andesine), olivine (forsterite), clinopyroxene (augite) and spinel (titano-magnetite). The refinement was performed utilizing an andesine structure with a Ca/Na molar ratio of 0.98 [21], a ferrous forsterite structure with a Mg/Fe molar ratio of 4.48 (unit cell volume of 294.60 $Å^3$) [22], a titanian augite structure [23] and a titanomagnetite structure [24]. A significant amorphous fraction was also present (one third of the total mass) in the as received raw material. The Fe^{2+}/Fe^{3+} ratio was estimated to be 1.50; Fe^{2+} ions could be located in the M1 and M2 sites of augite, in the octahedral site of ferrous forsterite and in the tetrahedral and octahedral sites of spinel, while Fe^{3+} ions could be located in the M1 site of augite and in the tetrahedral and octahedral sites of spinel.

SEM microstructural analyses on scoria particles showed their fine-grained, vesicular and hypo-crystalline nature. The texture was porphyritic, with microphenocrysts of plagioclase, olivine, clinopyroxene and sporadic spinel characterized by subhdral shapes and dimensions between 50 and 200 μm (**Fig. 3a**). The groundmass (**Fig. 3b**) had an intersertal texture, with tabular plagioclase microlites surrounded by glass and cryptocrystalline phases. The vacuoles were characterized by irregular to spherical shape and size from few tens of microns to 1 mm. EDS analyses (**Fig. 3c, d, e, f**) confirmed the chemical compositions of plagioclases, olivines and clinopyroxenes determined by XRD (andesine, ferrous forsterite and titanian augite, respectively), while spinel crystals resulted to be frequently zoned and possessed heterogeneous composition, typical for chromite-titanomagnetite and chromite-spinel series. The glass matrix shows a silicoaluminate composition, with relevant amounts of calcium and iron and minor amounts of magnesium, titanium and alkalis. The mineralogical, chemical and textural characteristics of the analyzed volcanic materials are typical for basalt scoriae from the lava fields (harrats) of the Arabian continental alkali basalt province [25].

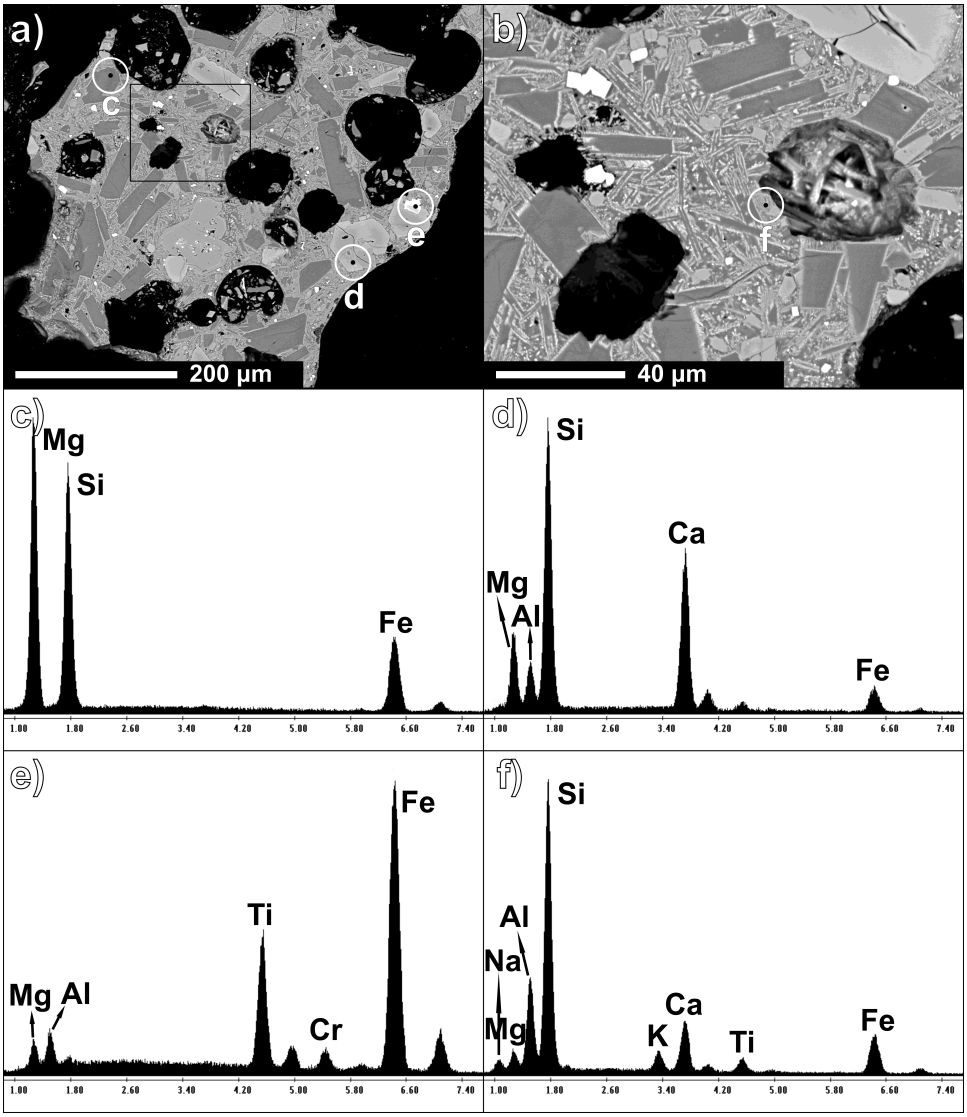

Fig. 3 – SEM-EDS microanalyses on a basalt scoria particle: a) Backscattered electron image (BEI) at low magnification, showing the porphyritic texture; b) BEI of the groundmass, showing the intersertal texture; c, d, e, f) EDS microanalysis of olivine, clinopyroxene, spinel and glass, respectively (point analyses locations are indicated in the BEI's)

As reported in **Tab. 3**, the basalt scoria had significant variations of both mineralogical and chemical characteristics after firing at different temperatures. The thermal treatments at 1050°C and 1100°C caused a decrease in glass content, more marked at lower temperatures and counterbalanced by a significant increase in plagioclase and hematite and a less significant clinopyroxene increase. Such analytical evidences indicate that partial melting phenomena occur in the glass glass matrix and crystallization of Al-rich silicates – e.g. plagioclase over clinopyroxene – is favored due to the peraluminous nature of the material. Furthermore, the oxidizing firing condi-

tions favored oxidation processes of the Fe^{2+} ions in the glass matrix, with consequent crystallization of hematite. Spinel and olivine were also interested by iron oxidation phenomena, according to well known processes [26-27]: the spinel underwent partial conversion into Ti-rich maghemite [28], more effective at higher temperatures, while olivine underwent a depletion of structural iron clearly testified by a d-spacing variation of (hkl) planes. For this reason, it was referred to a new structural model, consisting of olivine [29], with a Mg/Fe molar ratio of 9.53. The structural change caused an unit cell contraction, with consequent cracking of olivine crystals and precipitation of extracted iron in form of iron oxides inside the microcracks, as seen by SEM-EDS analyses (**Fig. 4**). A greater unit cell contraction is observable at 1100°C (290.46 $Å^3$ vs 290.92 $Å^3$), indicating a higher degree of Fe oxidation and consequent extraction from the olivine crystal structure. Such analytical evidence is consistent with previous analytical studies and can be related to the temperature-dependent thermodynamic stability of olivines [27]. The changes in Fe oxidation state are characterized by a steep drop in the Fe^{2+}/Fe^{3+} ratio to a value of 0.11.

After firing at 1150°C, a partial melting of silicate phases, in particular clinopyroxene, is observable, with formation of glass phase. The degree of Fe oxidation is still high, as testified by the hematite formation and by the total conversion of spinel into maghemite. The residual olivine is also interested by limited Fe oxidation, as shown by the lower unit cell contraction (290.77 $Å^3$), still related to thermodynamic factors [27]. Nevertheless, the overall degree of Fe oxidation is lower than the one observed for the lower heating temperatures, as testified by the higher Fe^{2+}/Fe^{3+} ratio of 0.19. At 1200°C, the degree of melting of the silicate phases is significantly accentuated, in particular for clinopyroxene, with relevant formation of glass phase. Furthermore, the Fe oxidation process led to a preferential crystallization of maghemite over hematite, being the hematite amount lower with respect to the other samples and the maghemite presence not fully justifiable with the spinel oxidation process. On the whole, the degree of Fe oxidation is lower than the other samples, as testified by the higher Fe^{2+}/Fe^{3+} ratio of 0.21.

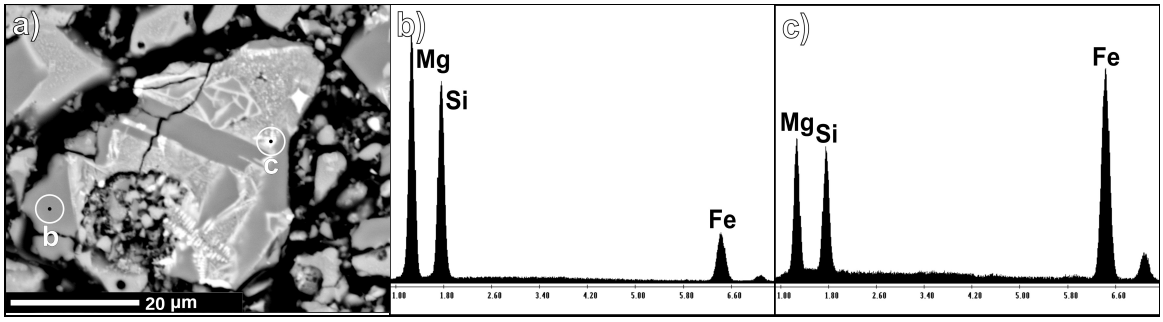

Fig. 4 – SEM-EDS microanalyses on a relict olivine crystal after firing at 1050°C. a) BEI, showing the effect of iron oxidation (cracking of the crystal and precipitation of iron oxides); b) EDS microanalysis of the olivine relict, with clear iron depletion; c) EDS microanalysis of iron oxide dendrites (Mg and Si are due to the interaction of the electron beam with the surrounding olivine relict).

All the Fe oxidation phenomena are consistent with the TGA analysis of the scoria (**Fig. 2b**), which revealed a mass increase starting above 700°C, with the exception of the treatment at 1200°C; in fact, the chemical titration revealed a decrease of the Fe^{2+}/Fe^{3+} ratio from 1150°C to 1200°C. This discrepancy between the chemical analysis and the TGA is reputed to be apparent, since it could be simply due to the fact that the TGA was recorded by applying a heating rate of 10°C/min whereas the titration was measured for samples directly fired at selected temperatures. Moreover, as the diffusion coefficient of oxygen in a basalt melt is less than $1.65 \cdot 10^{-6}$ cm^2/s [30], atmospheric oxidation is not effective after the formation of the melt unless the layer of the melt is very thin.

The prediction of the redox state of iron ions into the mixture is even more complicated by the fact that the soda lime cullet softens at a relatively low temperature, thus limiting the surface area of the basalt which is exposed to the atmospheric oxygen and by the fact that both basalt and cullet have a different redox equilibrium. The redox reaction between polyvalent ions, such as iron, and oxygen may be written in terms of the ionic species present in the system, as proposed by several authors [31-33]:

$$FeO_n^{(3-2n)+} = Fe^{2+} + \frac{1}{4}O_2 + \left(n - \frac{1}{2}\right)O^{2-} \qquad \text{(Eq.1)}$$

The equilibrium between ferrous and ferric oxides complexes is regulated by the atmospheric oxygen O_2 whereas according to Toop and Samis, [34, 35] a “free” oxy-

gen anion (O^{2-}) is bonded only to modifier ions and is related to the bridging (O^0) and nonbridging oxygen (O^-) ions by:

$$2O^- = O^{2-} + O^0 \qquad \text{(Eq.2)}$$

It is worth mentioning that Eq.2 is a shorthand notation for the various reactions that involve more complex entities with various proportions of bridging and non-bridging oxygens.

1.3.2 Glass Ceramic Foams Characterization

Considering the chemistry of the starting materials, shown in

Tab. 2, the introduction of cullet reduces the content of network glass modifier and the same occurs to the concentration of O^{2-}. Furthermore a number of studies performed on glass melts confirmed that for achieving the thermodynamic equilibrium between polyvalent ions and environmental oxygen, several hours or even days are required [31, 36-41]. The thermal treatment applied to the selected mixtures was far from the equilibrium, as when the B and C mixtures softened, oxygen gas was virtually cut off from the bulk of the melt. These two effects shifted the equilibrium to the right of Eq.1 and provided oxygen evolution, in turn causing the foaming of glass/basalt mixtures, by reduction of Fe^{3+} to Fe^{2+}.

It was reported by Fincham and Richardson [42] that sulfur solubility under reducing conditions increases with increasing temperature and decreasing pO_2, thus meaning that more reducing conditions are required at lower temperatures to maintain the same sulfur solubility in reduced melts. [31] This effect is called reboil when bubble-free materials exhibit bubble formation upon reheating from the solid state [43]. Similarly, cullet contains not negligible amount of sulfur, hence the previously mentioned reduction of solubility may justify the slight smell of sulfur perceived when crushing the specimens.

Tab. 4 – Mineralogical quantitative phase analysis of the C5B5 mixture at room temperature and after firing at 1100°C with different heating ramps (wt%), obtained by full profile fitting of the experimental XRD patterns according to the Rietveld method (R_{wp}, R-factor of the weighted profile for each refined pattern is reported). Forsterite unit cell volume (Å^3) for each thermal treatment is also reported.

	Room T	1100°C, 10 °C/min	1100°C, 20 °C/min	1100°C, 40 °C/min	1100°C, DF
R_{wp}		3.25	3.13	3.27	3.19
Amorphous	66.00	68.79	71.01	69.89	68.29
Andesine	19.97	0.67	0.29	0.17	-
Augite	5.33	25.41	23.21	24.37	26.11
Forsterite	7.57	3.49	3.84	4.11	3.95
Spinel	1.13	0.29	0.28	0.24	0.27
Hematite	-	0.19	-	-	-
Maghemite	-	0.76	0.73	0.71	0.74
Quartz	-	0.42	0.64	0.52	0.64
Forsterite cell volume	294.60	291.36	291.96	291.89	292.42

The mineralogical composition obtained by Rietveld quantitative phase analysis of C5B5, fired at 1100°C with different heating rates, is reported in **Tab. 4**. Significant variations in the mineralogical profile of the samples occurred with respect to the mixture at room temperature. A slight increase in the content of amorphous phase – markedly dominant over the crystalline fraction – is always observable, while the most evident variation in the composition of the crystalline fraction is the marked decrease in plagioclase amount, slightly correlated to the heating rate. The plagioclase decrease is counterbalanced by a significant increase in clinopyroxene concentration, caused by the introduction in the mixture of a silicate-rich material proportional to the amount of scoria. The transition from basic to intermediate composition as regards silica content, from peraluminous to peralkaline conditions as regards alumina saturation, and the drastic increase in calcium concentration, caused the dissolution of alumina-rich phases – e.g. the plagioclase - and the precipitation of calcium-rich ones – e.g. the clinopyroxene – during the thermal process. Furthermore, the presence of low but clearly recognizable quartz amounts suggests a slight systematic silica oversaturation of the mixture.

As for the other Fe-bearing phases, a partial oxidation of spinel, with maghemite formation, is always observable, associated with a decrease in olivine concentration. As for the thermal treatment of the scoria samples, an oxidation process of ferrous

iron in relict olivine is observable, testified by the unit cell contraction of the phase. The unit cell contraction is always smaller with respect to the one in the pure scoria sample treated at the same temperature, with values around 291 $Å^3$ for the mixtures treated with heating ramps, and it is larger in the samples that were directly fired. These analytical evidences suggest a lower oxidation of iron with respect to the thermally treated scoria, also confirmed by the detection of hematite only in the sample heated at 10°C/min. Furthermore, the directly fired sample apparently shows lower degree of oxidation with respect to the other ones.

SEM-EDS analyses (**Fig. 5**) confirmed the analytical evidences deduced by XRD analyses. The foams were constituted by a dense glass matrix, with clinopyroxene, olivine and spinel primary crystals. Plagioclase primary crystals were almost totally absent, whereas diffuse newly-formed microcrystals of clinopyroxene were present in the groundmass, often preferentially nucleated around relict phases. As observed for the thermally treated scoria samples, the olivine oxidation process is clearly observable, as testified by the presence of fractured crystals with precipitation of extracted iron in form of iron oxides inside the microcracks (**Fig. 5b, d**). Nevertheless, relict olivine crystals were less stressed with respect to the one observed in the thermally treated scoria samples, with lower occurrence of iron oxides dendrites: such evidence is in agreement with the lower degree of olivine oxidation observed by XRD analyses. Furthermore, the olivine crystals in the directly fired sample were less oxidized with respect to the ones of the other foams (**Fig. 5d**), confirming the lower degree of reaction.

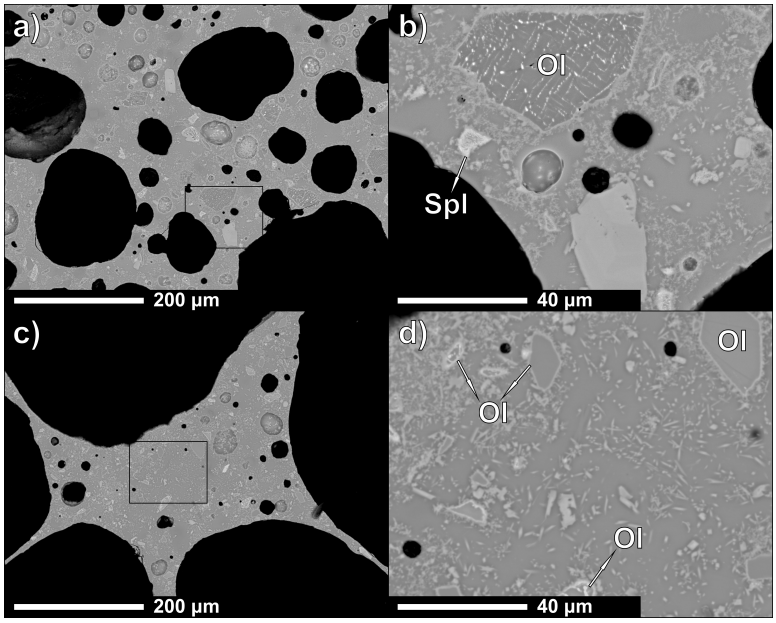

Fig. 5 – SEM images of C5B5 foams fired at 1100°C with a 10°C/min ramp (a, b) and by direct insertion (c, d). a, c) low magnification; b, d) high magnification of the highlighted areas. Oxidized olivine (Ol) and spinel crystals (Spl) are indicated

As reported in **Tab. 5**, bubbles formation was strongly promoted by direct firing, determining a total porosity of 86%, of which only 8% was closed. By decreasing the heating rate to 10°C/min, the total porosity decreased to 53%, of which only 8% was open. By applying heating rates of 20 and 40°C/min, intermediate total porosities were achieved. The specimens produced by applying a progressive heating at 40°C/min, showed a water absorption after boiling of about 0.3 wt%, which decreased to 0.1 wt% for the samples treated with a heating rate of 10°C/min and 20°C/min.

X-ray computed micro-tomography (X-µCT) measurements were carried out on the C5B5 set of samples, in order to evaluate the effect of different heating rates on the pore space properties (open and closed porosity fractions, pore size distribution). The results were then compared with those previously obtained from gas pycnometry on the same samples. As opposed to other techniques for the investigation of porosity, X-µCT offers the great advantage of directly visualizing in 3D the pore space, providing at the same time important information about size, shape and position of the pores. X-µCT experiments also allowed to extract some relevant morphometric indices of the three-dimensional porous structure, such as the structure thickness, that can be correlated with the mechanical properties of the foams.

Tab. 5 – Characterization data for foam samples fired at 1100°C for 15 minutes at different heating rates (data between square brackets obtained from X-ray computed micro-tomography; *=data obtained from bars cut from panel samples)

Sample type	C5B5					C4B6		C6B4
15 min at: (°C)	1100				1050	1050	1100	1050
Heating rate (°C/min)	10	20	40	DF	DF	DF	DF	DF
W_{AB} (wt %)	<0.2	<0.2	0.3	>100	93	24	78	42
Density (g/cm^3)								
Bulk [ρ_b]	1.27 ± 0.08	1.03 ± 0.05	1.05 ± 0.03	0.37 ± 0.02	0.53 ± 0.08	0.88 ± 0.09	0.51 ± 0.05	0.44 ± 0.01
Apparent [ρ_a]	1.38 ± 0.01	1.15 ± 0.01	1.18 ± 0.01	1.70 ± 0.05	1.49 ± 0.07	1.80 ± 0.03	1.39 ± 0.04	0.79 ± 0.04
True [ρ_t]	2.70 ± 0.01	2.69 ± 0.01	2.69 ± 0.01	2.69 ± 0.01	2.69 ± 0.01	2.68 ± 0.01	2.68 ± 0.01	2.62 ± 0.01
Porosity (%)								
Total porosity [TP]	53 ± 3 [44]	62 ± 2 [53]	61 ± 1 [53]	86 ± 1 [73]	80 ± 3	67 ± 3	81 ± 2	83 ± 1
Closed porosity [CP]	8 ± 6[1]	10 ± 4 [3]	11 ± 3 [7]	78 ± 1 [72]	65 ± 6	51 ± 5	63 ± 4	44 ± 3
Open porosity [CP]	45 ± 6 [43]	52 ± 5 [50]	50 ± 3 [46]	8 ± 1 [1]	16 ± 6	16 ± 6	18 ± 4	39 ± 4
Elastic modulus (GPa)*	26.9 ± 0.5	19 ± 2	18.6 ± 0.6	-	-	-	-	-
Strength (MPa)								
Bending strength [σ_{flex}]*	17 ± 4	11 ± 1	13 ± 2	-	-	-	-	-
Crushing strength [σ_{cr}]	50 ± 10	22 ± 7	18 ± 6	2.5 ± 0.7	5 ± 2	15 ± 7	4 ± 1	2 ± 1
Mean struct. Thickness (μm)								

The analysis of the pore size distribution was carried out only on the *closed porosity fraction* of each sample; the results are reported in the histograms of **Fig. 6e**. For clarity of representation, the graphs were limited to a maximum diameter of the pores of 1 mm; only a few, very large coalesced pores were excluded from the results in this way. The increase of the heating rate from 10 to 40°C/min seems to have a clear effect on the size of the pores. In particular, a shift of the main peak of the distribution towards larger values (an effect of the coalescence of pores) and a broadening of the distribution curve are observed. Again, also for what concerns the pore size distribution, the samples prepared with heating rates of 20 and 40°C/min are very similar. As expected, the pellet obtained by direct firing is completely different and cannot be directly compared with the other three. In fact, only a minor fraction of pores is reported in the relative pore size distribution histogram, being the porosity of the sample almost completely open. However, as confirmed by X-μCT slices (**Fig. 6e**), the maximum size of the pores is limited in this case to significantly lower values (< 500 μm).

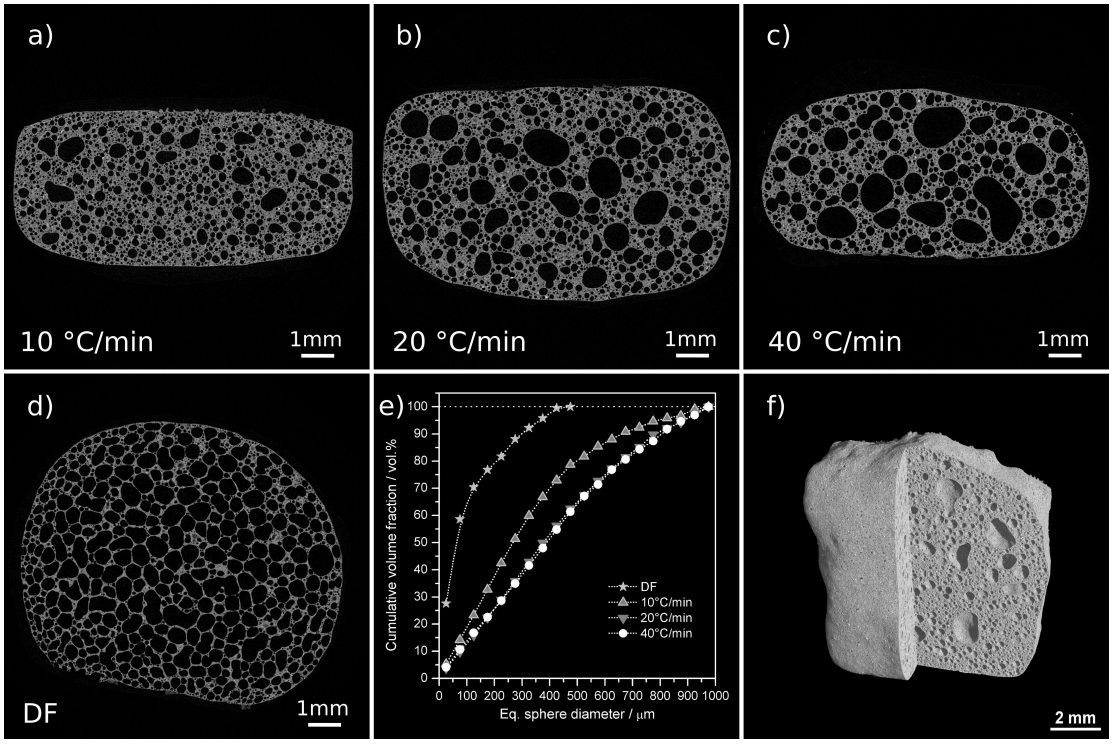

Fig. 6 – Results from X-ray microtomography: a,b,c,d) reconstructed cross-sections of selected samples from the C5B5 series; e) pore size distribution of the closed porosity fractions; f) 3D rendering of a pellet (C5B5, 10°C/min heating rate - a portion of the sample was virtually cut out to display the interior).

The results from X-μCT, as shown by **Tab. 5**, are in good agreement with those from gas pycnometry. However, it is easy to notice that the values of total porosity measured with X-μCT are always significantly lower compared to those obtained with gas pycnometry. This can be explained in terms of the limited spatial resolution of the technique, which makes the fraction of pores smaller than a few microns practically not detectable. Sub-microns spatial resolutions could be obtained, though on significantly smaller samples, using synchrotron-based X-ray computed microtomography. A 3D rendering of one of the investigated pellet is shown in **Fig. 6f**. The actual appearance of glass ceramic samples is visible in **Fig. 7**, showing a C5B5-type sample heated at 10°C/min.

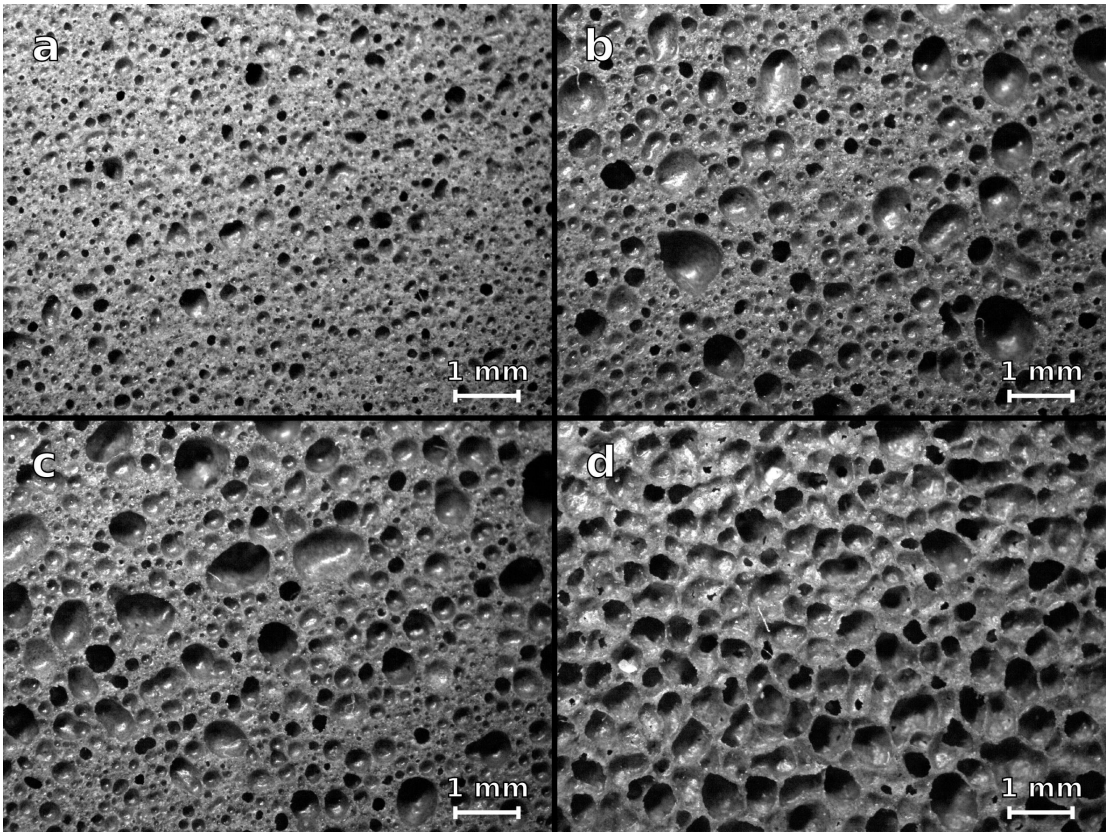

Fig. 7 – Microstructure of a C5B5-type sample fired at 1100°C (10°C/min heating rate).

The structure thickness (also referred to as the trabecular thickness in biomedical applications) was calculated using 3D algorithms for the investigated samples. The determination of this index [44] is based on the fitting of maximal spheres inside an object (the foam walls in this specific case). The mean structure thickness evaluated in 3D is calculated as the volume weighted average of the local thicknesses and represents an important parameter for comparing the wall thickness of porous solids. However, also the distribution of thicknesses has to be considered to better define the mechanical properties of such materials. The values of the mean structure thickness obtained for the investigated samples are reported in **Tab. 5**. The sample prepared by direct firing showed the lower value of mean structure thickness (47.4 μm), as a consequence of its very large amount of porosity. Significantly higher values were obtained for the other samples, showing a slight increase of the mean structure thickness with the increasing heating rate. However, the mean structure thickness was evaluated as 54.2 μm for the sample obtained by heating at 10°C/min,

whereas almost identical values were obtained with heating rates of 20 and 40°C/min (57.9 and 58.1 μm, respectively).

The limited mean structure thickness and the high porosity determine low crush strength values for the directly fired samples (2.5 MPa). Nevertheless a reduced mean structure thickness might provide higher strength as observed for the sample obtained by heating at 10°C/min. Indeed the high concentration of pores with a size less than 100 μm determines the struts thickness reduction without worsening the mechanical properties.

The decomposition of the organic residues present in the cullet, may be beneficial for the enhancement of the porosity when applying a fast heating rate. However, the experiments conducted with a heating rate of 10°C/min provided the lowest TP, probably because the decomposition of the organic residues present in the raw materials started well below the softening of the mixture and even below the T_G of cullet. On the contrary by applying a fast heating to the samples, the specimen surface softened and created a sealing layer which embedded all the gases released within the material. The decomposition of the organics to form CO and CO_2 may not be limited to the oxygen trapped within the pores of the green body, but also from the oxygen evolution occurring at high temperatures upon reduction of Fe^{3+} to Fe^{2+}. Contemporary it is not well understood if the enhancement of porosity at the increasing of the heating rate is given by the limited exposition at the environmental oxygen. For example, samples fired with a heating rate of 10°C/min took 110 minutes to reach 1100°C, while samples directly fired were kept only for 15 minutes at 1100°C. The longer the time spent by the sample at high temperature, and the easier is for the gas bubbles to coalesce, producing an inhomogeneous morphology and increasing the mean pore size. At the same time, the kinetic of crystallization and phase transformation played a pivotal role, along with the viscosity of the amorphous phase, in the dynamics of the microstructural development. Low heating rates might favor the reaction and re-crystallization of the system, thereby increasing the viscosity and reducing the viscous flow and possibility of coalescing the bubbles. For this reasons, it was important to observe the pore size for the whole sample without restricting the investigation to limited areas.

In **Fig. 8** are shown two other slices of samples heated with a rate of 10°C/min and 20°C/min, and showing the evidence of coalescence of gas bubbles.

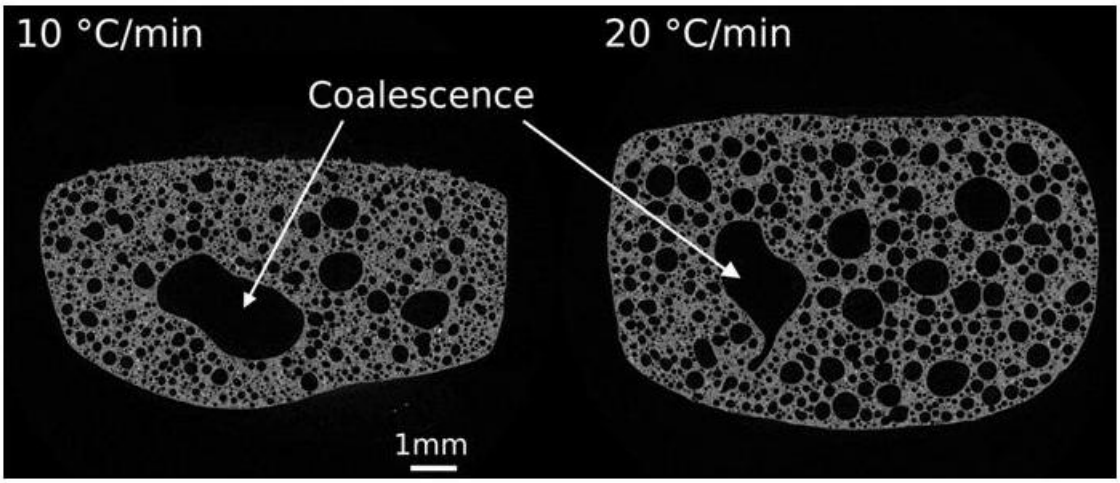

Fig. 8– Coalescence of the pores for the samples, of composition C5B5 fired at 1100°C for 15 minutes, heated with a rate of 10°C/min and 20°C/min.

Mineralogical Analysis

The changes occurring in the C5B5 samples depending on the heating rates, stimulated further tests on the effect of composition and temperature. The results of treatments at 1050 and 1100°C, in terms of mineralogical composition, are summarized in **Tab. 6**, while density and strength data are reported again in **Tab. 5**. A progressive decrease in plagioclase concentration with increasing temperatures, counterbalanced by an increase in clinopyroxene, is confirmed. The presence of the calcium silicate phase is related to the intermediate and peralkaline composition of the mixtures, highly enriched in calcium, whereas its occurrence at low temperatures only is related to its thermal stability field. Traces of quartz are detectable in all the samples, indicating a slight silica oversaturation for all the mixtures. Furthermore, spinel and olivine underwent Fe oxidation processes in all the samples, with maghemite formation and olivine unit cell contraction due to iron extraction. As for the C5B5 mixtures treated with different heating ramps, the unit cell contraction was always lower with respect to the ones observed for the thermally treated scoria samples, suggesting lower overall degrees of iron oxidation. No clear correlations between the measured olivine unit cell contraction and temperature or composition variations were observable.

Tab. 6 – Mineralogical quantitative phase analysis of C4B6, C5B5 and C6B4 mixtures at room temperature and after firing at 1050°C and 1100°C, obtained by full profile fitting of the experimental XRD patterns according to the Rietveld method (Rwp, R-factor of the weighted profile for each refined pattern is reported). The forsterite unit cell volume (Å^3) resulting from the refinement after each thermal treatment is also reported.

	C4B6, T room	C4B6, 1050°C	C4B6, 1100°C	C5B5, T room	C5B5, 1050°C	C5B5, 1100°C	C6B4, T room	C6B4, 1050°C
R_{wp}		3.15	3.32		3.20	3.19		3.12
Amorphous	59.20	58.10	61.17	66.00	68.31	68.29	72.80	74.08
Andesine	23.96	7.85	2.86	19.97	2.57	-	15.97	0.57
Augite	6.40	24.38	27.84	5.33	20.35	26.11	4.27	17.31
Forsterite	9.08	6.53	6.70	7.57	5.86	3.95	6.06	4.91
Spinel	1.35	0.76	0.25	1.13	0.44	0.27	0.90	0.36
Hematite	-	0.45	-	-	-	-	-	-
Maghemite	-	0.68	0.97	-	0.71	0.74	-	0.48
Quartz	-	0.33	0.20	-	0.31	0.64	-	0.24
Wollastonite	-	0.93	-	-	1.44	-	-	2.04
Forsterite cell volume	294.60	291.57	292.17	294.60	292.79	292.42	294.60	291.04

Mechanical properties and potential applications

As previously observed, directly fired samples show mostly open pores, whereas the samples fired using a defined heating rate featured mostly closed cells. As illustrated by **Fig. 6e**, the samples with closed cells had also a practically continuous pore cell distribution, while the open porosity was associated to a defined maximum pore size (a sort of threshold level) and was generally much more uniform. These differences could be ascribed to the mechanism of pore formation itself. Operating with direct firing, lots of pore nuclei formed almost simultaneously; on the contrary, operating at defined heating rates, some pores could form and collapse during the heating period. Larger pores, for defined heating rates, likely incorporated smaller ones; this effect (cell coalescence) is well known to cause a reconstruction of the cell struts, which become increasingly thicker, and in turn contain secondary pores [3]. In **Fig. 6c**, as an example, some very large pores are present and surrounded by very thick and porous struts.

The presence of open porosity generally implies a degradation of mechanical properties; thick and porous struts, however, make closed-cell foams practically as weak as open-celled foams [3]. As a general approach, it may be noted that a com-

ponent with uniformly distributed open cells is mechanically as efficient as one with closed cells, which are not homogenously distributed, and with thick struts. The Ashby's plot [45] in **Fig. 9a** may be seen as a confirmation of this interpretation: the studied samples are nicely aligned in terms of specific crushing strength (the line in the graph represents materials with the same ratio between crushing strength and density, σ_c/ρ), except for C5B5-type samples fired at 10°C/min (well above the line, meaning that they are mechanically more efficient). Interestingly, the specific strength of these glass ceramic foams is higher or equal to that of variants of light-weight concrete, suggesting their use as new lightweight aggregates in the building industry.

The plots of bending strength and elastic modulus for denser samples, in the form of panels and fired with a defined heating rate, also indicate the suitability of these materials for possible applications in the building industry; in fact, the indices for the design of lightweight panels [45], i.e. the specific flexural strength index ($\sigma_{flex}^{1/2}/\rho$, **Fig. 9b**) and the specific Young's modulus index ($E^{1/3}/\rho$, **Fig. 9c**), well exceed the values for most non-technical ceramics, including traditional ceramics (brick and tiles), natural stones (granite) and concrete. Considering the low water absorption (not exceeding 0.3 wt%), C5B5-based panels could be applied in the so-called ventilated façades, i.e. a new generation of cladding components that can be applied on the surface of large buildings, aimed at improved the thermal insulation, as an alternative to conventional porous ceramics (fired at higher temperature and requiring the addition of specific foaming agents to develop a homogenous cellular structure) [46,47], especially if coated with a glaze [48,49].

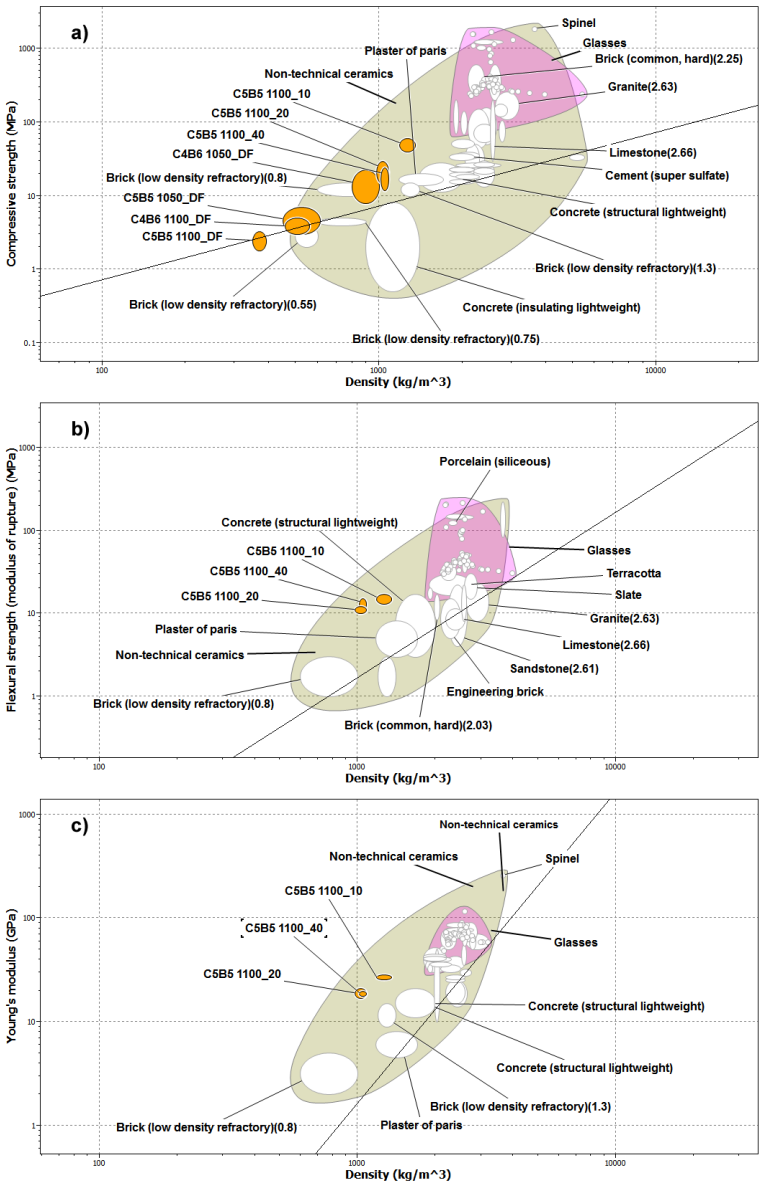

Fig. 9 – Ashby's plots of developed glass ceramic foams compared with non-technical ceramics and glasses (a) compressive strength; b) flexural strength; c) Young's modulus); the lines correspond to guidelines for lightweight design.

NOTE: It is not well understood how the nucleation of acicular clinopyroxenes in the amorphous matrix may influence the mechanical strength. Although the mixtures richer in scoria are richer in clinopyroxene, neoformation of clcinopyroxene is higher in the samples rich in cullet, since the formation of the phase is favored by the higher presence of calcium in the resulting mixture. Surprisingly, samples C4B6 and C5B5 fired at 1100 and 1050°C respectively, presented approximately the same porosity values and comparable strength, but different mineralogical composition. In fact, samples C5B5 show lower clinopyroxene formation and a relative enhance-

ment of the amorphous phase. This might suggest that the crystallization slightly modifies the strength of the studied foams. However, samples C5B5 and C6B4 fired at 1100 and 1050°C respectively, have approximately the same total porosity and crushing strength, despite the much higher OP evaluated for sample C5B5 (high OPs are known for being detrimental for the mechanical strength). Samples C5B5 fired at 1100°C are more crystallized than samples C4B6 fired at 1050°C and show higher clinopyroxene formation, but lower olivine content. As previously reported the olivine oxidation process determine relevant fracturing of crystals (**Fig. 5b, d**) that may reduce the strength of the foams. A possible explanation of the detriment of the mechanical properties of sample C6B4 fired at 1050°C, may be found in the percentage of olivine formed and into its volume cell contraction.

The introduction of cullet reduces the content of network glass-modifiers and consequently by equation (2) the same occurs to the concentration of the free oxygen ion O^{2-} which shifts the equilibrium to the right of equation (1) and provides oxygen evolution by reduction of Fe^{3+} to Fe^{2+}.

It is worthy to mention that the viscosity of the mixture may vary strongly with the composition. For example at 1050°C the percentage of the amorphous phase goes from 58 wt% for C4B6 to 72 wt% for C6B4. Reasonably at the increasing of the amorphous phase the viscosity of the mixture decreases thus favoring an enhancement of the porosity.

Then it is not trivial to determine if the enhancement of porosity at the increasing of wt% of cullet is due to the reduction of the alkali content only or if other effects give a contribute.

The decrease of density by increasing the firing temperature may be explained for all the studied mixtures considering that by increasing the temperature, reaction (1) is favored and the viscosity decreases.

1.3.2 Lightweight Concrete Characterization

The traditional aggregates were substituted in a limited percentage (30 vol%) considering that the amorphous aluminosilicates are strongly corroded at high pH values and the samples were cured in water for 28 with a pH of 13, which might be detrimental for the mechanical properties. Secondly aggregates produced using the tunnel furnace presented a relatively large size distribution and only a small fraction

could be used according to the Bolomey's and Fuller's curves. Fuller's curve is generally used for pastes with an improved packing of the aggregates whereas the Bolomey's curve is used for pastes with an improved workability. In particular the expression for the Bolomey's curve is:

$$P = 100\frac{A + (100 - A)\sqrt{d/D} - C}{100 - C}$$

where P is the percentage of aggregate passing through a sieve with an opening d, D is the diameter of the larger aggregates used, C is the fraction of cement and A is the workability coefficient. We decided to realize a semifluid paste selecting the parameter A=10 and 25mm for the maximum size of the aggregate. The plot in **Fig. 10** shows the distribution of the aggregate and sands sizes used to obtain the experimental Bolomey's curve.

In **Fig. 11a** is shown a standard specimen set up with the strain gauges used to evaluate the deformation for the elastic modulus and compression strength determination. The sample failure reported in **Fig. 11b** shows the lateral cracks formed in the external walls of the specimens due to the lateral expansion during compression (tensile failure) that are satisfactory according to the requirements reported in the standard EN 12390 (**Fig. 11c**). The Brazilian test set up is reported in **Fig. 12a**, whereas the typical failure of samples for both the sets are shown in **Fig. 12b** and **c**.

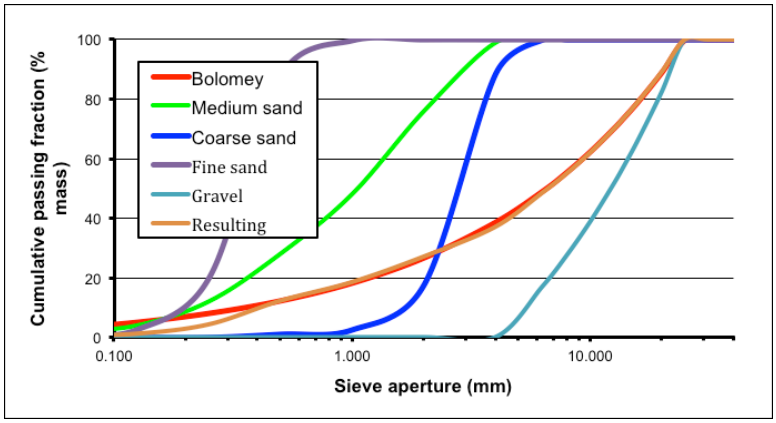

Fig. 10 – Aggregates and sands size distributions used to obtain the experimental Bolomey's curve.

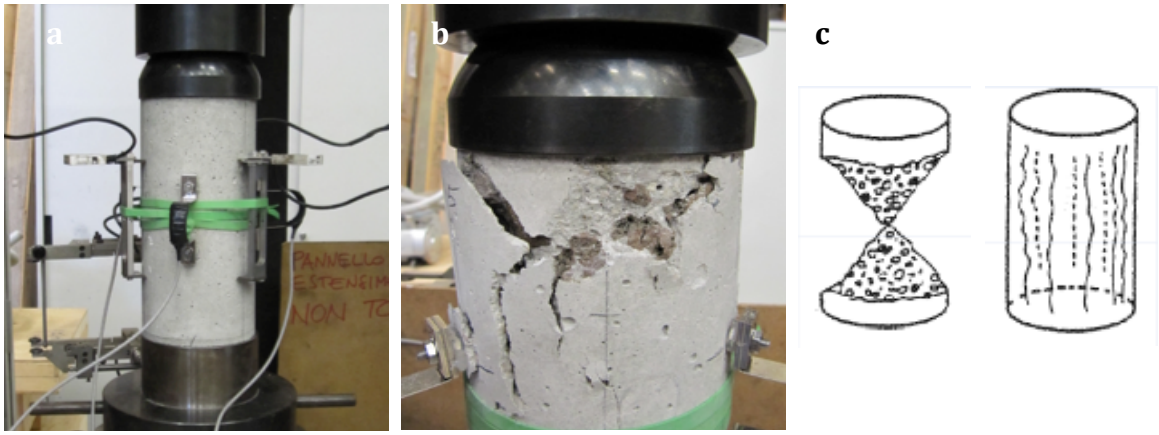

Fig. 11 – a) Experimental set up for the determination of the elastic modulus and compressive strength. b) Failure of a LWAC sample in compression. c) Satisfactory failures of standard specimens according to EN 12390.

According to the Italian's law requirements concrete is considered structural when the failure of the standard cylinder samples occurs at 15/20 MPa (C15/20). The materials developed using the traditional aggregates presented a strength values at the upper limit of the C25/30 (see **Tab. 7**) whereas the LWAC samples were closer to the lower limit of the class. Although the LWAC samples were 15% lighter and 12% weaker in compression than when using the traditional aggregates the specific strength resulted 4% higher. It is rather interesting to observe that a similar difference (13%) occurred for the tensile strength and only the elastic modulus was lower of about 17% for the LWAC. The low elastic modulus resulted from the low elastic modulus of the LWA (< 20 GPa, see **Tab. 5**) comparing with the traditional aggregates (~70 GPa).

Fig. 12 – a) Brasilian test set up. b) Failure of a sample using traditional aggregates. c) Failure of a LWAC sample.

Tab. 7 – Mechanical properties of concrete samples using traditional and LWA.

	Apparent density	Compression strength	Specific compression strength	CoV	Elastic modulus	Tensile strength	CoV
	[kg/m^3]	MPa	MPa/(g/cm^3)	%	GPa	MPa	%
Traditional	2431	29.9 ± 0.5	12.3	1.5	33.2	3.9 ± 0.1	1.4
Light weight	2055	26.4 ± 1.1	12.8	4	24.3	3.4 ± 0.3	7.5
C 25/30*		25			30.5	3.3	
C30/35*		30			32	3.8	
Traditional LWAC Difference %	*-15*	*-12*	*+4*		*-17*	*-13*	

* Standard table of strength requirements provided by EN 12390.

1.4 Conclusions

Cellular Glass Ceramics Manufactured in Laboratory Conditions

The addition of cullet to basalt scoria enabled the fabrication of highly porous glass ceramic foams with good mechanical strength at relatively low temperature and with fast firing. Total porosity ranged in a wide range of values, depending on the composition and processing schedule adopted, and components with either closed cells and low water absorption values, or with open cells were fabricated. No foaming agents were necessary, and the self-foaming mechanism was related to the redox reactions occurring between different iron oxide species. The choice of the most appropriate processing will depend on the type of application pursued for the specific components produced. For instance the data here presented demonstrate that C5B5-based light weight aggregates obtained by applying a heating rate of 10°C/min could be used to realize lightweight concrete considering that the specific strength of these glass–ceramic foams is higher or equal to that of typical lightweight concrete. Furthermore C5B5-based panels obtained by applying a heating rate of 40°C/min or 20°C/min could be applied in the so-called ventilated façades considering their high specific flexural strength index, the limited water absorption and that porous materials may further improve the thermal insulation.

Lightweight Aggregates and Concrete

When changing type of cullet and firing conditions passing from a muffle to a tunnel furnace and using a process not well optimized, the control of the porosity is rather complicated. The cellular glass ceramics manufactured at SASIL were affected by larger pores and by a substantial difference from the results obtained during the preliminary experiments performed in laboratory. Although the pore size distribution of the aggregates strongly varied from the results obtained in laboratory conditions, LWA in sufficient amount were produced for manufacturing LWAC. The concrete using conventional materials was in the class C25/30 of structural concretes and its strength lowered of 12% when substituting 30 vol% of aggregates with the LWA. Although the main focus of the actual regulations is the absolute compression strength and when using LWAC the value was lowered (still in the class C25/30) the specific strength of the LWAC was improved of about 4%. This result is encouraging and demonstrates that optimized LWA could compete with traditional aggregates.

Future investigations will be carried on by personnel from CIRCE to investigate lighter LWAC by substituting a higher fraction of LWA.

Bibliography

1 G. Scarinci, G. Brusatin, E. Bernardo, Production Technology of Glass Foams, in: M. Scheffler, P. Colombo (Eds.), Cellular Ceramics. Structure, Manufacturing, Properties and Applications, Wiley-VCH, Weinheim, Germany, 2005.

2 W. Owen (Pittsburgh Plate Glass, USA), US Patent 2,310,457 (1943).

3 E. Bernardo, F. Albertini, Glass foams from dismantled cathode ray tubes, Ceram. Int. 32 (2006) 603–608.

4 F. Méar, P. Yot, M. Ribes, Effects of temperature, reaction time and reducing agent content on the synthesis of macroporous foam glasses from waste funnel glasses, Mater. Lett. 60 (2006) 929–934.

5 E. Bernardo, R. Cedro, M. Florean, S. Hreglich, Reutilization and stabilization of wastes by the production of glass foams, Ceram. Int. 33 (2007) 963–968.

6 H.R. Fernandes, D.U. Tulyaganov, J.M.F. Ferreira, Preparation and characterization of foams from sheet glass and fly ash using carbonates as foaming agents, Ceram. Int. 35 (2009) 229–235.

7 E. Bernardo, Micro- and macro-cellular sintered glass–ceramics from wastes, J. Eur. Ceram. Soc. 27 (2007) 2415–2422.

8 F. Defrancesco, A. Tomasi, G.D. Soraru, Expanded materials from quartz-porphyrite sands, J. Mater. Sci. 22 (1987) 2493-2496.

9 I. Ponsot, E. Bernardo, Self glazed glass ceramic foams from metallurgical slag and recycled glass, J. Clean. Prod. 59 (2013) 245-250.

10 Jones MR, McCarthy A. Behaviour and assessment of foamed concrete for construction applications. In: Dhir RK, Newlands MD, McCarthy A, editors. Use of foamed concrete in construction. London: Thomas Telford; 2005. p. 61–88.

11 J. A. Rossignolo, M. V. C. Agnesini. Mechanical properties of polymer-modified lightweight aggregate concrete. Cement and Concrete Research 32 (2002) 329–334.

12 H. B. Basri, M. A. Mannan, M. F. M. Zain. Concrete using waste oil palm shells as aggregate. Cement and Concrete Research 29 (1999) 619–622.

13 K.M. Anwar Hossain. Properties of volcanic pumice based cement and lightweight concrete. Cement and Concrete Research 34 (2004) 283–291

14 R. Demirboga, R. Gül. The effects of expanded perlite aggregate, silica fume and fly ash on the thermal conductivity of lightweight concrete. Cement and Concrete Research 33 (2003) 723–727.

15 H.M. Rietveld, A profile refinement method for nuclear and magnetic structures. J. Appl. Crystallogr. 2 (1969) 65-71.

16 Gualtieri AF. Accuracy of XRPD QPA using the combined Rietveld–RIR method. J. Appl. Crystallogr. 33 (2000) 267–278.

17 W.A. Dollase, Correction of intensities for preferred orientation in powder diffractometry: application of the March model, J. Appl. Crystallogr. 19 (1986) 267–72.

18 L.A. Feldkamp, L.C. Davis, J.W. Kress, Practical cone-beam algorithm. J. Opt. Soc. Am. 1 (1984) 612-619.

19 M. Boin, A. Haibel, Compensation of ring artefacts in synchrotron tomographic images. Opt. Express, 14 (2006) 12071-12075.

20 J. Sijbers, A. Postnov, Reduction of ring artefacts in high resolution micro-CT reconstructions, Phys. Med. Biol. 49 (2004) 247-253.
21 I.D.R. Mackinnon, J.B. Parise, J.D.F. Gerald, Average structure of an An48 plagioclase from the Hogarth Ranges, Am. Mineral. 71 (1986) 1399-1408.
22 G. Ottonello, F. Princivalle, A. Della Giusta, Temperature, composition and fO_2 effects on intersite distribution of Mg and Fe^{2+} in olivines, Phys. Chem. Miner. 17 (1990) 301-312.
23 G.M. Crisci, P.F. Zanazzi, G. Molin, D. Pasqual, Clinopyroxene from Lipari: Comparison with analogues from other Aeolian Islands, Italy, Can. Mineral. 36 (1998) 97-105.
24 Wechsler, B.A., Lindsley, D.H., Prewitt, C.T., Crystal structure and cation distribution in titanomagnetites ($Fe_{3-x}Ti_xO_4$), Am. Mineral. 69 (1984) 754-770.
25 V.E. Camp, M.J. Roobool, The Arabian continental alkali basalt province: Part I. Evolution of Harrat Rahat, Kingdom of Saudi Arabia, Geol. Soc. Am. Bull. 101 (1989) 71-95.
26 B. Gillot, F. Jemmali, A. Rousset, Kinetics and mechanism of ferrous spinel oxidation studied by electrical conductivity and thermogravimetry, J. Mater. Sci. 21 (1986) 4436-4442.
27 D. Świerczyński, C. Courson,L. Bedel, A. Kiennemann,and S. Vilminot, Oxidation reduction behavior of iron-bearing olivines $(Fe_xMg_{1-x})_2SiO_4$ used as catalysts for biomass gasification, Chem. Mater. 18 (2006) 897-905.
28 S. Collyer, N.W. Grimes, D.J. Vaughan, G. Longworth, Studies of the crystal structure and crystal chemistry of titanomaghemite, Am. Mineral., 73 (1988) 153.
29 Yu Shu Cheng, Effects of pressure on the crystal structure of olivine in harzburgite xenolith of basalt. Proceedings of the National Science Council, Republic of China, Part A: Physical Science and Engineering 21 (19979 173-179.
30 R.F. Wendlandt, Oxygen diffusion in basalt and andesite melts: experimental results and discussion of chemical versus tracer diffusion, Contrib. Miner. and Petr. 108 (1991) 463-471.
31 S. Holmquist, Ionic Formulation of Redox Equilibria in Glass Melts, J. Am. Ceram. Soc. 49 141 (1966) 228-29.
32 D.S. Goldman, Oxidation Equilibrium of Iron in Borosilicate Glass, J. Am. Ceram. Soc. 66 (1983) 205–209.
33 M. Cable, A Century of Developments in Glassmelting Research, J. Am. Chem. Soc., 81 (1998) 1083–1094.
34 G. W. Toop and C. S. Samis, Some New Ionic Concepts of Silicate Slags, Can. Metall. Quart. 2 (1962) 129-52.
35 B. Mysen and P. Richet, Silicate Glasses and Melts, Elsevier 1sd edition (2005) 179-183.
36 F. Irmann, A Study of Molten Borates with the Cr(VI)—Cr(III) Indicator, J. Am. Chem. Soc. 74 (1952) 4767-4770.
37 W. D. Johnston, Oxidation-Reduction Equilibria in Iron-Containing Glass, J. Am. Ceram. Soc. 47 (1964) 198-201.
38 W. D. Johnston, Oxidation-Reduction Equilibria in Molten $Na_2O{\cdot}2SiO_2$ Glass, J. Am. Ceram. Soc. 48 (1965) 184-190.

39 W. D. Johnston, A. Chelko, Oxidation-Reduction Equilibria in Molten $Na_2O{\cdot}2SiO_2$ Glass in Contact with Metallic Copper and Silver, J. Am. Ceram. Soc. 49 (1966) 562-564.
40 S. Banerjee, A. Paul, Thermodynamics of the System Cu-O and Ruby Formation in Borate Glass, J. Am. Ceram. Soc. 57 (1974) 286-290.
41 A. Paul, Chemistry of Glasses, Chapman & Hall 2nd edition (1990) 228-230.
42 C. J. B. Fincham and R. D. Richardson, The Behaviour of Sulphur in Silicate and Aluminate Melts, Proceedings of the Royal Society A , 223 [1152] (1954) 40-62.
43 J. E. Shelby, Introduction to Glass Science and Technology, The Royal Society of Chemistry 2nd edition (2005) pp 40-42.
44 T. Hildebrand, and P. Rüegsegger. A new method for the model-independent assessment of thickness in three-dimensional images. Journal of Microscopy, 185(1), (1997) 67-75.
45 M.F. Ashby, Materials Selection in Mechanical Design, third edition, Butterworth Heinemann, Oxford, 2005.
46 E. Bernardo, M. De Lazzari, P. Colombo, A. Saburit Llaudis, F. Javier Garcìa-Ten, Lightweight Porcelain Stoneware by Engineered CeO_2 Addition, Adv. Eng. Mat. 12 (2010) 65-70.
47 EU. patent application 13162767.1-1354 A porous glass ceramic composition and method for manufacturing the same
48 M.A. Binhussain, M. Marangoni, E. Bernardo, P. Colombo, Sintered and glazed glass ceramics from natural and waste raw materials, Ceram. Int. 40 (2014) 3543-3551.
49 EU. patent application 13162770.5-1354 A glaze composition, method for manufacturing the glaze composition and methods for glazing.

Chapter 2 – Basalt derived glass ceramics

2.1 Introduction

Basalt is a gray to black, fine-grained volcanic rock that forms large lava flows on oceanic islands and is also common at many continental sites. Chemically it is composed of major oxides: SiO_2, Al_2O_3, FeO, CaO, MgO, and to a lesser degree Fe_2O_3, Na_2O, K_2O, TiO_2, MnO, and P_2O_5, with many other trace ingredients. The two major minerals that are always present are monoclinic pyroxene and plagioclase feldspar, but magnetite, olivine, and glass are often present as well as other accessory minerals.

Many authors [1, 2] reported that basalts are easily melted at 1400°C or above and are readily cooled to a glass. Upon reheating and keeping the Fe_2O_3/FeO ratio sufficiently high (>0.5) fine-grained glass ceramics were formed. The major crystalline phase in these glass ceramics, and sometimes the only crystal specie is monoclinic pyroxene: a complex solid solution of $CaMgSi_2O_6$ (diopside), $CaFeSi_2O_6$ (hedenbergite), $MgSiO_3$, (enstatite), $FeSiO_3$, $NaFeSi_2O_6$ (acmite), $CaAl_2SiO_6$, $CaTiAl_2O_6$, and $MnSiO_3$. The authors [1] described that the role of iron oxide in the nucleation has been attributed to a clustering of Fe^{3+} in the glass that upon heating yields magnetite (Fe_3O_4) as the nucleating agent. Sometimes the magnetite persists and can be seen as nuclei within clinopyroxene crystals or clusters; in other cases it is resorbed by soda to produce acmite ($NaFeSi_2O_6$) and other species capable of solid solution in pyroxene.

Basalts exist as compact rocks, porous tuffs and scoria. The rocks are formed during slow cooling of lava, resulting in high crystallinity and hardness. Disintegration and milling of these rocks is energy intense and requires high maintenance, then re-melting of basalts is carried out in special shaft furnaces working with crushed rock pieces with size of 10–20 cm. On the contrary the vesicular structure of tuffs and scoria reduces the costs for milling, Karamanov et al. [3] obtained a ceramic tile with a bending strength of 100 MPa sintering a powdered basalt tuff at 1100°C. In the work was provided the proof of concept that the cost

for the production of sintered basalt should be significantly lower than one of the "traditional" petrurgical glass ceramics (refused rock industry) [1] and competitive to that of the traditional tiling ceramic materials (as porcelain stoneware or earthenware). Basaltic compositions or iron-rich silicates have been employed in the petrurgy, to produce building tiles, pipes and bends and glassy insulation fibers.[1]

In the present chapter the basalt scoria already introduced in Chapter 1 was investigate to find a new use as a starting material for the manufacturing of ceramic tiles or proppant.

2.1.1 Ceramic Proppants

Owing to the increasing cost of petroleum-based products and the decline of petroleum supplies, economical interest in oil shale resources is arising, as testified by the intensive research on novel mining techniques, e.g. high-volume, "slick-water hydraulic fracturing" also known as "fracking"[4]. An example of fracking is the extraction of shale gas accomplished by pumping high-pressure water with additives resulting in the formation of fissures in the rocks that favor the gas escape. However when the pumping of the fracturing fluid is interrupted, the fissures may close and decrease the conductive pathway to the wellbore. To avoid this inconvenience and to enhance the exploitation of the well, propping agents or proppants are employed. Proppants are selected on the basis of economic and practical considerations to optimize the flow conductivity and to minimize the losses in the fracture during production [5].

The proposed method for sintering proppants and the choice of the starting material aims to develop a cheap, acid/base resistant, strong and reliable material in alternative to the most common materials employed for the manufacture of proppants. The novel employment of basalt is the sintering of basalt powders to manufacture proppants without a melting step. The scoria could be considered as a glass naturally quenched in air that can be used to sinter glass ceramic.

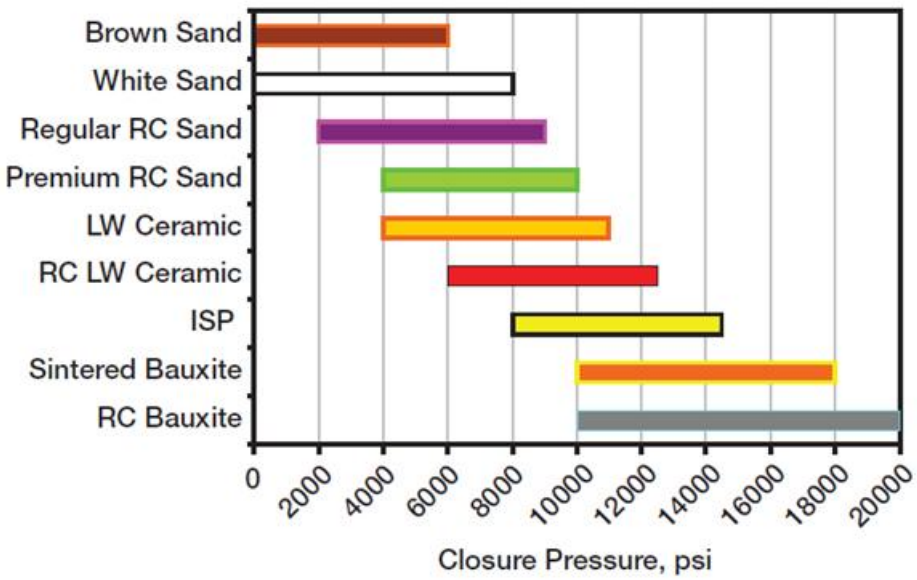

Fig. 13 – Proppant application range vs. closure stress (from Predict K, 2007)

A large variety of proppants are available, from natural occurring sand to the man-made ceramics or calcined bauxite. Sands are employed for applications requiring lower closure stresses[a] than those of more performing man-made ceramics as reported in **Fig. 13**.

The most important characteristics of proppants, tested according to the ISO 13503-2 standard are:

- *Roundness and sphericity* – the proppant should be almost smooth (without asperity) and spherical. The surface stresses are more uniform on well-rounded, spherical particles, in fact they are capable of carrying higher loadings than a less-rounded particle.
- *Density* – the proppants density influence the choice of the composition of the fracturing fluid. Relatively high-density proppants require high-viscosity fluids for the suspension and the transport in the fracture.
- *Resistance to acid attacks* – acid solubility evaluation is used to determine the suitability of a proppant for the use in acid environments.

[a] Closure pressure or closure stress is defined in the Schlumberger Oilfield Glossary as "an analysis parameter used in hydraulic fracture design to indicate the pressure at which the fracture effectively closes without proppant in place".

- *Proppant strength* – the determination of the highest stress level that proppants can bear is fundamental when a hydraulic fracture is created. The proppant strength is a significant parameter, in fact successively to the fracture formation the pressure of the fracturing liquid is decreased and the proppants have to withstand the stresses that tend to close the fracture.
- *Proppant crushed and fine particles generation* – the fragmentation of proppants after failure strongly affect the permeability of the pack. The crushed particles that are smaller than 100 mesh (149 μm) are generally considered to be fines.

2.1.2 Proppants Granulation

Over the past decades, increasing interest and progress were accomplished in understanding the fundamental processes that influence granulation. The three key stages for the process of wet granulation are:

1. Wetting and nucleation.
2. Consolidation and coalescence.
3. Attrition and breakage.

These three phenomena are competitive and occur simultaneously. After the collapse of a grain due to impact or friction new fragments are created and act as triggers for the growth of new particles. **Fig. 14** shows the comparison between the traditional model and the modern approach.

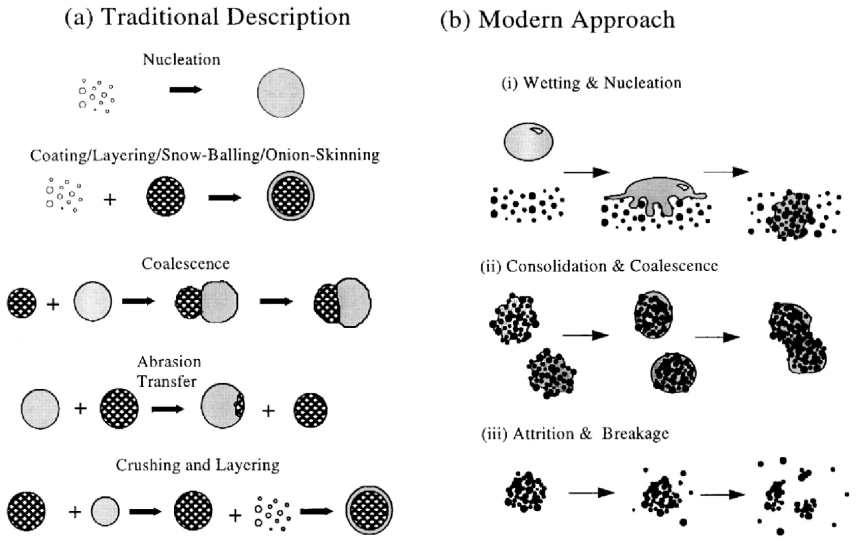

Fig. 14 – Traditional granulation (a) and modern approach (b).

The green proppants or green granules were prepared using the previously prepared mixtures (see above) and the equipment of **Fig. 15**.

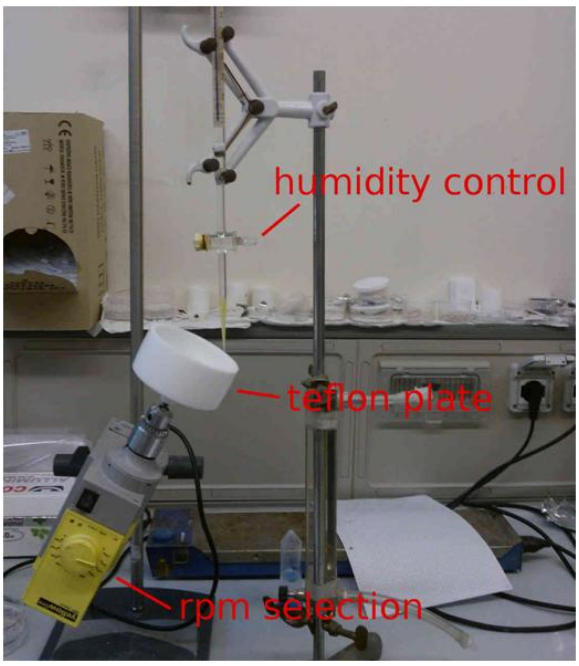

Fig. 15 – Experimental setup: at the bottom left of the image is a food mixer equipped with a selection of the angular velocity (rpm) and working angle, in the middle a teflon plate where the green granules are formed, at the top a burette for humidity control of the granules.

2.1.3 Basalt as Construction Material

Studying the realization of ceramic proppants, it was found that basalt was suitable to shape black and strong glass ceramics. For this reason it was decided to investigate the feasibility of using sintered basalt as a construction material. Sintered basalt forms glass ceramic tiles having water absorption and mechanical strength close to those of commercial glass ceramics. Considering the valuable chemical durability of natural basalt the same is expected for sintered basalt tiles, thus suggesting the possible realization of hardwearing tiles used for paving. In literature a large number of publications concerning basalt glass ceramics or fibers may be found, but only few refers to natural basalt sintered without previously melting the raw material. Therefore, we thought that it would have been very interesting to perform an innovative work concerning sintered basalt as novel construction material. Furthermore the information acquired on studying basalt as construction material may extend the understanding of the thermal

processes that could be used to improve the mechanical strength of basalt-based proppants.

2.2 Materials and Methods

2.2.1 Basalt Based Proppants Manufacturing

The granulator was tilted at a working angle of 45 deg and set at 160 rpm for 10 minutes. To produce the aggregates, the mixtures were placed in the drum of the granulator and moistened by adding 20 wt% of PVA solution (5 wt%) drop by drop. Very fast agglomeration was limited increasing the speed to 250 rpm, and a spatula was used to fragment the coarse granules. After 2 minutes the granulator was stopped and the granules were dried in air for 20 minutes. After water evaporation, the granules were sieved below 1 mm and over 1.32 mm, placed on a refractory previously covered with alumina powder and dried overnight at 80°C.

The burning out of the polymer was accomplished at 300°C for 30 minutes applying a heating rate of 10°C/min. The proppants sintering was performed at 1160°C for 15 minutes afterwards the samples were directly cooled at room temperature.

A pivotal role on the strength of basalts is played by the oxide state of iron hence we studied the effect of a slightly reducing atmosphere during the fast firing of the proppants. It was thus chosen to cover the refractory with alumina powder, then with graphite powder, then to place the green aggregates over the refractory and then to cover again the granules with graphite. The graphite mixed with the aggregates was confined in a circular area in the refractory and was covered with a kyanite crucible turned upside down. The refractory was then placed in the kiln at 1160°C in air for 20 minutes and finally directly cooled at room temperature. Considering the very quick heating the crucible limited the warming up of the specimen, thus we found that 5 minutes more were required to obtain aggregates with sphericity equivalent to the previous experiment. This technique created a small chamber where the thermal decomposition of graphite was confined and the proppants were not exposed to environmental oxygen. The

crucible turned up was placed also for safety reasons because graphite exposed at the environmental oxygen at 1160°C burns.

In the text the sintered basalt proppants are labeled with B whereas the sintered proppants in reducing atmosphere are labeled RB.

2.2.2 Basalt as Construction Material

The basalt scoria was ball-milled in an agate jar and sieved to obtain particles with a size below 90 μm. Successively, 4 samples were prepared by ball mixing 25 grams of basalt powder at 300 rpm for 30 minute in an agate jar with 1.7 g of polyvinyl alcohol (PVA) solution at 7 wt%. The mixture was pressed at 40 MPa in a 50x50 mm^2 mold and dried overnight. Preliminary studies showed that an optimal sintering interval for the basalt powder goes from 1150 to 1160°C and that the heating rate strongly influences the final shape of the sintered body. To study the effect of the thermal treatment it was decided to sinter 3 samples at 1160°C by applying respectively a 2, 5 and 10°C/min heating rate. A fourth sample was fired at 1150°C by applying a 5°C/min heating rate. The samples were fired at the selected temperature for 60 minutes and a preliminary 30-min step at 300°C to burn out the PVA.

The Young's module of the fired samples was determined using the resonant frequency in the flexural mode of vibration (GrindoSonic Mk5, Leuven, Belgium). The geometrical density was calculated measuring the dimension of the bar specimens using a caliper and the mass weight with a laboratory scale. In order to remove surface flaws, all samples were carefully polished to a 6 μm finish before testing, using abrasive papers and diamond paste. Four-point bending tests (30 mm outer span and 8 mm inner span) were performed using an Instron 1121 UTS instrument (Instron, Danvers, MA) on at least 8 specimens for each sample type with the cross-head speed of 1 mm/min until fracture. The edges of the bars were beveled using fine abrasive papers and diamond paste.

2.3 Results and discussion

2.3.1 Basalt Based Proppants

On the basis of the Krumbien-Sloss chart, **Fig. 16**, the sphericity and roundness of ceramic proppants were evaluated to be, respectively, around 0.9 and 0.9. High roundness reduces point loads in correspondence of the asperities of the surface roughness, and good sphericity improves the control of flow and the packing of proppants during fracturing.

As already described in **Tab. 3** (Chapter 1) the basalt scoria presented a crystallinity of 68% that slightly decrease to about 65% after heating at 1150°C for 60 min. Among the most significant mineralogical transformations occurring spinel and forsterite are oxidized and newly formed hematite and maghemite are observed. Differently from the previous investigation here the aggregates were exposed to high temperature for a shorter time thus we expect a lower oxidation (higher Fe^{2+}/Fe^{3+}). The mineralogical transformations and the limited amorphous phase determined strongly influenced the powders sintering. As previously mentioned in the introduction the obtainment of spheres is relevant to improve the packing of the proppants and then to prop more efficiently and from preliminary studies it was found that when exposed for more than 15 minutes at 1160°C the aggregates were excessively softening reducing the final sphericity.

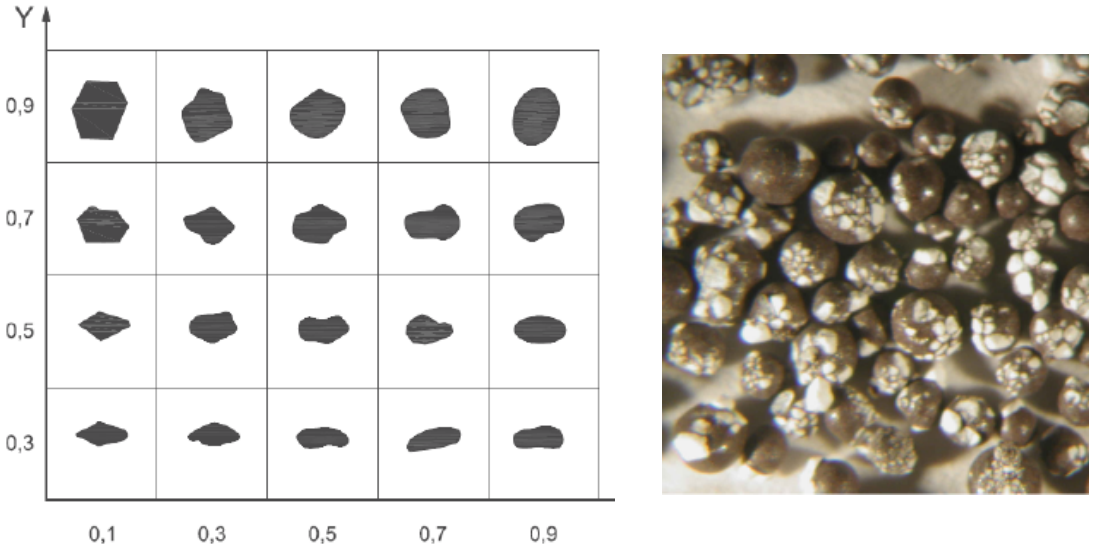

Fig. 16 – On the left, the Krumbien-Sloss chart of Roundness (X) Vs Sphericity (Y). On the right, stereo microscope images of basalt based proppants.

The strength values reported in **Tab 1** referred to proppants having a relatively large diameter range due to the complexities on the control of the granulation. The commercial LWC proppants Versprop® produced by Saint Gobain were used as benchmark to compare the mechanical strength of our proppants. According to the data sheet, Versaprop® have an average diameter of 0.74 mm. As an approximation the Weibull modulus of our materials were considered independent of the volume. Then the characteristic strength of the materials was transformed using the following relationship:

$$\frac{\sigma_1}{\sigma_2}=\left(\frac{V_2}{V_1}\right)^{1/m}$$

where σ_1 is the strength of a proppant of volume V_1, σ_2 is the strength of a proppant of volume V_2 and m is the Weibull modulus. According to the standard UNI EN ISO 13503-2-2010 a known mass of proppants is placed inside a cylindrical steel container (d = 50.8 mm), this is subjected to a compressive force. A determination of the highest stress level at which proppant generates no more than 10% crushed material, rounded down to the nearest 6.9 MPa (1000 psi), represents the maximum stress, σ_m, that the material can withstand without exceeding 10% crush. This constraint imposes a surviving probability for proppants of 90%.

Going into details, σ_m is the ratio between the maximum applied load, F_m, over the area of the cylinder, $A_{cylinder}$:

$$\sigma_m=\frac{F_m}{A_{cylinder}}$$

Considering that F_m is applied on a monolayer of N_p proppants, a single proppant bears only a small fraction of the maximum load. The maximum, F_{90}, that a single proppant having a surviving probability of 90% can withstand is derived from the Hiramatsu and Oka formula which gives:

$$F_m=N_p\cdot F_{90}=N_P\left(\frac{d^2}{0.9}\sigma_{90}\right)$$

The close-packing of proppants is far from being ideal due to their limited sphericity; then the numerical density, δ, of a monolayer was assumed to be about

0.64.[b] The number of proppants contained in the cylinder is function of the area of the cylinder, the numerical density and the area occupied by a single proppant, $A_{proppant}$:

$$N_p = \frac{A_{cylinder}\,\delta}{A_{proppant}} = \frac{A_{cylinder}\,\delta}{\frac{\pi}{4}d^2}$$

Substituting the previous, the final relationship between σ_m and σ_{90} is:

$$\sigma_m = \frac{F_m}{A_{cylinder}} = \frac{N_p \cdot F_{90}}{A_{cylinder}} = \frac{N_P\left(\frac{d^2}{0.9}\sigma_{90}\right)}{A_{cylinder}} = \frac{\frac{A_{cylinder}\,\delta}{\frac{\pi}{4}d^2}\left(\frac{d^2}{0.9}\sigma_{90}\right)}{A_{cylinder}} = \frac{4}{0.9\,\pi}\,\delta\,\sigma_{90} \approx 0.905\,\sigma_{90}$$

Finally, σ_{90} was derived from the Weibull statistic providing the results reported in **Tab. 8**. In spite of the limits on the production, which forced us to test proppants having dimensions much bigger than those commercially available, it was demonstrated that the materials produced in the current project are indeed not far from the proppants commercially available in terms of achievable strength.

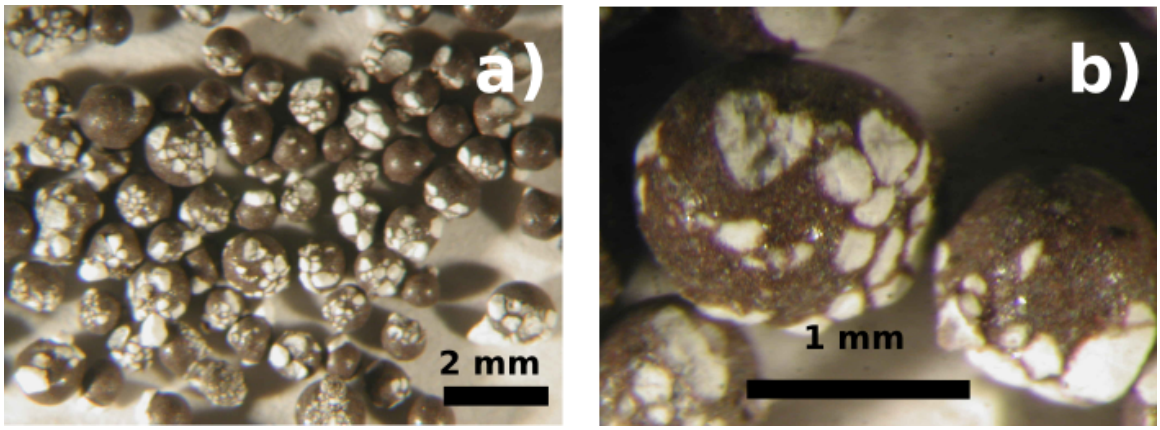

Fig. 17 – a) Basalt proppants at low magnification. b) Significant embedding of alumina powder at the surface of the basalt proppants.

[b]) In geometry, close-packing of equal spheres is a dense arrangement of congruent spheres in an infinite, regular arrangement. The highest average density that is, the greatest fraction of space occupied by spheres, that can be achieved by a regular lattice arrangement is ≈ 0.74048.

It should be noted, however, that the previous considerations about the theoretical strength of smaller size proppants contain some approximations that can strongly influence the correspondence between the theoretical and real data, but we believe that the results help us anyway to understand which characteristics influence more the properties of the final products.

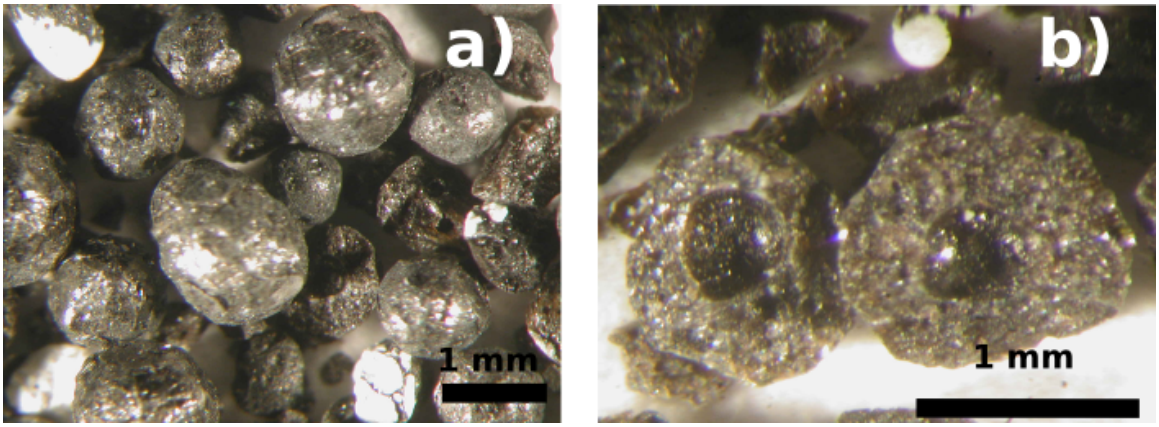

Fig. 18 – a) Low magnification micrographs of basal proppants fired in reducing b) No embedding of alumina powder at the, but significant bubbles formation.

In **Fig. 17** are reported the micrographs collected at the stereomicroscope of the basalt proppants; a significant embedding of alumina powder at the surface can be observed. These imperfections may affect the mechanical properties. In **Fig. 18** are reported the micrographs collected at the stereomicroscope of the basalt proppants fired in reducing atmosphere; in this case there is no embedding of alumina powder at the surface, but bubbles were formed in the bulk of the spheres.

An interesting functionality of the basalt proppant was linked to the presence of magnetite, which conferred a weak attraction to a permanent magnet. This functionality may be used for separating the proppants from other substances, e.g. in a continuous liquid/solid stream.

The compressive strength was measured compressing one by one 20 to 25 individual specimens per type of basalt proppants (B, and reduced basalt proppants RB respectively). In **Fig. 19** is reported the Weibull plot for both B and RB proppants and in **Tab. 8** the mechanical data. Obviously, the bubbles strongly decreased the mechanical strength of RB specimens. In spite of the alumina granules embedded at the surface of samples B, their specific strength, σ_0, was

considerably high. Moreover the σ_{90}, which correspond to the strength at which the survival probability was 90% (failure probability 10%), was 77.5 MPa for B proppants with an average diameter of 1.02 mm.

Using the same considerations previously described, we calculated the characteristic strength of proppants having an equivalent diameter of 0.74 mm, using Weibull statistics. The characteristic strength of proppants having an equivalent diameter of 0.74 mm calculated using the Weibull statistics gave a strength enhancement of about 20%, which resulted comparable to the commercial Versaprop® proppants. The results for the RB proppants were less promising, considering that the characteristic strength was quite low even for Ultra Light Weight (ULW) proppants.

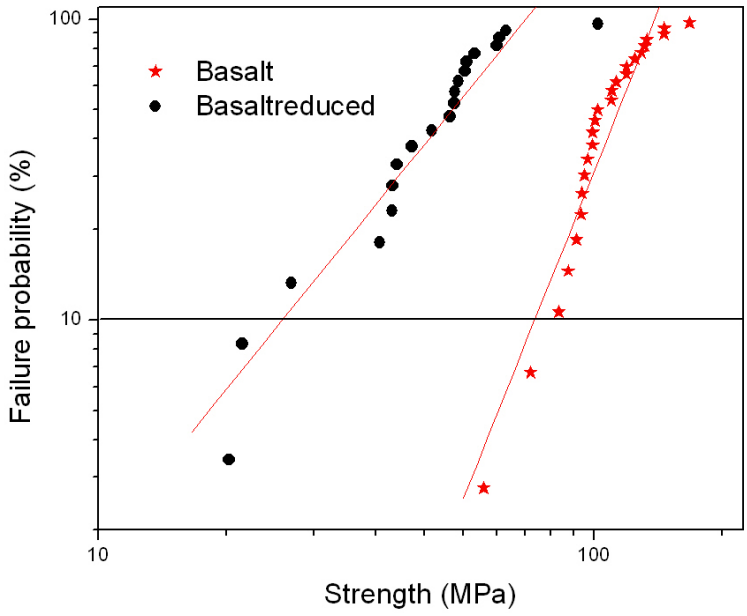

Fig. 19 – Weibull plot for both B and RB proppants; the straight line sets the failure probability of 10%, limit required for the definition for the crash classification according to the standard UNI EN ISO 13503-2-2010.

Tab. 8 – Weibull modulus, m, characteristic strength, σ_0, for proppants characteristic strength for a surviving probability of 90%, σ_{90}, maximum stress, σ_m, both in Mpa and psi and crash classification according to the standard UNI EN ISO 13503-2 2010.

Composition	T °C	m	σ_0 MPa	σ_{90} MPa	σ_m MPa	σ_m MPa	Crash classification
B	1160	5.62	115.7	77.5	70.2	10200	10K
B*	1160	5.62	137.5	92.1	83.4	12094	12K
RB	1160	2.63	65.5	27.9	25.2	3660	3K
RB*	1160	2.63	100.8	42.8	38.8	5620	5K

* calculated values using the Weibull statistics for proppants having d = 0.74 mm.

2.3.2 Basalt as Construction Material

As clearly shown in **Fig. 20**, the heating rate strongly modifies the final shape of the sintered tile. Specifically, a loss of the final shape is observed at the higher heating rates owing to an improved viscous flow sintering. The different shapes observed probably result from the evolution of the crystal phases during firing. Crystallization is promoted until 1050-1150°C and successively the silicate crystal phases together with the remaining glassy phase start to melt leading to viscous flow sintering. A low heating rate enhances the formation of crystal phases, consequently at the firing temperature the high viscosity due to the presence of the crystals limits the sintering by viscous flow. The sample heated at 1150°C with a heating rate of 5°C/min showed a much lower loss of shape than the sample fired at 1160°C at the same heating rate, and provided a result close to the sample fired at 1160°C with a heating rate of 2°C/min.

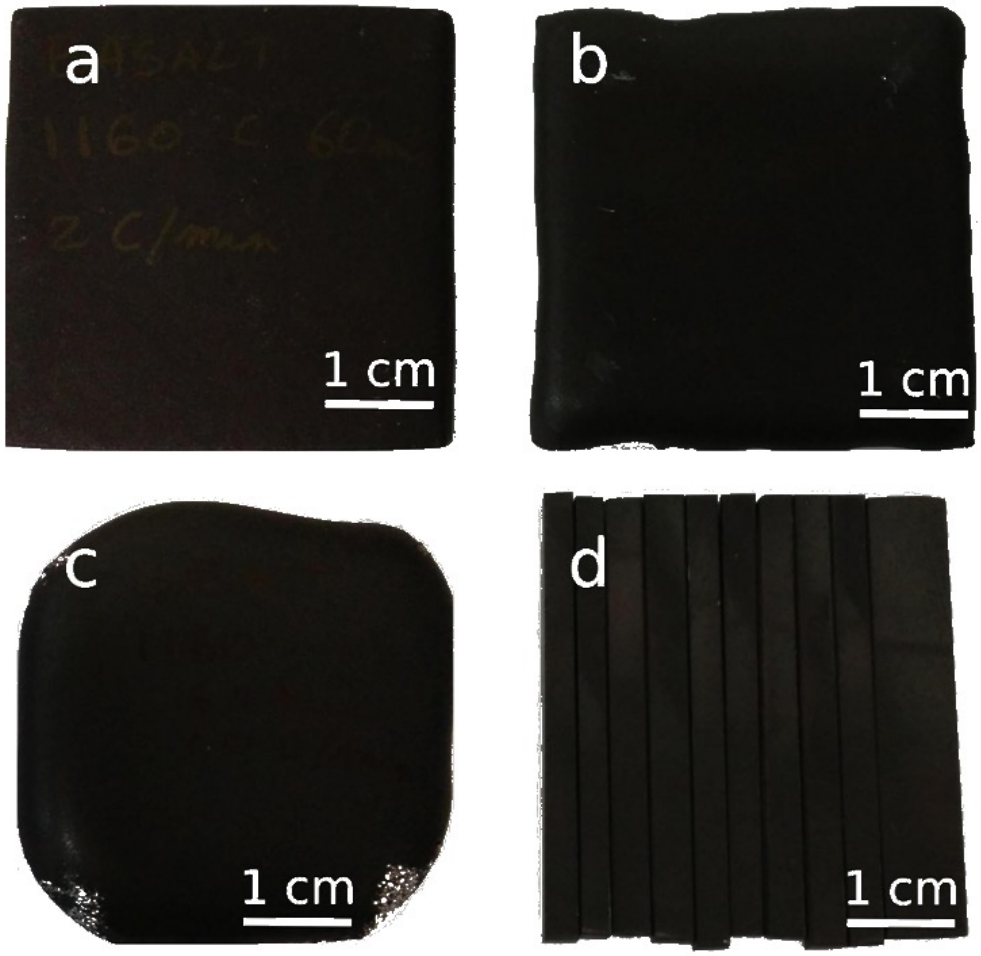

Fig. 20 – a) basalt glass ceramic fired at 1160°C for 60 minutes applying a 2°C/min heating rate. b) basalt glass ceramic fired at 1160°C for 60 minutes applying a 5°C/min heating rate. c) basalt glass ceramic fired at 1160°C for 60 minutes applying a 10°C/min heating rate. d) cut basalt glass ceramic fired at 1150°C for 60 minutes applying a 5°C/min heating rate.

The sintered basalt glass ceramics exhibited physical properties similar to that of commercial glass ceramics used for paving, which in turn possess largely better properties than traditional natural stones, as shown in **Tab. 9**. In particular, the basalt glass ceramics obtained in this work feature the same or higher flexural strength (>47 MPa) than the other reference materials.[6]

	E	ρ	σ	Wab
	GPa	g/cm³	MPa	Wt%
Basalt 1160°C 60 min 2°C/min	74 ± 6	2.72 ± 0.04	47 ± 4	0.48 ± 0.05
Basalt 1160°C 60 min 5°C/min	80 ± 5	2.68 ± 0.04	64 ± 16	0.94 ± 0.09
Basalt 1160°C 60 min 10°C/min	83 ± 7	2.69 ± 0.04	61 ± 6	0.31 ± 0.07
Basalt 1150°C 60 min 5°C/min	84 ± 4	2.73 ± 0.02	70 ± 9	0.29 ± 0.09
Neoparies glass ceramics*	51-86	2.70-2.72	41-50	
Cryston glass ceramics*	95	2.76	49	
Marble*	27-82	2.70	13.7-16.7	
Granite*	42-60	2.60	13.5-14.7	

Tab. 9 – Characterization data for sintered basalt glass ceramic samples for 60 minutes at different heating rate. * ref [6]

We should also stress the fact that the produced glass ceramics possess a very low water absorption, making them suitable candidates for high performance paving material.

2.4 Conclusions

2.4.1 Basalt as Propping Agent

From the present investigation we found that the granulation is a critical step that requires a specific equipment to avoid defects during production. However the manufacture of spherical glass ceramics proppants instead of ceramics because the viscous flow at 1160°C allowed for an almost perfect spheroidization. Although basalt proppants, fired only for 15 minutes at 1160°C, gave specific strengths that are probably close or even higher than the commercial Versaprop® proppants to compare their properties it would be important to test the commercial proppants using the same procedure. A possible improvement of the mechanical strength can be achieved avoiding the use of alumina powder as a substrate and using the same technology currently used for proppants manufacturing, i.e. substituting the kiln furnace with a rotary kiln.

Another process that could be investigated is an intermediate procedure between B and RB firing. Placing B granules on a refractory substrate previously covered with graphite and alumina may give a lower embedding of alumina into a proppant's surface.

2.4.2 Basalt as Construction Material

From an industrial point of view, it may be interesting to reduce the sintering time by applying a faster heating rate at a lower temperature to observe if the resulting sample holds the shape uniformly. A further issue, which might be explored is the realization of a functional tile performing magnetic properties, due to the presence of iron oxide in the glass ceramics, by firing the sample in a reducing atmosphere.

As previously discussed basalt embeds effectively the alumina powder bed placed between the refractory and the sample. To avoid such inconvenience it was found that dolomite and limestone might be a cheaper alternative to alumina powder. Limestone probably formed a calcium silicate or calcium aluminosilicate layer that prevents the sample to stick. However even if limestone was the most effective alternative to alumina, it must be considered that calcined calcite produces lime that is caustic when hydrated.

A further experiment could be performed by fast firing a mixture of basalt and alumina platelets to investigate if such combination enhances the fracture toughness of the basalt glass ceramic. Alumina platelets are relatively economic and largely used in the abrasive industry

Bibliography

1 G. H. Beal, H. L. Rittler. 'Basalt Glass Ceramic', American Ceramic Society Bulletin (1976) 55 [6] , 579-582.

2 A. Karamanov, S. Ergul, M. Akyildiz, M. Pelino. 'Sinter-crystallization of a glass obtained from basaltic tuffs', Journal of Non-Crystalline Solids 354 (2008) 290–295.

3 A. Karamanov, L. Arrizza, S. Ergul. 'Sintered material from alkaline basaltic tuffs' Journal of the European Ceramic Society 29 (2009) 595–601.

4 R.W. Howarth, and A. Ingraffea & T. Engelder, Natural gas: Should fracking stop?, *Nature*, 477 (7364) (2011) 271–273.

5 M.J. Economides, T. Martin, Energy Tribune Publishing Inc., Modern Fracturing Enhancing Natural Gas Production, 2008.

6 E. Bernardo et al., Journal of Non-Crystalline Solids 352 (2006) 4017–4023.

Chapter 3 – Double Layer Glass Ceramics From Waste Materials

3.1 Introduction

3.1.1 Vitrification – Pros and Cons

Vitrification has proved to be the safest technology for the treatment and remediation of non-combustible hazardous waste, among the various disposal technologies [1]. The process implies the thermal destruction of waste and, when properly formulated, the resulting glass features a high chemical inertness, so that it can be landfilled without any particular concerns. Despite the soundness of vitrification technology, confirmed by numerous scientific studies and experimental tests [2], this approach has found difficulties in establishing itself, being particularly cost and capital intensive. In the case of inorganic waste for which, differently from radioactive waste, environmental safety is not an absolute priority over cost, a vitrification treatment may be justifiable only if the obtained glass could be reused in high value applications. The most significant application of waste-derived glasses is undoubtedly represented by glass ceramics, starting from the well-known Russian "Slag Sitals" (developed nearly 50 years ago), based on the vitrification of metallurgical slags. Slag Sitals may be considered a sort of prototype for glass ceramics derived from glasses belonging to the CaO-Al_2O_3-SiO_2 (CAS) system [3], since they combine good mechanical properties (bending strength, abrasion resistance) and chemical stability, suitable for their main application in the construction industry for buildings façades.

The production of high value glass ceramics is associated to additional costs in the overall treatment of inorganic waste: as an example, Slag Sitals imply the rolling of waste-derived glass into sheets, following the melting procedure, and a secondary ceramization treatment. Recent investigations have been applied to waste-derived CAS glasses in order to reduce the transformation costs. In particular, sintering of glass powders, leading to "sinter-crystallized" glass ceramics, is

receiving a growing interest [4]. Glass powders may be easily obtained by the grinding of glass fragments possessing high internal stresses, such as those produced by pouring a glass melt in water to produce a frit. With this approach, energy savings are associated to both the vitrification and ceramization steps, since waste glasses may be poured just after homogenization, i.e. avoiding the expensive refining step, and crystallization may occur very rapidly (in 1h or less, at an adequate sintering temperature), on the basis of surface nucleation, even for glasses with a very low amount of oxides that could act as nucleating agents (i.e. oxides with a poor solubility in glass, such as TiO_2, ZrO_2 etc.). [5]

The direct sintering of mixtures of inorganic waste including recycled glasses, acting as fluxing agents, is an important alternative. The products cannot be nominally considered as glass ceramics, since there is no vitrification, i.e. a stage in which the starting raw materials are mixed and converted into a glass, is involved. However, a rich literature supports the classification of such products as "sintered glass ceramics", owing to the generally observed phase evolution [6-7]. In fact, the recycled glass component, besides promoting the densification by viscous flow sintering, reacts with the waste, leading to silicate and aluminosilicate crystals similar to those developed by devitrification of waste glasses. The process, evidently resembling that of traditional ceramics, offers remarkable energy savings, due to the absence of a high temperature (>1350-1400°C) melting stage and its simplicity. The impact on the chemical stabilization of waste is quite controversial: on one hand, if treatments at moderate temperatures prevents some pollutants from decomposition and escape as gasses (as an example, fluorine gas from F-containing waste [8]), on the other one the chemical homogeneity of a sintered body is much lower than that of a glass obtained from melting (pollutants may selectively accumulate in regions not completely dissolved in the liquid phase provided by the flux).

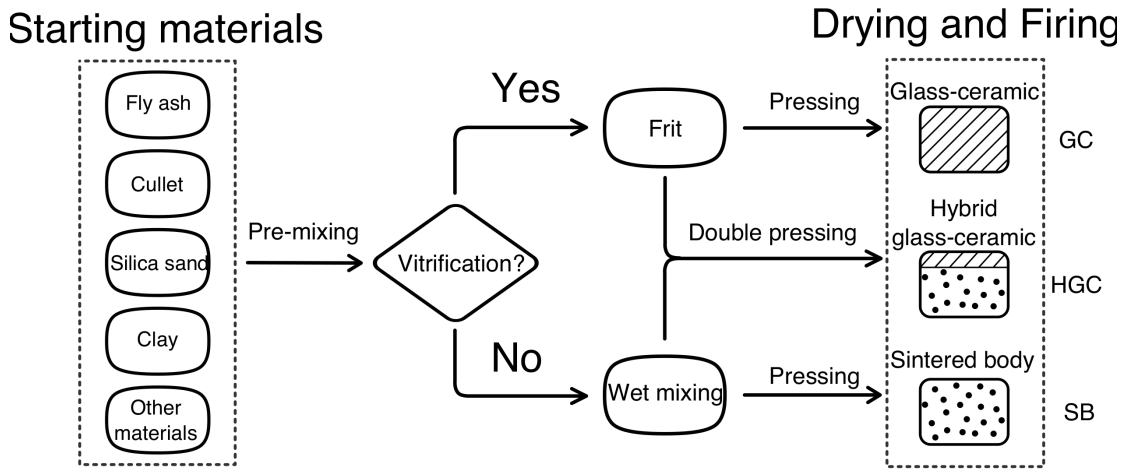

Fig. 21 – Schematic representation of three routes for the production of ceramic materials employing selected natural and waste raw materials.

3.1.2 Limiting the Vitrification

As illustrated by **Fig. 21**, the present chapter aims at combining direct sintering of waste mixtures and sintering of waste-derived glasses, with the development of layered *hybrid glass ceramics* (HGC). The good mechanical properties and the homogeneous microstructure of sinter-crystallized glass ceramics (GC) are exploited in a glaze, white or colored, deposited on a porous base body obtained from direct sintering (SB). The production process described hereafter has the aim of combining direct sintering of waste mixtures and sintering of waste-derived glasses, with the creation of layered HGC (see **Fig. 21**). Vitrification of waste is sustainable, since it is applied only to a limited amount of the starting materials; the single firing reduces the costs associated to the deposition of a glaze. Owing to the negligible water absorption (at the glazed side) and the limited density, the developed layered glass ceramics could be a valid alternative to the lightweight tiles currently developed for building façades.

3.2 Materials and Methods

3.2.1 Starting Materials

The starting waste raw materials for the production of the sintered body and the glass ceramics in this study were a basalt waste and fly ash residues from a cement plant in the Riyadh region of Saudi Arabia, soda lime cullet (the fraction of recycled material that is difficult to reuse in conventional glass production owing to its impurities), and panel glass from dismantled cathode ray tubes (CRTs). The other starting natural raw materials were ball clay, limestone, and silica sand from the Riyadh region. **Tab. 10** reports the data for X-ray fluorescence analysis (Philips XRF Sequential Spectrometer PW2400, Eindhoven, The Netherlands) of the starting raw materials and the percentages of raw materials employed for the preparation of the samples.

Tab. 10 – Chemical composition of the starting raw materials and formulation of the investigated glass ceramics.

Oxide	Silica sand	Limestone	Clay	Fly ash 1	Fly ash 2	Basalt	Cullet	CRT panel glass	SB/GC1	GC2
Chemical composition (wt%)										
SiO_2	98.6	2.3	41.6	14.2	12.8	47.4	71.9	57.3	55.7	60.3
Al_2O_3	0.6	0.9	39.1	4.8	4.5	15.9	0.7	3.8	12.8	11.3
P_2O_5			0.1			0.5				0.1
Na_2O	0.1		0.1	0.1	1.2	3.4	13.3	12.8	2.6	2.2
K_2O		0.1	0.1	0.5	14.5	1.0	0.1	7.2	4.1	0.4
MgO		0.6	0.2	0.7	0.6	9.6	3.3		0.8	2.6
CaO		52.7	0.5	58.3	50.4	7.7	10.1		22.0	18.6
BaO								7.9		
SrO								8.4		
Cr_2O_3						0.1				
Fe_2O_3		0.3	1.3	2.8	2.2	11.4	0.1	0.2	1.0	3.4
TiO_2	0.4		2.9	0.3	0.2	1.9		0.4	1.0	1.1
MnO_2						0.2				
ZnO								0.6		
ZrO_2								1.4		
L.O.I.	0.3	43.1	14.1	18.3	13.6	0.9	0.5			
Formulation (wt%)										
SB/GC1	25	10	25		25		15			
GC2	30		15	25		20	10			

3.2.2 Samples Preparation

Sintered body (SB) – The raw materials of composition SB were firstly independently ground into a fine powder using a ball mill, and then sieved below 90 μm. About 300 grams in total of the ground raw materials were mixed thoroughly in a food mixer, adding 30 wt% of water. After mixing, the homogeneous mixture was dried in an oven at 80°C for 24 h and then ground again, keeping only the powder with a diameter below 90 μm. Sintering experiments were performed on samples SB prepared by pressing 15 grams of the dry powder mixture in a rectangular die (cross-section of 50 mm ×34 mm) at a pressure of 30 MPa. The samples were further dried at 120°C for 30 minutes and then fired at 1000, 1100, 1150 and 1250°C for 60 minutes with a heating rate of 10°C/min.

Glass ceramic frits (GC) – Glasses from mixtures GC1 and GC2 were obtained by melting at 1300°C for 2 h and poured in cold water. The frits were then collected, dried at 80°C and then ball milled in an agate jar and sieved to obtain particles with a size below 90 μm.

Dilatometric and differential thermal analysis (DSC 404, Netzsch Gerätebau GmbH, Selb, Germany, 10°C/min heating rate) were performed on both fine powders (< 90 μm) and coarse powders (> 90 μm) of glass GC1 in order to infer the conditions for optimum processing. Preliminary sintering experiments were performed on disks (30 mm diameter) obtained uniaxially pressing at 40 MPa 2 grams of powder. The discs were fired directly at 900, 950, 1000°C temperatures for 30 and 60 minutes. After selection of the preferred firing temperature, two samples were obtained by uniaxially pressing 15 grams of the dry powder GC1 in a rectangular die (cross-section of 50 mm × 34 mm) at a pressure of 30 MPa without adding binders. The samples were fired at 950°C for 30 minutes with a heating rate of 40°C/min.

Hybrid glass ceramic (HGC) – A hybrid glass ceramics (HGC) was obtained firstly by lightly pressing (at 10 MPa) 15 grams of the dry powder mixture SB in a rectangular die (cross-section of 50 mm × 34 mm) and subsequently, on this substrate, 3 grams of a glass frit were deposited (0.176 g/cm^2). Then, the layered sample was uniaxially pressed at 30 MPa. We found, in fact, that pressing firstly the substrate at 30 MPa, followed by the deposition of the frit and second pressing at 30 MPa, led to a limited adhesion between the frit and the substrate, prob-

ably because of limited interpenetration between the glaze and the substrate during pressing.

The glass frit for HGC was produced by mixing GC1 frit with some additives in order to obtain a white color and to find the perfect match in terms of physical properties (e.g. coefficient of thermal expansion) between this top layer and the substrate. The GC1 frit (40 wt%) was mixed with a whitening agent ($ZrSiO_4$, 0.8 μm mean particle size, Industrie Bitossi SpA, Vinci, Italy, 20 wt%) and a flux (CRT panel glass, 40 wt%). The GC2 frit with no additive was employed, as an alternative, for the firing of a HGC sample of green color. The HGC samples were fired at 1150°C for 60 minutes, with a heating rate of 10°C/min.

3.2.3 Characterization Techniques

The Young's modulus of glass ceramic samples was determined using the resonant frequency in the flexural mode of vibration (GrindoSonic Mk5, Leuven, Belgium). Four point bending tests (30 mm outer span, 8 mm inner span) were performed using an Instron 1121 UTS (Instron, Danvers, MA) on at least 15 specimens with dimensions of 3.8 mm × 2.7 mm × 46 mm size. In order to remove surface flaws, all samples were carefully polished to a 6-μm finish before testing, by using abrasive papers and diamond paste. The edges of the bars were baveled by using fine abrasive papers and diamond paste. The cross-head speed was 1 mm/min speed until fracture. The HGC samples were tested by positioning the SB layer on the compression (upper) side and the GC layer on the tensile (lower) side.

The morphological features of sintered samples were characterized by Scanning Electron Microscopy (SEM-ESEM Quanta 200, FEI Company, Eindhoven, The Netherlands). The crystalline phase assemblage was investigated on powdered samples by X-ray diffraction (Bruker D8 Advance, Karlsruhe, Germany), employing CuKα radiation (0.15418 nm) and collecting data in the range 2θ=10–60° (0.05° steps, 3 s counting time). The identification was performed by means of a semi-automatic software package (Match!, Crystal Impact GbR, Bonn, Germany), supported by data from PDF-2 database (ICDD-International Centre for Diffraction Data, Newtown Square, PA).

3.3 Results and Discussion

3.3.1 Sintering of Waste-derived Glass and Direct Sintering of Waste

As reported above, **Fig. 21** illustrates the three different routes followed for the production of the various samples using the selected raw materials. The first route refers to the formation of a dense glass ceramic body by sinter-crystallization of a waste-derived glass frit. The second one consists of the direct firing of an uniaxially pressed green-body, and the third one corresponds to the production of a hybrid glass ceramic glazed body based on the two previous mixtures. In this case, the glass ceramic frit was employed as a glaze to provide a dense, aesthetically pleasing layer on the surface of the brown-colored fired body derived from natural and waste raw materials.

As shown in **Fig. 22**, the composition selected for samples SB/GC1 is quite similar to that of the previously cited Slag Sitals. In our samples, the content of iron oxide was much decreased, in order to achieve a light coloration; the content of TiO_2, that could act as nucleating agent, was also very low, considering that the glass from the same composition (GC1 frit) was expected to crystallize by surface nucleation.

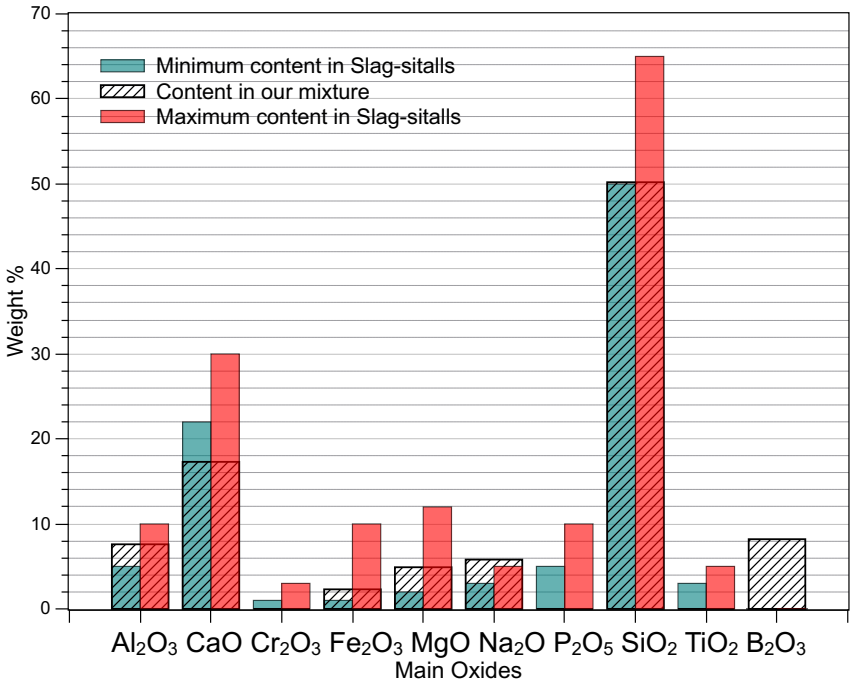

Fig. 22 – Comparison between the investigated glass composition and Slag Sitalls

Thermal Analysis – The DTA analysis for the GC1 frit (see **Fig. 23**) clearly shows that the investigated glass is prone to surface crystallization; in fact, the main crystallization exothermic peak is more intense for fine powders (< 90 μm) than for coarser ones and, more importantly, the crystallization temperature is also lowered for fine powders at about 1000°C. A secondary crystallization peak, located at ~900°C for the coarse powder, is also shifted to a lower temperature with decreasing particle size.

Both the DTA and dilatometric plots enable to establish the glass transition temperature (T_G), at about 700°C. The remarkable difference between the glass transition and the crystallization temperature (~300°C) is useful for promoting the sinter-crystallization process, i.e. the possibility to successfully densify glass powders via viscous flow and simultaneously achieve a high crystallization degree. The sintering temperature was selected at 1000°C, to enhance crystallization, and this temperature was high enough also for achieving a remarkable densification, since viscous flow starts above T_G; more precisely, viscous flow sintering is generally optimized 50-100°C above the dilatometric softening point [9]. In our case the dilatometric softening occurs at ~770°C (see **Fig. 23**), that is far below 1000°C.

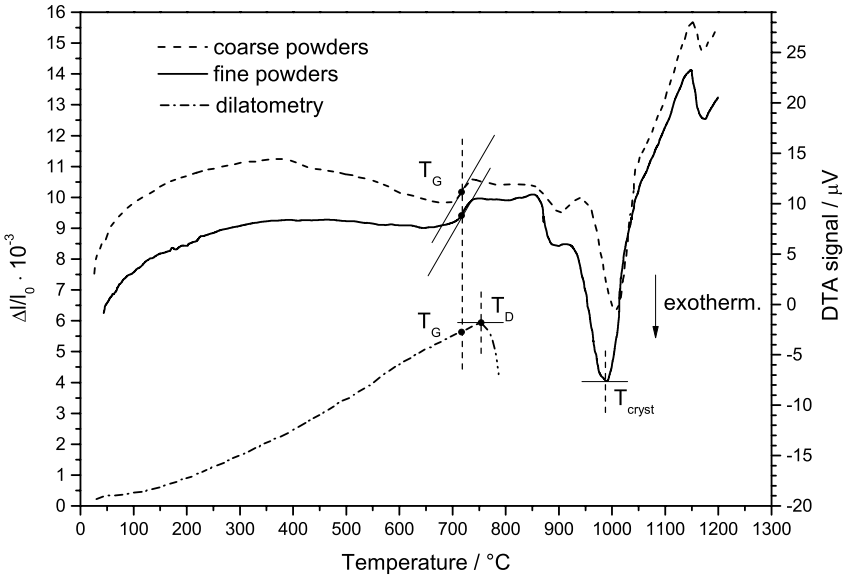

Fig. 23 – DTA and dilatometric plots for GC1 glass

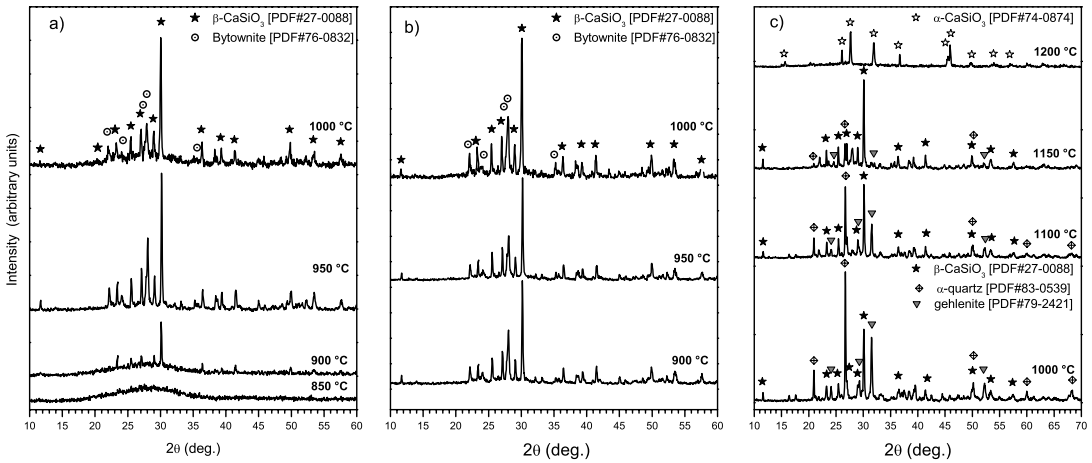

Fig. 24 – X-ray diffraction patterns of GC1 and SB samples: a) GC1 glass, sintering for 30 min; b) GC1 glass, sintering for 60 min; c) SB, sintering for 60 min (heating rate: 10°C/min)

Mineralogical Composition – The effectiveness of surface nucleation, for GC1 frit, is confirmed by **Fig. 24a** and **Fig. 24b**, which show that crystals started developing already after 30 minutes at 900°C, and after 1h at 1000°C little evidence remained of the presence of a residual amorphous phase. The first crystalline phase to appear, after the heat treatment at 900°C, was wollastonite (β-$CaSiO_3$, PDF#27-0088), followed by the crystallization of and Ca-Na feldspar (sodium exchanged anorthite or bytownite, $Ca_{0.85}Na_{0.14}Al_{1.83}Si_{2.16}O_8$, PDF#76-0832). Both phases are typical of waste-derived CAS glass ceramics [3]. Anorthite crystallization was actually optimized at 950°C, if we consider that its peak is well visible for a holding time of 30 min (see **Fig. 24a**); for a longer treatment (60 min) the precipitation of this phase was well recognizable even at 900 and 1000°C (see **Fig. 24b**).

Tab. 11 – Summary of density and shrinkage values for sintered samples [n.d. = not determined; *: samples with no regular shape; **: samples were glued to the refractory substrate after firing]

Type	Sintering T (°C)	Time (min)	Density (g/cm^3)	Linear Shrinkage (%)
GC1	900	30	2.63 ± 0.02	21
	900	60	2.65 ± 0.02	21
	950	30	2.65 ± 0.02	25
	950	60	2.66 ± 0.02	25
	1000	30	2.65 ± 0.02	n.d. *
	1000	60	2.68 ± 0.02	n.d. *
SB	1000	60	1.94 ± 0.04	2
	1100	60	1.87 ± 0.04	3
	1150	60	1.83 ± 0.04	7
	1200	60	n.d. **	n.d. **

As reported by **Tab. 11**, the difference in density and shrinkage was not particularly significant in samples sintered in different conditions; however, we observed that the samples heat treated at 1000°C displayed an even excessive viscous flow, resulting in the loss of the original disc shape. Considering the optimized crystallization of both wollastonite and anorthite and the retention of shape, we chose 950°C as the reference temperature for the manufacturing of larger samples. Rectangular tile samples (cross-section of 50 mm × 34 mm) of composition GC1 were fired at 950°C for 30 minutes, applying a heating rate of 40°C/min, which are conditions suitable for an industrial process.

The mechanical properties of bars cut from the tiles, as reported in **Tab. 11**, were of the same order of magnitude of those of similar CAS waste-glass sinter-crystallized glass ceramics, and compare favorably with the data typical for traditional ceramics [10]. In particular, the good strength is associated with a negligible water absorption, in turn due to the smooth and compact surface, as shown by **Fig. 25a**. It should be noted that a similar smooth and impermeable surface is achieved in conventional stoneware ceramics only if sintered much above 1000°C [11]. The compact surface is accompanied by a homogeneous distribution of micro-crystals, as shown by **Fig. 25b** (polished surface). The total residual porosity, evaluated by gas pycnometry, is of the order of 5 vol%.

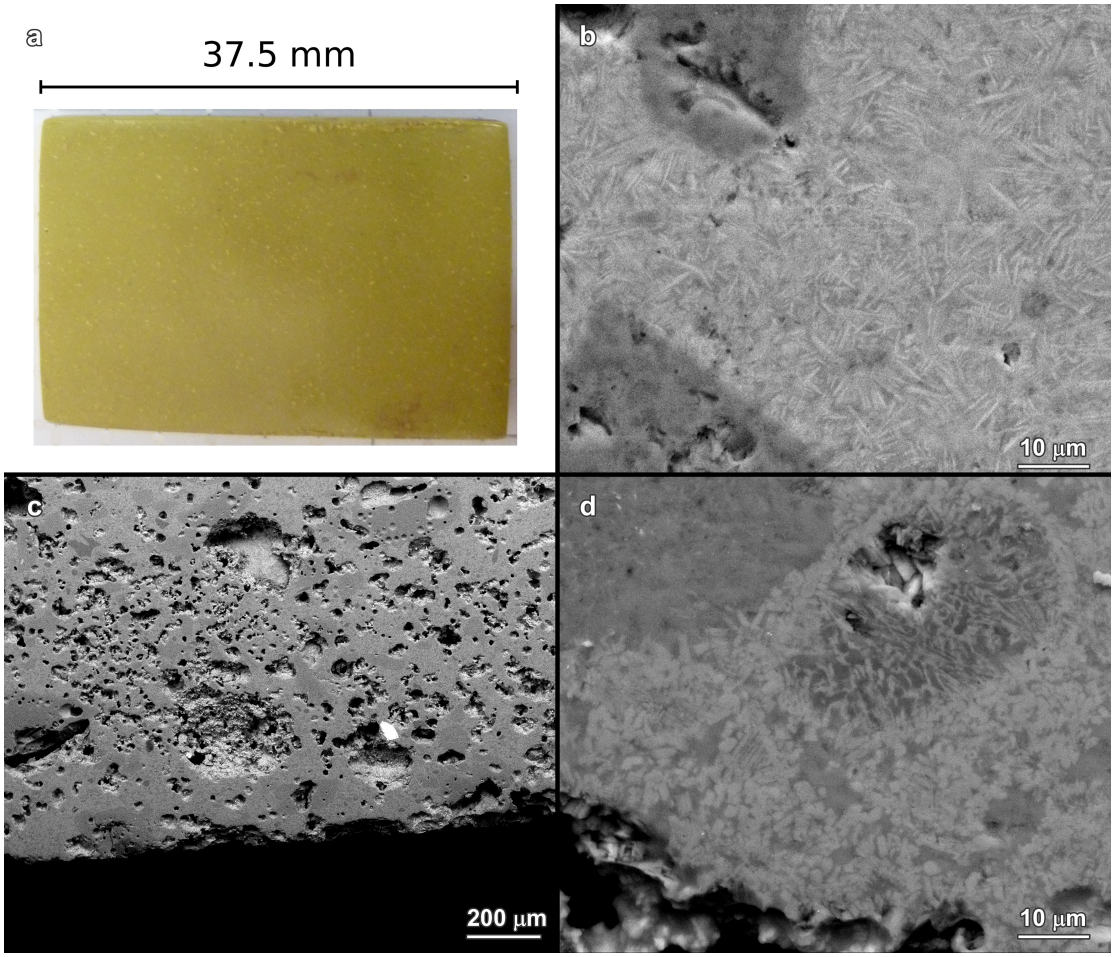

Fig. 25 – Microstructural details of sintered materials from GC1 mixture: a,b) sintered glass ceramic (GC1); c,d) ceramic from direct sintering.

The phase evolution of SB samples heat treated at different temperatures is shown in **Fig. 24c**. At 1000°C, the sintering had just started to occur (see the limited shrinkage value in **Tab. 11** and the interactions between the constituents are evident. Intense quartz peaks, associated with the use of silica sand, were accompanied by peaks related to a calcium silicate, i.e. wollastonite (β-$CaO{\cdot}SiO_2$, PDF# 27-0088), and a calcium alumino-silicate, i.e. gehlenite ($2CaO{\cdot}Al_2O_3{\cdot}SiO_2$, PDF#79-2421), another typical phase in waste-derived CAS glass ceramics [3].

The phase assemblage changed with increasing sintering temperature, due to the progressive dissolution and reaction of some components. At 1150°C, the peaks associated to gehlenite practically disappeared, whereas those related to quartz much decreased. The liquid phase promoted by the softening of the soda-lime glass gradually incorporated silica from sand, and partially crystallized into a specie with a relatively high silica content (while alumina-rich gehlenite disap-

peared, wollastonite exhibited a slight increase of intensity of the associated peaks). The significant softening of the glass component was also testified by an enhanced shrinkage (7%). For the highest sintering temperature, 1200°C, the only phase detected was pseudo-wollastonite (α-$CaO{\cdot}SiO_2$, PDF#74-0874, a high temperature variant of calcium silicate), indicating that the other crystalline species dissolved in the residual glass. In other words, the assemblage of crystal phases resembled that of conventional glass ceramics (only "newly-formed" crystals) even without preliminary vitrification of components. However, the loss of shape at this temperature (the sample actually remained glued to the refractory substrate upon firing) forced us to consider treatments below 1200°C.

The mechanical properties of SB sample sintered at 1150°C were quite lower than those of GC1 glass ceramic and are justified, above all, by the presence of a significant amount of residual porosity, of the order of 35 vol%. Part of porosity is open, as testified by the remarkable water absorption of 8% and illustrated by **Fig. 25c**. **Fig. 25d** confirms the substantial microstructural similarity of directly sintered bodies with conventional glass ceramics.

3.3.2 Layered Hybrid Glass Ceramics

The main aim of the fabrication of hybrid glass ceramics was the preparation of a low-cost waste-derived tile, from direct sintering, with a limited water absorption (at least at the surface exposed to the environment, when the tile is mounted), provided by a glass ceramic top layer, preferably of white color. Since glazes from pure GC1 glass featured an unpleasant yellow color, despite the limited content of Fe_2O_3, zircon ($ZrSiO_4$) was used as whitening agent, in form of micropowders mixed with the glass frit, as common for commercial glass ceramic glazes [12]. While GC1 glass, after firing at the same temperature (1150°C) used for the substrate, had a very similar coefficient of thermal expansion (7.6 $10^{-6}°C^{-1}$ for the coating compared to 7.7 $10^{-6}°C^{-1}$ for the substrate), there was a significant mismatch with zircon (4.9 10^{-6}°C-1 [13]); in order to compensate this, panel glass was considered as a further additive (9.9 10^{-6}°C-1 [14]). Moreover, being itself a waste, panel glass was consistent with the overall approach of obtaining low-cost waste-derived materials.

Predicting the coefficient of thermal expansion of a composite material is not straightforward [15], but a GC1 frit/panel glass/zircon weight balance of 40/40/20, was found to be the most appropriate choice (expected coefficient of thermal expansion close to 8 $10^{-6}°C^{-1}$). Samples fired at 1150°C, with a base body coated with a GC1/panel glass/zircon composite frit (GC1/panel glass/zircon=40/40/20, by weight) were effectively crack-free and possessed a continuous, dense and brilliant white layer on the top surface, as testified by **Fig. 26a**. While the water absorption became negligible, the mechanical properties did not practically change, compared to the uncoated sintered body (see **Tab. 12**). This was reasonably due to the fact that also the glaze, although perfectly interprenetrated with the base body, contained some bubbles, as shown by **Fig. 26c**. The development of the pores could be favored by the presence of the panel glass, a highly oxidized glass known to release dissolved oxygen upon sintering [14]. The limited mechanical properties could be justified also by the almost complete absence of crystalline phases, as illustrated by **Fig. 26e** and **Fig. 27**; besides un-dissolved zircon ($ZrSiO_4$, PDF#72-0402), only weak traces of wollastonite were visible.

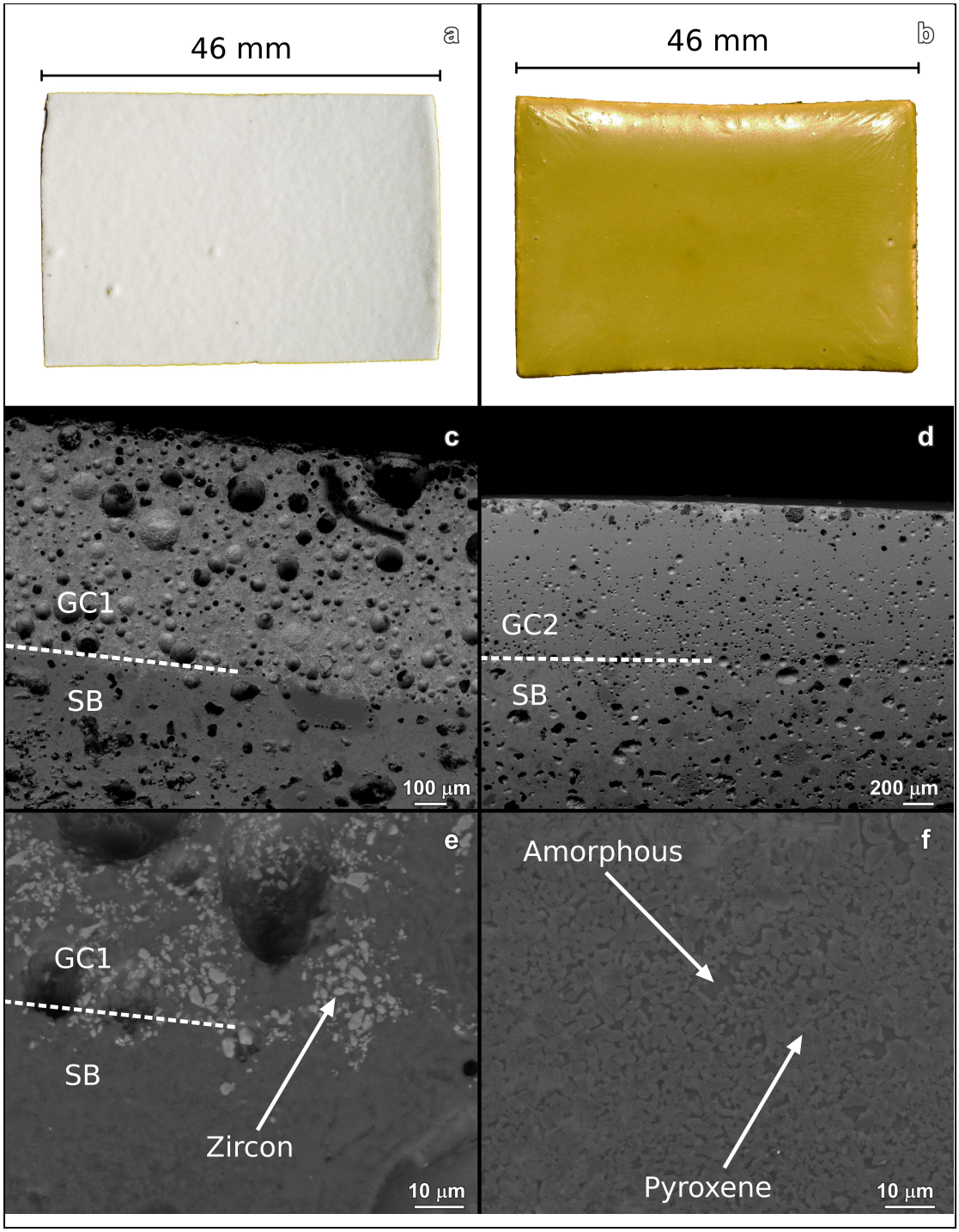

Fig. 26 – Microstructural details of layered hybrid glass ceramics: a) sintered glass ceramicHGC1; b) sintered glass ceramic HGC2; c) interface between the GC1 and SB layers; d) interface between the GC2 and SB layers; e) magnification of the interface between the GC1 and the SB layers; f) pyroxene crystals embedded in a glass matrix at the surface of the layer GC2.

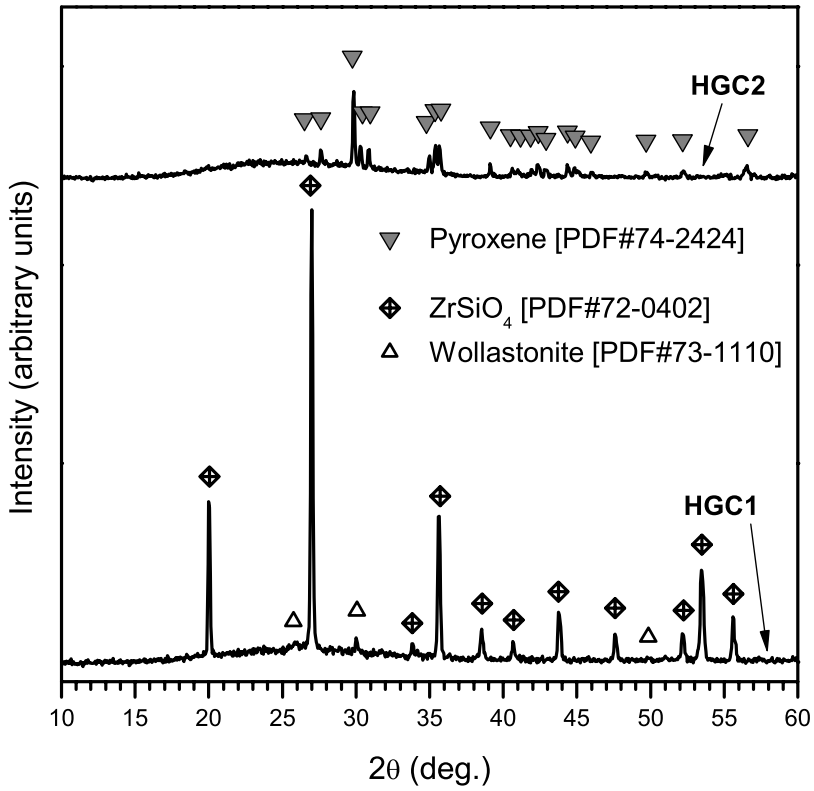

Fig. 27 – X-ray diffraction patterns of glaze materials

GC2 glass was prepared from a selected mixture of waste, in the compositional range of Slag Sitals (as for GC1), but without the constraint of having a low amount of Fe_2O_3. This choice led to a brilliant olive green color, when applied as glaze, without additives, as visible in **Fig. 26b**. As demonstrated by the same **Fig. 26f** and **Fig. 27**, GC2 actually also led to a crystallized layer, with a pyroxene (ferrous diopside, $(Ca_{0.92}Fe_{0.08})(Al_{0.14}Fe_{0.33}Mg_{0.53})Si_2O_6$, PDF#74-2424) as the main crystal phase. This specific phase is obviously consistent with the enhanced iron content in the glass ceramic formulation. The partial crystallization, the absence of bubbles and the close matching of coefficient of thermal expansion (7.2 10^{-6}°C-1) had a positive effect on the mechanical properties of the component.

Tab. 12 – Physical and Mechanical characterization data for the different samples

Samples	Sintering temperature	Residual porosity	Water absorption	Density ρ	Elastic modulus, E	4-pt bending strength, σ	$\sigma^{1/2}/\rho$
	°C	%	%	g/cm^3	GPa	MPa	MPa$^{0.5}$·cm^3/g
GC1	950	5	<0.5	2.63 ± 0.02	84 ± 6	73 ± 8	3.3
Sintered Body	1150	35	8	1.83 ± 0.04	41 ± 3	27 ± 5	2.8
Zr-HGC *	1150	32	<0.5, on glazed surface **	1.89 ± 0.05	48 ± 5	26 ± 4	2.7
HGC2	1150	30	<0.5, on glazed surface **	1.99 ± 0.03	60 ± 4	40 ± 10	3.2

** 20% Zircon 40% panel glass 40% GC1.*

*** Data inferred from measurements on frits sintered at the same conditions.*

Due to the enhanced mechanical properties (see **Tab. 12**), the second series of layered glass ceramics could find interesting applications as structural materials. In fact, although lighter than GC1 glass ceramic, the hybrid glass ceramic HGC2 possessed an almost identical specific strength (which is the index ruling the mechanical efficiency of panels, as proposed by Ashby [15]). In addition, this value was quite close to that of lightweight stoneware tiles (2.9 MPa$^{0.5}$·cm^3/g), previously developed for high values applications such as the so-called ventilated façades [16]. Zr-HGC (first series) could be used for tiles subjected to moderate loads, although improvements by revision of formulations (type and content of additives) will be the object of future investigations.

3.4 Conclusions

A selected mixture of waste and low cost minerals was converted into glass ceramic components either by vitrification and subsequent crystallization or by direct sintering. The proposed method provides a cost effective method to manufacture economically competitive materials for building applications using a large amount of waste materials of which only a limited amount requires a melting step before firing.

A sinter-crystallization approach led to strong glass ceramics, under particularly simple conditions (pressing of fine powders and sintering at 950°C for only

30 min). Furthermore, the surface porosity of a glass ceramic body from direct sintering was sealed by a glass ceramic glaze, developed from the same starting mixture of waste and minerals;

The characteristics of waste-derived glass ceramic glaze were tailored by the addition of secondary components (panel glass from dismantled CRTs, zircon). Owing to their characteristic specific strength, the developed layered glass ceramics could find applications in the building industry as lightweight tiles.

Bibliography

1 U.S. Environmental Protection Agency, Handbook on vitrification technologies for treatment of hazardous and radioactive waste, 1992, Office of Research and Development, Washington DC. Report EPA/625/R-92/002.

2 P. Colombo, G. Brusatin, E. Bernardo, G. Scarinci, Inertization and reuse of waste materials by vitrification and fabrication of glass-based products, Curr. Opin. Solid St. M. 7 (2003) 225–239.

3 W. Höland, and G. Beall, Glass ceramic technology; 2002, Westerville OH, The American Ceramic Society.

4 L.M. Schabbach, F. Andreola, E. Karamanova, I. Lancellotti, A. Karamanov, L. Barbieri, Integrated approach to establish the sinter-crystallization ability of glasses from secondary raw material, J. Non-Cryst. Solids, 357 (2011) 10–17.

5 I. Gutzow, R. Pascova, A. Karamanov, J. Schmelzer, The kinetics of surface induced sinter crystallization and the formation of glass ceramic materials, J. of Mater. Science, 33 (1998) 5265-5273

6 A.A. Francis, R.D. Rawlings, R. Sweeney, A.R. Boccaccini, Processing of coal ash into glass ceramic products by powder technology and sintering, Glass Technol., 43 (2002) 58-62.

7 C. Dimech, C. R. Cheeseman, S. Cook, J. Simon, A. R. Boccaccini, Production of sintered materials from air pollution control residues from waste incineration, J. Mater. Sci. 43 (2008) 4143–4151.

8 I. Ponsot, R. Falcone, E. Bernardo, Stabilization of fluorine-containing industrial waste by production of sintered glass ceramics, Ceramics International, 39 (2013) 6907–6915.

9 A. Ray and A.N. Tiwari, Compaction and sintering behaviour of glass alumina composites, Mater. Chem. and Physics, 67 (2001) 220–5.

10 E. Bernardo, M. Varrasso, F. Cadamuro, S. Hreglich, Vitrification of wastes and preparation of chemically stable sintered glass ceramic products, J. Non-Cryst. Solids, 352 (2006) 4017–4023.

11 E. Bernardo, L. Esposito, E. Rambaldi, A. Tucci, S. Hreglich, Recycle of Waste Glass into "Glass–Ceramic Stoneware", J. Am. Ceram. Soc., 91 (2008) 2156–2162.

12 M. Romero, J.Ma. Rincon, A. Acosta, Crystallisation of a zirconium-based glaze for ceramic tile coatings, J. Eur. Ceram. Soc.. 23 (2003) 1629–1635.

13 R.C. Garvie, Allen M. Alper (Ed.), High Temperature Oxides: Oxides of rare earths, titanium, zirconium, hafnium, niobium, and tantalum, Academic Press, New York and London (1970), p. 133

14 E. Bernardo, G. Scarinci, S. Hreglich, G. Zangiacomi, Effect of time and furnace atmosphere on the sintering of glasses from dismantled cathode ray tubes, J. Eur. Ceram. Society 27 (2007) 1637–1643.

15 M.F. Ashby, Materials Selection in Mechanical Design, Butterworth Heinemann-Elsevier 3rd edition, 2005.

16 E. Bernardo, M. De Lazzari, P. Colombo, A.S. Llaudis and F.J. Garcı`a-Ten, Lightweight porcelain stoneware by engineered CeO_2 addition, Adv. Eng. Mater. 12 (2010) 65–70.

Chapter 4 – Soda Lime Glass Based White Tiles

4.1 Introduction - Choice of Whitening Agents

In the present chapter we investigated a method to manufacture white ceramics recycling soda lime glass discarded from a local factory in Saudi Arabia. In the glaze technology there are two general methods of dispersing particles in glazes. The first is mechanical dispersion obtained grinding or mixing the whole glaze composition with a fine powder that promotes a higher opacity. In this case, the crystalline phase must be stable enough to be protected from dissolution in the glass at high temperatures. The second method is the controlled nucleation and growth of crystal phases in the glassy phase [1, 2].

The production of white tiles was realized sintering a mixture of cullet and a whitening agent (10-30 wt%). We employed four different whitening agents. The first was metakaolin, which is a reaction product deriving from the heating of kaolin. The second was silica sand (α-quartz) and limestone ($CaCO_3$) in stoichiometric ratio 1:1 in order to favor the formation of β-wollastonite ($CaSiO_3$). The third was a commercial frit produced by Bitossi (Italy), for glazes based on controlled wollastonite formation. The fourth whitening agent was CaF_2, which is a mineral used for the realization of optical glass of low refraction index, opal glass and in glazes. Calcium fluoride has been used for several hundred years for bubble removal from glass melts in the fining processes and many other applications, e.g. to improve the kinetics of slag-iron separation in steelmaking.

The sintering of cullet mixed with a whitening agent (10-30 wt%) under the appropriate conditions enables the production of an opaque glass composite using a ceramic processing. The whitening agent used provided a white opacity to the material because of scattering and reflection of the light that is incident on the material. Among the factors controlling the opacity are included the difference in refractive index between the glass and opacifier, the number, size, shape

and distribution of the opacifier particles, the incident light wavelength and the thickness of the material.

The traditional routes for glass ceramic manufacturing require to produce a frit melting a parent glass of appropriate composition that is successively processed to obtain a controlled formation of crystal phases. The different approach proposed in this work is focused on the limitation of the thermal treatments and raw materials costs. In fact, using soda lime cullet was possible to avoid the glass melting directly going to the green-body forming and the sintering steps.

4.1.1 Some Further Remark About CaF_2

The choice of CaF_2 is related to the fact that fluorine is the most electronegative element of the periodic table and it replaces the oxygen ions making non-bridging bond of Si-F. Important effects due to the CaF_2 content on the structural property are provided as reported in literature by many works. CaF_2 decreases the viscosity and the glass transition temperature reducing the polymerization degree of the silicate network. FTIR studies display the diminishing of intensity of the vibrations related to the Si-O bound, this effect is explained as the increase of non-bridging oxygen to silicon atoms ratio (NBO/Si). Fluorine ions replace either bridging (O^0) or non-bridging (O^-) oxygen modifying the electronic environment of silicon atoms because of higher electronegativity of fluorine relative to oxygen [3-6].

The fluorine ion modifies the silica tetrahedral structure, because of the higher electronegativity of fluorine relative to oxygen, changing the bond angle Si-O-Si. In fact the electronic clouds of the Si-O valence bonds are attracted by fluorine ions. The repulsion forces *F* among the bonding electron pairs in the silica tetrahedra are identical, but the substitution of oxygen with fluorine ion create a distortion which modify the angles of the tetrahedra, as depicted schematically in **Fig**. **28** using a simple two-dimensional representation. The SiO_2 and $[SiO_3F]$ tetrahedron top view shows the Si-O-Si bond angle changes from 120° in silica to a greater value in fluorinated silica.

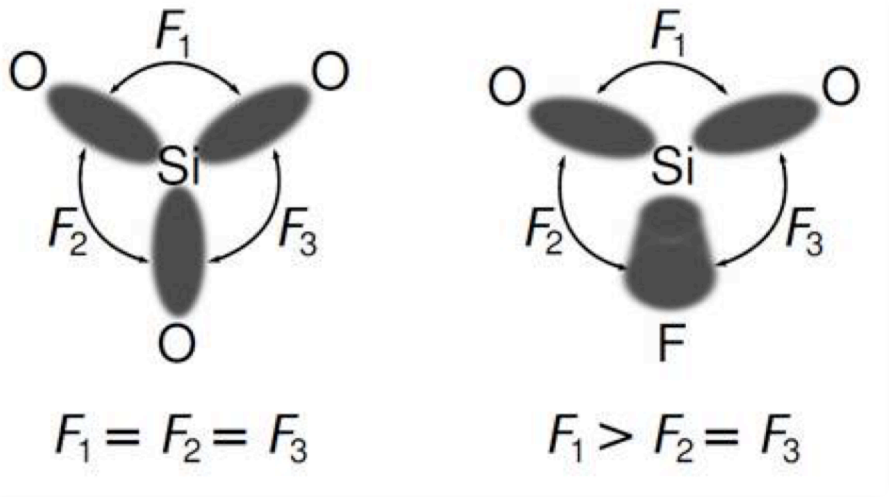

Fig. 28 – The figure represent the top view of a pure silica tetrahedron on the left and a fluorinated silica tetrahedron on the right. The repulsive forces are represented by the letter F and the black arrows empathize the angle between the valence bound electronic clouds.

The role of fluorine ions on the glass network is widely studied, but fewer works were dedicated to the reaction between soda lime cullet and CaF_2 at relatively low temperatures. In some silicate glasses fluorine probably promotes the decrease in the energy barrier necessary for crystallization as effect of the increasing of the NBO/Si ratio [7-9].

4.2 Materials and Methods

In order to improve the plasticity of the glass powder and to increase the green body strength, 7-10 wt% of water without binders was added to the powders.

Disk samples preparation – The composition was mixed at 200 rpm for 30 minutes in an agate jar and successively uniaxially cold pressed in a cylindrical mold (Ø = 20 mm) at a pressure of 10 MPa. All the disks were fired applying a 10°C/min heating rate with a holding time of 30 minutes to different temperatures.

Tile samples preparation – 12 grams of moistened raw powder mixture (80%wt of cullet and 20%wt of CaF_2) was uniaxially cold pressed in a mold 50 mm x 50 mm, at a pressure of 50 MPa. The green body was successively transferred on a refractory slab and dried at 80°C overnight. The produced sample

was then fired in air in an oven at 900°C for 30 minutes applying a 5°C/min heating rate.

The green body was successively transferred on a refractory slab and dried at 80°C overnight. In the present investigation no binder was used to avoid the burning out step before sintering. The samples were handled carefully because the green body strength is strongly related to the capillary forces which hold together the particles when the green body is wetted by the solvent and during drying, this capillary force disappears because the liquid evaporates [10]. During drying, the capillary force of the solvent may be replaced by the cohesive force of a binder.

The sample was subjected to a preliminary mechanical characterization, after being cut into small bars (3 mm x 3 mm x 43 mm, approximately). All bars were carefully polished to a 6 μm finish and beveled at the edges, by using abrasive papers and diamond paste. The Young's modulus was measured by non-destructive resonance frequency testing (GrindoSonic Mk5, Leuven, Belgium). Four point bending tests (40 mm outer span, 20 mm inner span) were performed on 10 samples by using an Instron 1121 UTS (Instron, Danvers, MA), with a crosshead speed of 1 mm/min.

4.3 Results and Discussions

4.3.1 Visual Appearance and Water Absorption

The preliminary experiments were focused on the verification of the aesthetical appearance and the water absorption of white opaque glass ceramics produced varying the whitening agent percentage and the firing temperature.

The photographs of the resulting samples, collected in **Fig. 29**, are not sufficient for the interpretation of the color, but show that a good quality of white color was indeed obtained.

The water absorption tests (**Tab. 13**), accomplished after 2h soaking in boiling water, were employed for the selection of the preferred composition and firing temperature, in order to produce a larger specimen for the mechanical tests. In fact a low water absorption is representative of a low open porosity and effective sintering.

The commercial frit (wollastonite) produced by Bitossi was employed as a sort of standard for the comparison of the whiteness of the samples produced. It was, in fact, our intention to use cheap natural raw materials instead of commercial frits. The whitened samples were all satisfactory from an aesthetical point of view, but all of them presented greater water absorption when fired at the highest temperature (950-1000°C). The composition prepared mixing limestone and silica gave a pleasant color, but also a very high percentage of water absorption; this composition was not further investigated considering that the additive employed probably increased the apparent viscosity of the sample thus meaning that a higher sintering temperature should be used. Excellent results concerning the water absorption were achieved using metakaolin (0.2%) and CaF_2 (0.3-0.4%) at 900°C, which are very close to zero although the best result was obtained using 30% of the commercial frit (<0.1%).

Fig. 29 – White glass ceramics composed prevalently of cullet 95 -70 wt% and a whitening agen. The samples of larger diameter (20% CaCO3 + SiO2) were pressed in a mould with Ø=31 mm.

Tab. 13 – Water absorption values of the glass ceramics

Whitener	Wt %	T °C	Water absorption %
Wollastonite*	10	900	0.7
Wollastonite*	10	950	9.6
Wollastonite*	30	900	<0.1
Wollastonite*	30	950	1.1
$CaCO_3$+SiO_2	20	900	38.8
$CaCO_3$+SiO_2	20	1000	6.6
Metakaolin	10	900	0.2
Metakaolin	10	950	15.4
CaF_2	5	900	0.3
CaF_2	10	900	0.5
CaF_2	20	900	0.4

* commercial frit

4.3.2 Mineralogical Analysis

The samples selected for further characterization were:

- 10 wt% of metakaolin and 90 wt% of cullet;
- 20 wt% of CaF_2 and 80 wt% of cullet.

The X-ray diffraction analysis of the metakaolin glass ceramic presented a prevalently amorphous structure, that is justified by the fact that 90% of the starting material was amorphous glass. Among the four different crystal phases identified, the most expected was the anorthite formation from the reaction between metakaolin and the glass matrix:

$Al_2O_3 \cdot 2SiO_2$ (metakaolin) + CaO (glass matrix) → $CaO \cdot Al_2O_3 \cdot 2SiO_2$ (anorthite).

The remaining crystal phases were calcium silicates such as wollastonite ($CaSiO_3$) and devetrite, which is a sodium-calcium silicate. The remaining peaks were attributed to the α-quartz pattern, but due to a shift of the peaks positions they are probably associated to a solid solution of a quartzoid derivative with alkali or alumina substitutions in the crystal lattice.

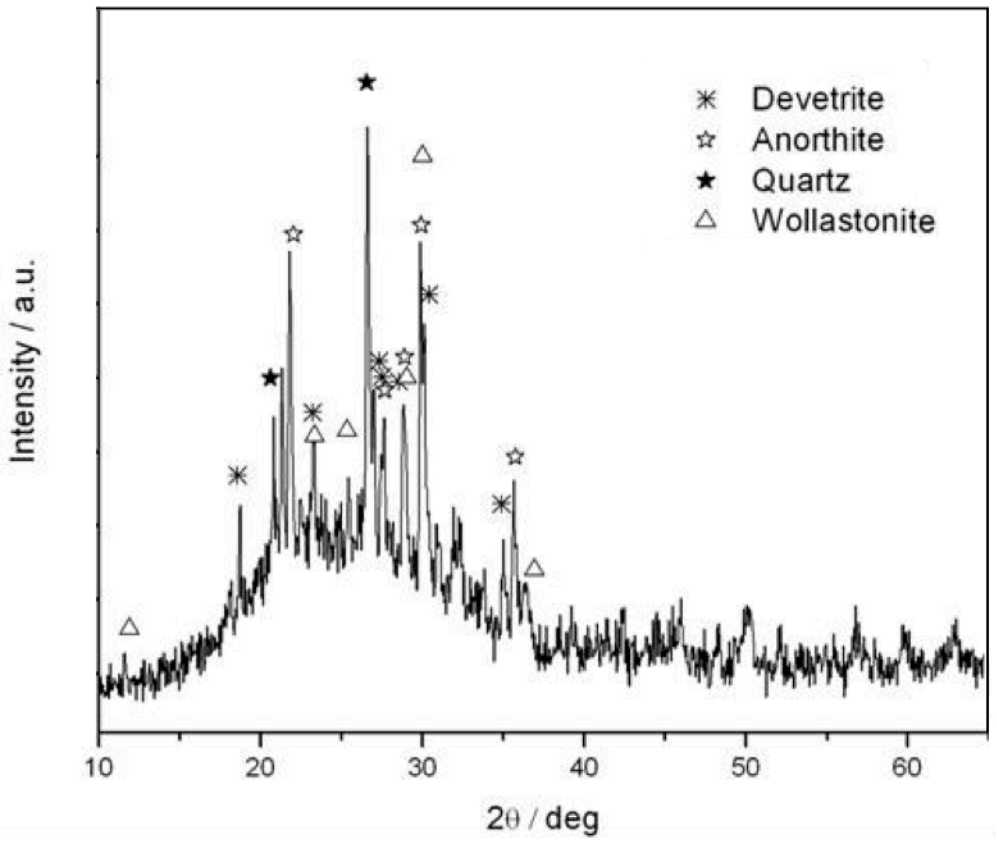

Fig. 30 – XRD pattern of the glass ceramic composed of 90% of cullet and 10% of metakaolin fired at 900°C for 30 minutes

The X-ray diffraction analysis, reported in **Fig. 31**, of the sample containing CaF_2 (20 wt%) gave a completely different result consisting in the formation of a highly crystalline glass ceramic. We can therefore observe that the presence of a fluorine-containing specie influence the crystal phases formation in the form of:

- Fluorite, CaF_2
- Agrellite, $NaCa_2Si_4O_{10}F$;
- Cuspidine, $Ca_4Si_2O_7F_2$;
- A solid solution of Na-Ca silicates in the form of albite-calcian $NaCaAlSi_3O_8$ and Na_2CaSiO_4;
- β-wollastonite ($CaSiO_3$);

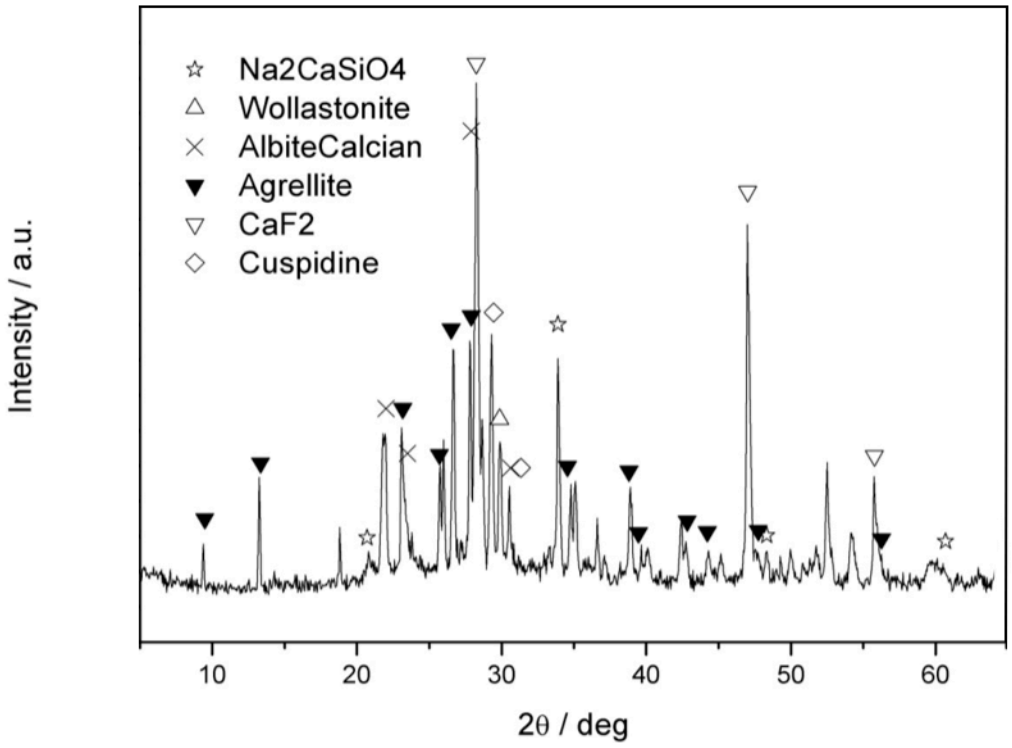

Fig. 31 – XRD pattern of the glass ceramic composed of 80 wt% of cullet and 20 wt% of CaF_2 fired at 900°C for 30 minutes

The presence of a large amount of fluorite in the diffractogram is probably given by two different mechanisms. The first mechanism concerns the droplet phase separation at high temperatures, which is well known in the opaque silicate glass production. Metastable immiscibility is observed in many glass systems and is a technique for achieving a controlled precipitation of nuclei that start the crystal growth in glass ceramics. The second mechanism concerns a saturation of the reactions taking place between cullet and CaF_2. The most interesting crystal phase formed was agrellite, that in nature is present as a white translucent mineral with a 5.5 hardness [11]. Agrellite presents a structure quite close to fluorcanasite ($Na_4K_2Ca_5Si_{12}O_{30}F_4$), these amphiboles were reviewed by Beall et al. [12] for their remarkable mechanical strength (e.g. a stoichiometric fluorcanasite glass ceramic is dense and highly crystalline, with a microstructure of interpenetrating lamellae that confers to the material a flexural strengths of 300 MPa and toughness values up to 5 $MPa \cdot m^{1/2}$). Moreover, the production method for fluorcanasite, and also agrellite, glass ceramics were patented (U.S. patent 4,386,162) according to a totally different route. The main difference between their inven-

tion and the process studied in this work is the *absence* of a melting step in our process, because we used a *direct sintering* of the starting mixture.

To study more in details the CaF_2 glass ceramic, the DTA and TGA analysis of the mixture composed of 80 wt% of cullet and 20 wt% of CaF_2 are reported in **Fig. 32**. The analysis show the exothermic peak of sintering and crystallization at 750°C and 850°C respectively. Both the effects are exothermic due to the fact that sintering involves surface energy reduction and therefore the crystallization of an amorphous phase releases heat. The crystallization band ends at ~900°C, while at 960°C a strong endothermic peak is shown. This endothermic effect is associated with a crystal phase transformation or possibly to fluorine gas evolution, although no evident mass loss was recorded. Samples based on CaO-CaF_2-SiO_2 are in fact involved in undesired production of inorganic fluorine gases according to the following reaction:

$$2\ CaF_2 + SiO_2 \leftrightarrow 2\ CaO + SiF_4\ (g)$$

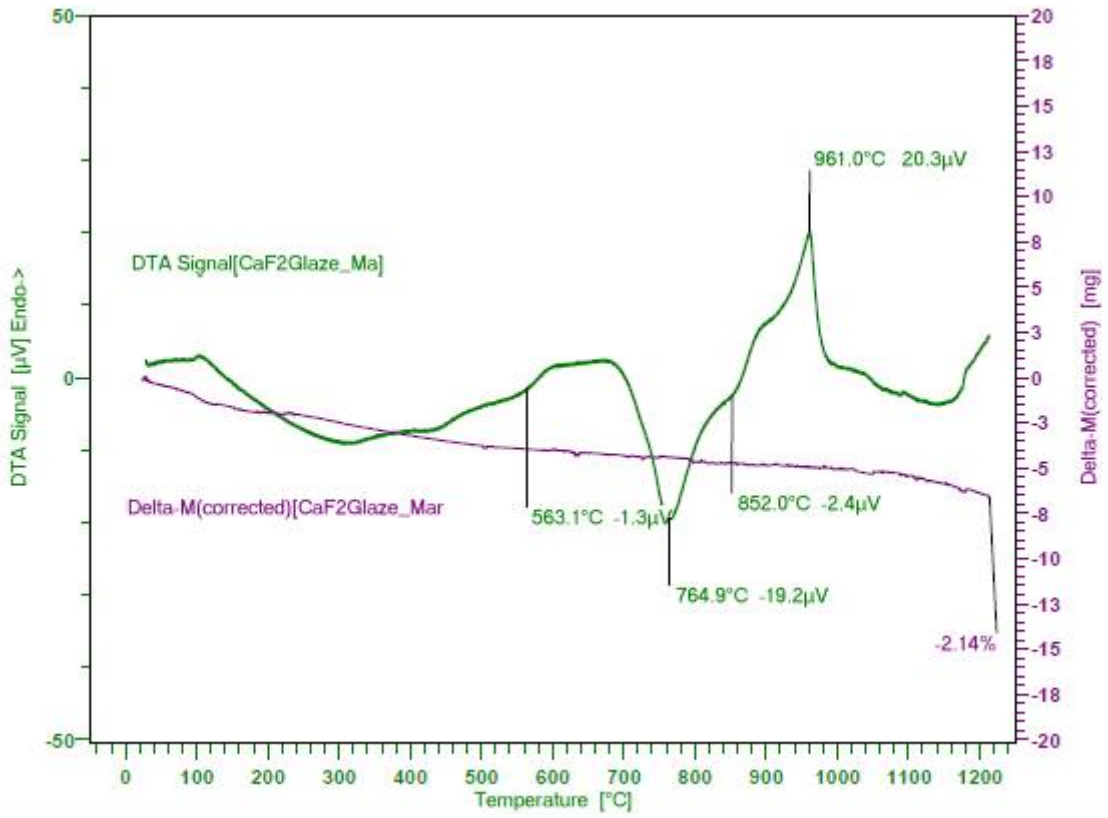

Fig. 32 – DTA curves at 10°C/min of a mixture composed of 80 wt% of cullet and 20 wt% of CaF_2

Tab. 14 – Dynamic Young's modulus, 4-pt flexural tests, and geometrical density values.

	E GPa	$\sigma_{4\text{-pt}}$ MPa	ρ g/cm³	Water absorption %
Ceramic substrate	34*	54 ± 6	1.83 ± 0.04	0.4

* The dynamic Young's modulus require a further investigation because the test for porous materials require larger samples

The mechanical strength (**Tab. 14**), at the 4-pt bending test, of about 54 MPa for a glass ceramic with a low density and low water absorption is a remarkable result that can compete with materials already used in the building industry.

4.3.3 Colored Glass Ceramics

A further study was accomplished concerning colored samples, with the 20 wt% CaF_2, 80 wt% cullet composition, which were prepared mixing four pigments produced by Sacmi (Italy). The pigments are transition metal silicates of blue, yellow, orange, and red colors. The realization of these colored samples required a high percentage of pigments (about 5 wt%). From a large scale production point of view, it is meaningless to consume high amounts of pigments for glass ceramics colored in bulk, as a more reasonable application of these colored material is glazing. However, for high wear applications, coloration in bulk is preferred.

By combining different pigments it was possible to create particular motives and to widen the range of colors achievable. In **Fig. 33** is shown, for example, a green sample produced from the combination of yellow and blue. It is also important to take into account that the pigments are applied in a white matrix that weakens the dyeing effects. These results are comparable to the U.S. patent 5,070,044, that is approximately the coloring process of canasite glass ceramics of the previously reported U.S. patent 4,386,162.

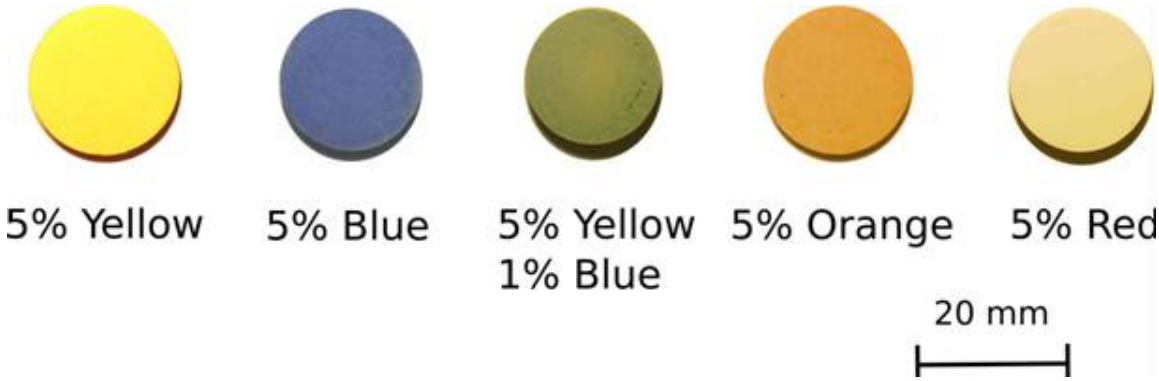

Fig. 33 – Colored glass ceramics composed of 80 wt% of cullet and 20 wt% of CaF2 mixed with a pigment.

4.4 Conclusions

The present investigation provided a method for manufacturing an environment friendly glass ceramic that is cost effective and has excellent mechanical properties. The low firing temperatures and the low cost of waste materials provide an interesting result, then considering that the materials employed are available in Saudi Arabia the glass ceramics realized are of industrial interest for the local ceramic companies.

The mechanical strength of 54 MPa for a low density ceramic with a low water absorption is an encouraging result that could be further improved in future studies. Although it was not well understood why the investigated samples presented a higher open porosity when fired at higher temperatures it was preferred to focus the research activities on other directions instead of continuing in the improvement of the white tiles from soda lime cullet.

A mechanical strength, at the 4-pt bending test, of about 54 MPa for a glass ceramic with a low density and low water absorption is an encouraging result that could be further improved increasing the translucence and luminescence for the production of luminescent panels, in a similar way of those marketed under the name of Veluna™, produced by Technical Glass Products (TGP) [13].

Bibliography

1 R. Casasola, J. M. Rincón, M. Romero. Glass–ceramic glazes for ceramic tiles: a review, Journal of Material Science (2012) 47:553–582.

2 A. Escardino. Kinetic Model for Crystallization in White Ceramic Glazes, Journal of the American Ceramic Society 84:23. (2001) 84:23-28.

3 D. B. Dingwell, C. M. Scarfe, and D. J. Cronin. The effect of fluorine on viscosities in the system Na_2O-Al_2O_3-SiO_2 - implications for phonolites, trachytes and rhyolites. American Mineralogist, 70(1-2):80–87, 1985.

4 J. H. Park, D. J. Min, and H. S. Song. FT-IR spectroscopic study on structure of CaO-SiO_2 and CaO-SiO_2-CaF_2 slags. ISIJ International, 42(4):344–351, 2002.

5 H. S. Park, H. Kim, and I. Sohn. Influence of CaF_2 and Li_2O on the viscous behavior of calcium silicate melts containing 12 wt pct Na_2O. Metallurgical and Materials Transactions B-Process Metallurgy and Materials Processing Science, 42(2):324–330, 2011.

6 Y. H. Kim, M. S. Hwang, H. J. Kim, J. Y. Kim, and Y. Lee. Infrared spectroscopy study of low-dielectric-constant fluorine-incorporated and carbon-incorporated silicon oxide films. Journal of Applied Physics, 90(7):3367–3370, 2001.

7 S. N. Salama, S. Salman, and H. Darwish. The effect of nucleation catalysis on crystallization characteristics of aluminosilicate glasses. Ceramics – Silikáty 46 (1) 15-23 (2002).

8 E. Y. Guseva, and M. N. Gulyukin. Effect of fluoride additives on glass formation in the SiO_2-CaO-Al_2O_3 system. Inorganic Materials, Vol. 38, No. 9, 2002, pp. 962–965.

9 D. P. Mukherjee, and S. K. Das. SiO_2-Al_2O_3-CaO glass ceramics: Effects of CaF_2 on crystallization, microstructure and properties. Ceramic International Volume 39, Issue 1, January 2013, Pages 571–578.

10 T. A. Ring. Fundamentals of Ceramic Powder Processing and Synthesis. Academic Press, 1996.

11 Mineralogy Database http://webmineral.com/

12 L. R. Pinckney, and GH Beall. Microstructural Evolution in Some Silicate Glass ceramics. Journal of the American Ceramic Society 91(3):773–779, 2008

13 Á. M. Rincon. Glass ceramic glazes for ceramic tiles: a review. Journal of Matererial Science 47 (2012) 553–582.

Chapter 5 – White Sintered Glass Ceramic Tiles With Improved Thermal Insulation Properties for Building Applications

5.1 Introduction

The improvement of the thermal efficiency of buildings, especially when exposed to arid environments, represents a challenge concerning the reduction of the overall costs for cooling. Cool roofing involves strategies to increase the solar reflectance in the visible and near infrared wavelengths or to enhance the thermal emittance at wavelengths close to 10μm of roofs in urban areas. Cool roofs also mitigate summer urban heat islands, lowering the citywide ambient air temperature and increasing human comfort. [1, 2, 3]

A valuable example of a cool roofing solution is represented by a functional engobe with a high albedo (i.e. with a high diffuse reflectivity or reflecting power) developed by Ferrarin et al. [4], that can be applied to conventional ceramic tiles used for roofing. Studies performed by Synnefa et al. demonstrated that the use of reflective coatings can reduce the temperature of a white concrete tile surface under hot summer conditions by 4°C during the day, and by 2°C during the night. [5] The surface of the concrete tiles was warmer than the ambient air by only 2°C during the day, and cooler than the ambient air by 5.9°C on average during the night.

Although a coating with a high albedo is valuable, a ceramic tile may warm up to environmental temperature, by contact with the air through conduction, transferring the heat into the building. A strategy to reduce this inconvenience is the use of a porous substrate that reduces the thermal conductivity. Thus the combination of a high reflective glaze and a porous substrate, as shown in **Fig. 34**, is a suitable strategy for obtaining “cool” tiles with improved thermal management properties [6].

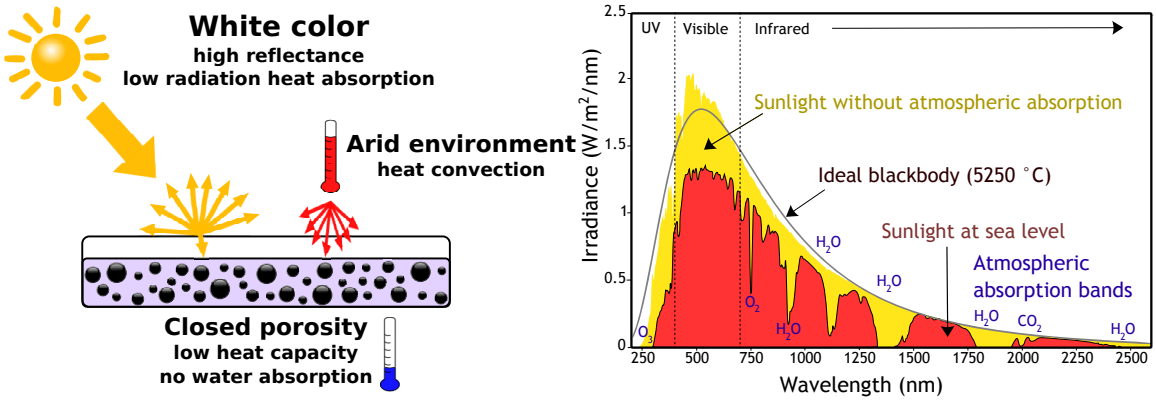

Fig. 34 – Schematic representation of an insulating tile engineered using a highly reflective coating deposited on a substrate possessing a low thermal conductivity. b) Spectrum of the solar radiation on the earth.

The porosity of the substrate needs to be tailored to provide sufficient mechanical strength and the lowest thermal conductivity possible. The matching of the coefficients of thermal expansion between glaze and substrate is simpler when the chemical composition of the two layers is similar, and therefore in this work we considered glass compositions suitable for the production of both dense and porous sintered glass-ceramics. Dense tiles can be considered for paving applications whereas porous tiles, both glazed and unglazed, can be used for cladding.

Porous tiles with a density and water absorption below 2 g/cm^3 and 2 wt%, respectively, were specifically investigated thus obtaining a compromise between mechanical strength, low thermal conductivity and limiting the absorption of water that might favor the formation of fungi and decrease the frost resistance. In order to realize white glass ceramics, natural raw materials possessing a limited amount of impurities (i.e. transition metals) were selected. Whiteness and opacity are provided by the refractive index difference between the glassy matrix and the crystal phases.

Tab. 15 – Chemical composition of NP glass and Neoparies™.

	NP glass		Neoparies™	
Oxide	(wt%)	(mol%)	(wt%)	(mol%)
Al_2O_3	7.7	4.8	7.0	4.4
B_2O_3	1.3	1.2	1.0	0.9
BaO	0.0	0.0	4.0	1.7
CaO	20.3	22.8	17.1	19.6
Fe_2O_3	0.4	0.1	0.0	0.0
K_2O	2.5	1.7	2.0	1.4
MgO	0.7	1.1	0.0	0.0
Na_2O	2.5	2.5	3.0	3.1
SiO_2	57.4	60.1	59.3	63.6
TiO_2	0.7	0.6	0.0	0.0
ZnO	6.5	5.0	6.5	5.2

	Clay (wt%)	Cullet (wt%)	Limestone (wt%)	Silica (wt%)	Pure chemicals (wt%)
Amount in NP glass	14.8	9.9	29.6	34.5	11.4

5.2 Materials and Methods

Neoparies™ glass-ceramics [7] were chosen as a reference material. A glass with chemical composition resembling that of Neoparies was reproduced using natural raw materials from Saudi Arabia and a limited amount of pure chemicals (~11 wt%, in the form of 3wt% ZnO, 3% borax and 5.4% K_2CO_3), as reported in **Tab. 15**. The chemical composition of the raw materials was evaluated by means of X-ray fluorescence (Philips XRF sequential spectrometer PW 2400, Eindhoven, The Netherlands). Different to Neoparies, BaO was substituted by increasing the mol.% of CaO, while the silica content was slightly reduced.

The raw materials were first dried and homogenized by ball milling in an agate jar for 30 minutes at 300 rpm and finally melted in kyanite (Al_2SiO_5) refractory crucibles at 1400°C for 90 minutes in static air. The molten glass did not corrode the crucible, thus not affecting the chemical composition of the parent glass. After achieving complete melting of the raw materials, the melt was poured into water to produce a glass frit. The drastic quenching provided a number of fragments that were successively dried at 80°C overnight, ball milled (30 minutes at 400 rpm) and sieved to obtain particles with a size below 90 μm.

Dilatometric and differential thermal analysis (DTA/TGA, STA 409; Netzsch-Gerätebau GmbH, Selb, Germany, operated at 10°C/min in static air) were performed both on powders below 90 μm and coarser particles (above 2-3 mm), to in-

vestigate the effect of the particle size on the crystallization behavior (surface induced vs bulk nucleation).

The investigation of the evolution of the density as a function of the amount of foaming agent added was performed by adding Si_3N_4 (samples labeled SN) and mixtures of Si_3N_4 and gypsum ($CaSO_4 \cdot 2H_2O$) used as oxidizer in a molar ratio Gypsym/Silicon Nitride of 3:1 (samples labeled G_3SN_1) or 6:1 (sample labeled G_6SN_1). For the preparation of dense samples, the pure frit was used whereas for the preparation of porous samples the foaming additives were introduced in the range 0.5 to 4 wt% with respect to the amount of dry frit, and the mixtures were cold pressed mixture in a 13 mm steel mold at a pressure of 40 MPa.

The water absorption, W_{AB}, apparent, ρ_a, bulk, ρ_b, densities of the fired samples were evaluated according to the UNI EN ISO10545 norm, by means of the Archimedes method. The true density, ρ_t, was evaluated on powdered samples of size below 90 μm by means of helium gas pycnometer (Micromeritics AccuPyc 1330, Norcross, GA)

After selection of optimum compositions, larger samples were realized using 25 g of the dry frit powder uniaxially cold pressed in a steel mold of 50×50 mm^2 at a pressure of 40 MPa. To obtain a porous substrate coated with the dense glass ceramic, 3 g of the dry frit powder were lightly pressed (at 10 MPa) and then 22 g of the glass frit mixed with the selected foaming agent were further deposited. The layered sample was then uniaxially pressed at 40 MPa. The produced samples were then fired in air at 950°C for 30 minutes applying a 10°C/min heating rate.

The Young's modulus of the glass-ceramic samples was determined using the resonant frequency method in the flexural mode of vibration (GrindoSonic Mk5, Leuven, Belgium). Four-point bending tests (40 mm outer span and 20 mm inner span) were performed using an Instron 1121 UTS instrument (Instron, Danvers, MA) on at least 15 specimens for each sample type, with dimensions of about 4 × 2.5 × 47 mm^3. In order to remove surface flaws, all samples were carefully polished to a 6 μm finish before testing, using abrasive papers and diamond paste. The edges of the bars were beveled using fine abrasive papers and diamond paste. The crosshead speed was 1 mm/min until fracture. The double layer samples were tested by positioning the porous layer on the compression (upper) side and the dense layer on the tensile (lower) side.

Ground glass–ceramics were investigated by powder X-ray diffraction (Bruker D8 Advance, Karlsruhe, Germany), employing CuKα radiation (0.15418 nm) and collecting data in the range 2θ = 10–70° (0.05° steps and 5 s counting time). The identification was performed by means of a semi-automatic software package (Match!, Crystal Impact GbR, Bonn, Germany), supported by data from PDF-2 database (ICDD-International Centre for Diffraction Data, Newtown Square, PA). A selected dense and polished sample was investigated using Vickers indentation (Officine Galileo DG 901, Florence, Italy), and the microhardness (H_V) was assessed by averaging 20 indentations produced at low load (5N).

Polished surfaces of the samples were characterized by scanning electron microscopy (SEM-ESEM Quanta 200, FEI Company, Eindhoven, The Netherlands). The cell size distribution was evaluated from the acquired SEM images using the image processing software ImageJ (Carl Zeiss, Oberkochen, Germany). The area of the cells, evaluated by means of ImageJ, was converted into the area of a circle of equivalent surface. The values obtained by image analysis were converted to 3D values using the stereological equation $\phi_{sphere} = \phi_{circle}/0.785$,[8] to determine the actual cell size.

The thermal diffusivity was evaluated at 25°C using the laser flash method. Samples were in the form of disks with 10 mm diameter and thickness of about 2 mm. A neodymium-glass laser operating at 1.053 μm which delivers a standard pulse of 30 J in 450 μs was used to heat up the front face of the cylindrical sample. The absorbed heat diffuses throughout the sample, and a liquid-nitrogen-cooled infrared detector (Hg-Cd-Te) was used to monitor the evolution of the back face temperature. Samples were coated with a thin graphite layer to increase the emissivity of the receiving and emitting faces. Thermal diffusivity was calculated by using the Degiovanni's expression, [9] which takes into account the heat losses from the sample during the experiment compared with the simpler Parker expression which only considers adiabatic conditions.[10] The thermal diffusivity (α) was measured in a direction perpendicular to the disk faces, and the thermal conductivity was then calculated by using the relation:

$$\lambda = \alpha \rho c$$

where ρ is the bulk density and *c* is the specific heat of the material. The specific heat was calculated using the rule of mixtures according to the glass composition given in Table 1. The rule of mixtures applied to the elementary oxide composition

for silicate glasses gives values which are in very good agreement with experimental measurements [11].

The reflectance was evaluated by means of a UV-Vis spectrophotometer (570 Jasco, Japan) equipped with integrating sphere (ISN-470). The white standard employed was a $BaSO_4$ plate.

5.3 Results and Discussion

The selection of a reference commercial glass-ceramic system (Neoparies™) and of specific foaming agents needs a preliminary discussion. The formation of specific crystal phases is beneficial for improved wear and chemical durability, when thinking of materials that should be applied both as cladding and floor tiles. Neoparies are well-known for featuring such optimum phase assemblage, combined with a white color, for formulations that do not contain any pigments. In addition, they are developed by viscous flow sintering with concurrent crystallization ("sinter-crystallization") of glass powders, i.e. by a process in which the introduction of additives (foaming agents, reinforcing phases) is particularly simple. [7]

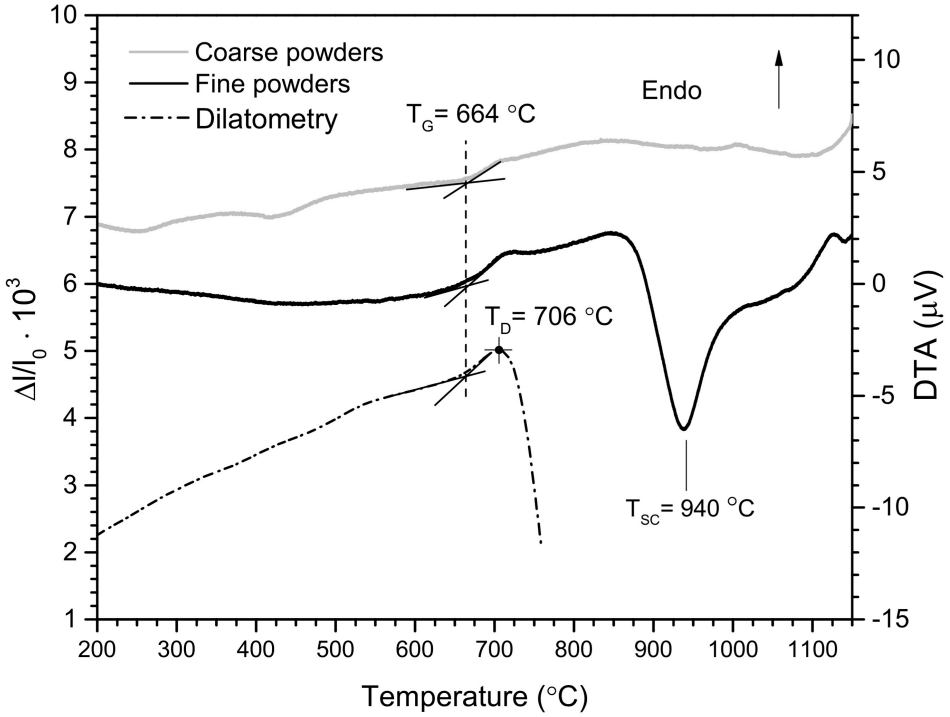

Fig. 35 – Dilatometric plot, for a rod, and DTA plots, for fine powders (below 90 μm) and coarse fragments (above 2-3 mm) of NP glass.

Concerning the development of porous samples, although a variety of foaming agents are available and well studied, only a few, such as CeO_2 and Si_3N_4, are suitable for generating porosity without affecting the final color. CeO_2 has been already shown to be an effective foaming agent in porcelain stoneware, due to the reduction to CeO and oxygen gas evolution at high temperature. [12] However, the sintering temperature of Neoparies-like compositions is in the 950-1100°C range, well below the temperatures suitable for using CeO_2. Although they are more expensive than CeO_2, Si_3N_4 powders can lead to gas generation in the desired temperature range; in particular, they release nitrogen gas and leave a silica residue when fired in an oxidizing environment even at temperatures as low as 800-850°C. [13-14] The oxidation of Si_3N_4 powders is mainly attributed to the reaction with the environmental oxygen diffusing through the porosity available inside the pressed powders. During sintering, the permeability decreases and the environmental oxygen becomes insufficient to fully oxidize the Si_3N_4 powders. Therefore, in the present study gypsum was added to enhance the oxidation of Si_3N_4.

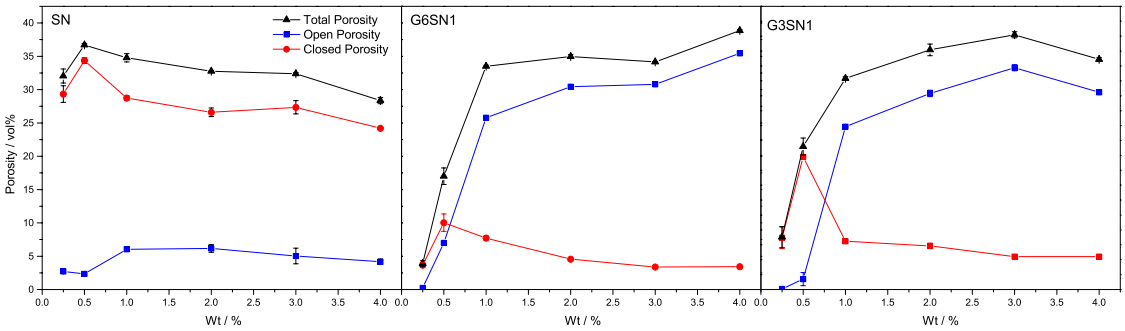

Fig. 36 – Total, open and close porosity of NP glass ceramic samples foamed using different foaming agents.

In **Fig. 35** are reported the dilatometry and DTA data for fine powders (below 90 μm) and coarse fragments (above 2-3 mm) of NP glass. The DTA plots for coarse and fine NP glass powders are in excellent agreement with the dilatometric plot for a NP glass rod, and show that the glass transition temperature (T_G) occurs at ~670°C. Coarse and fine glass powders remarkably differ from each other in terms of the exothermic peak, attributable to a crystallization event. Coarse glass powders do not exhibit any exothermic effect, whereas a large peak, centered at ~940°C (T_{SC}, with SC standing for "surface-activated crystallization"), is present for the fine glass pow-

ders. The data therefore are a proof that surface nucleation occurs in the system, which is the basis for the production of sintered glass-ceramics [15-16]. Moreover, crystallization occurs at a temperature higher than the dilatometric softening point (706°C), that is widely recognized as the minimum temperature at which significant sintering occurs by viscous flow. [17]

Considering the relatively large gap between the dilatometric softening point and the crystallization temperature (T_{SC}-T_D>200°C), NP glass was expected to lead to dense sinter-crystallized glass-ceramics when fired at T_{SC} (rounded at 950°C). This was effectively verified, with samples from pure NP glass exhibiting a bulk density of 2.56 ± 0.04 g/cm^3 after heat treatment at 950°C, very close to the true density of 2.68 ± 0.02 g/cm^3, indicating that a residual porosity not exceeding 4.5 vol% was present in the sample. The true density, ρ_t, was not affected by the presence of the foaming agents and was 2.68 ± 0.02 g/cm^3 for the set of samples analyzed.

From the porosity data reported in **Fig. 36**, we can note the efficient foaming action of Si_3N_4. Indeed, even at a very low amount such as 0.25 wt%, silicon nitride generated a total porosity (TP) of 32 vol%, that further increased to a peak value of 36.7 vol% for a 0.5 wt% of foaming agent added. Higher percentages of Si_3N_4 probably increased the apparent viscosity of the glass phase, thus limiting a further expansion. Although for both fired samples, mixing 0.25 or 0.5 wt% of Si_3N_4 yielded a density below 2 g/cm^3 and water absorption less than 2 wt% (see **Tab. 16**) , only the composition with the highest porosity was selected to manufacture a tile and further study of the material properties, in order to produce samples with better thermal insulation characteristics.

An enhancement of foaming was achieved by the addition of gypsum to the mixture. Gypsum completely dehydrates in the interval 120-180°C transforming into anhydrite (III), in turn decomposing into CaO and SO_3 at a temperature above 1180°C [18]. When coupled with a reducing agent, however, this calcium sulphate may transform to calcium sulphite and sulphide, with release of oxygen. This redox coupling is actually exploited for improving the oxidation of SiC in commercial glass foams [14]. By analogy, in our system Si_3N_4 was expected to be oxidized not only by reaction with atmospheric oxygen, but also by reaction with oxygen released from gypsum.

Both mixtures G_3SN_1 and G_6SN_1 formed a limited amount of porosity when the foaming agent was added in a small percentage (below 1 wt%), suggesting that the introduction of Si_3N_4 needs to be sufficiently high to enable the generation of porosity. In fact, performing some preliminary investigations we found that 0.5-2 wt% gypsum additions did not decrease the final density. Furthermore, in the G_3SN_1 and G_6SN_1 samples the role of gypsum is to oxidize Si_3N_4 particles and when the total amount of foaming agent is used in percentages of 0.25 or 0.5 wt%, only traces of silicon nitrides were introduced. However we can observe that for systems containing 1 wt% Si_3N_4 and above, the addition of gypsum in both formulations (samples G_6SN_1 and G_3SN_1) contributed to the expansion (allowing to obtain a total porosity greater than 40 vol%), but the main effect was to increase the amount of open porosity. The presence of open porosity led to high values for the water absorption (in some cases > 20 wt%), but the detrimental effect of its presence could be limited by the application of a dense glaze on the tile surface.

Tab. 16 – Water absorption (W_{AB}), bulk density (ρ_b) and apparent density (ρ_b) values for different mixtures. Samples directly inserted in the furnace at 950°C and heated for 3h.

Sample	Si_3N_4 (wt%)	W_{AB} (wt%)	ρ_b (g/cm^3)	ρ_a (g/cm^3)
SN	0.25	1.5 ± 0.1	1.80 ± 0.03	1.85 ± 0.03
	0.50	1.4 ± 0.1	1.68 ± 0.01	1.72 ± 0.01
	1.00	3.5 ± 0.2	1.73 ± 0.02	1.84 ± 0.01
	2.00	3.5 ± 0.3	1.78 ± 0.00	1.90 ± 0.01
	3.00	2.8 ± 0.7	1.79 ± 0.00	1.89 ± 0.02
	4.00	2.2 ± 0.2	1.90 ± 0.01	1.98 ± 0.00
G_6SN_1	0.25	0.1 ± 0.1	2.55 ± 0.01	2.55 ± 0.01
	0.50	0.1 ± 0.0	2.38 ± 0.03	2.38 ± 0.03
	1.00	14.6 ± 0.0	1.76 ± 0.00	2.37 ± 0.01
	2.00	17.7 ± 0.2	1.72 ± 0.01	2.48 ± 0.00
	3.00	17.7 ± 0.0	1.74 ± 0.00	2.52 ± 0.00
	4.00	21.9 ± 0.2	1.62 ± 0.00	2.51 ± 0.00
G_3SN_1	0.25	< 0.1	2.42 ± 0.05	2.42 ± 0.05
	0.50	0.9 ± 0.6	2.01 ± 0.04	2.05 ± 0.02
	1.00	16.0 ± 0.1	1.71 ± 0.01	2.35 ± 0.01
	2.00	20.8 ± 0.7	1.58 ± 0.03	2.36 ± 0.02
	3.00	24.5 ± 0.5	1.52 ± 0.01	2.42 ± 0.00
	4.00	20.3 ± 0.2	1.63 ± 0.01	2.43 ± 0.01

After these preliminary tests, further studies were performed on larger samples selecting an amount of foaming agent of 0.5 wt% (SN sample) and 2 wt% (G_3SN_1 sample), respectively. The first sample was manufactured without applying a glaze, because of its low water absorption. The second sample possessed the highest amount of porosity, and the mixture with 2 wt% of foaming agent was preferred in order to limit the amount of additive and considering that a sufficiently low density value was already obtained for that amount of foaming agent. Because of its high water absorption, a glaze with the same composition of the body was applied to this sample.

As determined by XRD analysis (**Fig. 37**), controlled surface crystallization of β-wollastonite ($CaSiO_3$ PDF #751396) and hardystonite ($Ca_2ZnSi_2O_7$ PDF #721603) occurred after heating at 950°C for 30 minutes; the presence of residual glass is also evident form the patterns. Hardystonite is part of the melilite group crystal structures of general formula $X_2YZ_2O_7$, where X is Ca^{2+} or Na^{+}, Y is Mg^{2+}, Zn^{2+} Al^{3+} or B^{3+} and Z sites are a combination of B^{3+}, Al^{3+} and Si^{4+}. Considering the chemistry of the studied glass ceramic, ion substitutions probably occurred in the hardystonite crystals with Al^{3+} and B^{3+} occupying the Y and Z sites [19-20].

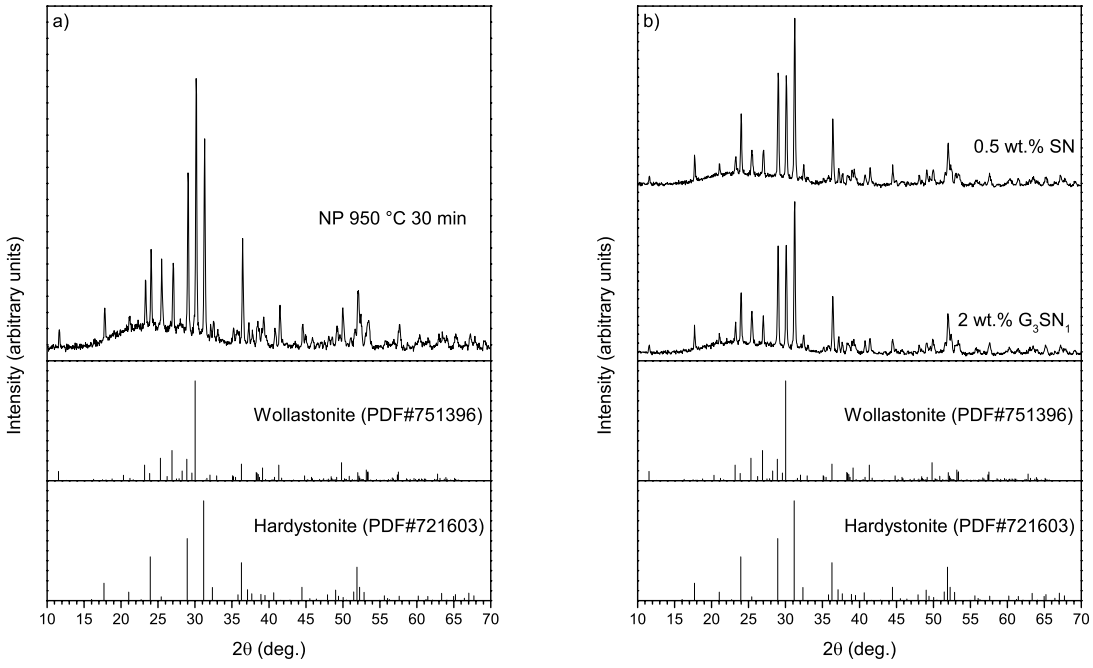

Fig. 37 – XRD patterns of sintered glass ceramics. a) Dense sample of composition NP fired at 950°C for 30 min. b) Cellular glass ceramics of composition NP foamed using different foaming agents, sintered at 950°C for 30 min.

Comparing the relative intensity of the diffraction peaks of β-wollastonite and hardystonite, we can observe that the porous samples presented a higher hardystonite to β-wollastonite ratio. A likely reason for this is that the pores could favor the heterogeneous nucleation of hardystonite. No evidence of Si_3N_4 or $CaSO_4$ traces were found in the XRD patterns, thus suggesting that the decomposition/reaction products of the introduced additives were dissolved in the glass ceramic.

Fig. 38 reports the back scattered image (BEI) and SEM-EDS analysis of the NP glass ceramic, showing the nucleation and growth of hardystonite and wollastonite crystals in regions richer in Zn or Ca, respectively.

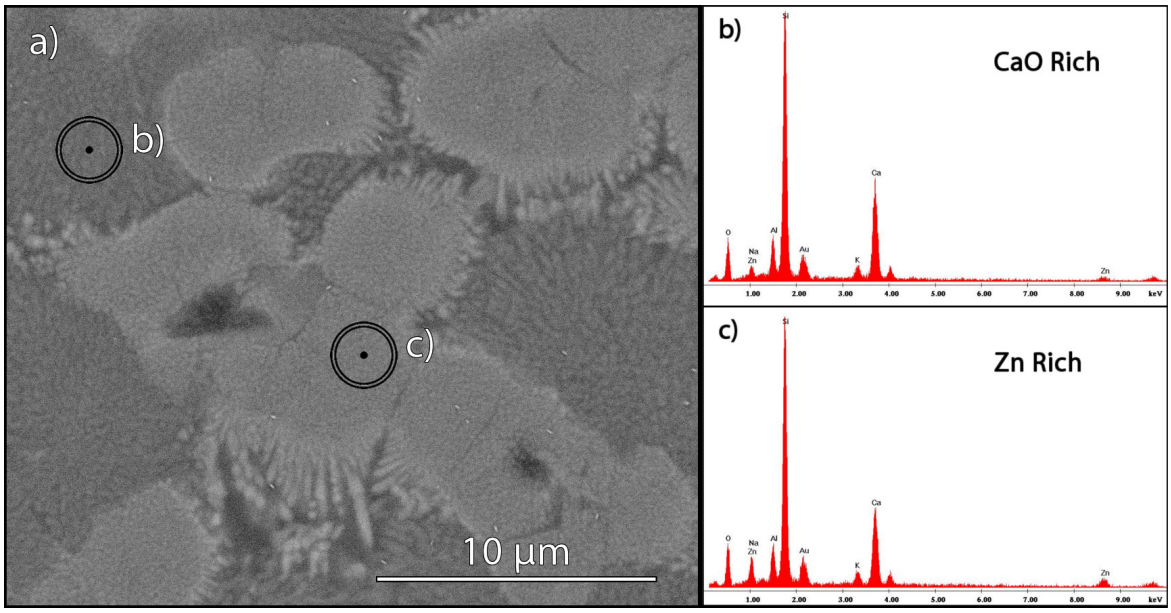

Fig. 38 – SEM-EDS microanalyses of a dense NP sample after firing at 950°C for 30 min. a) BEI, showing the phase separation; b) EDS microanalysis of the darker region, showing Zn depletion and higher Ca content; c) EDS microanalysis of the lighter region, showing Ca depletion and a higher Zn content.

In **Fig. 39a** is reported a top view of the dense NP glass ceramic, showing the formation of the hardystonite- and wollastonite-rich regions. A residual total porosity of 4.5 vol% was calculated from the ρ_b and ρ_t density. In **Fig. 39b** a perfect integration between the dense coating applied on the porous substrate realized adding 2 wt% of the foaming mixture containing gypsum (sample G_3SN_1) is shown. The same crystalline microstructure found in the bulk material is also present in the struts of the porous samples (see **Fig. 39c** and **d**).

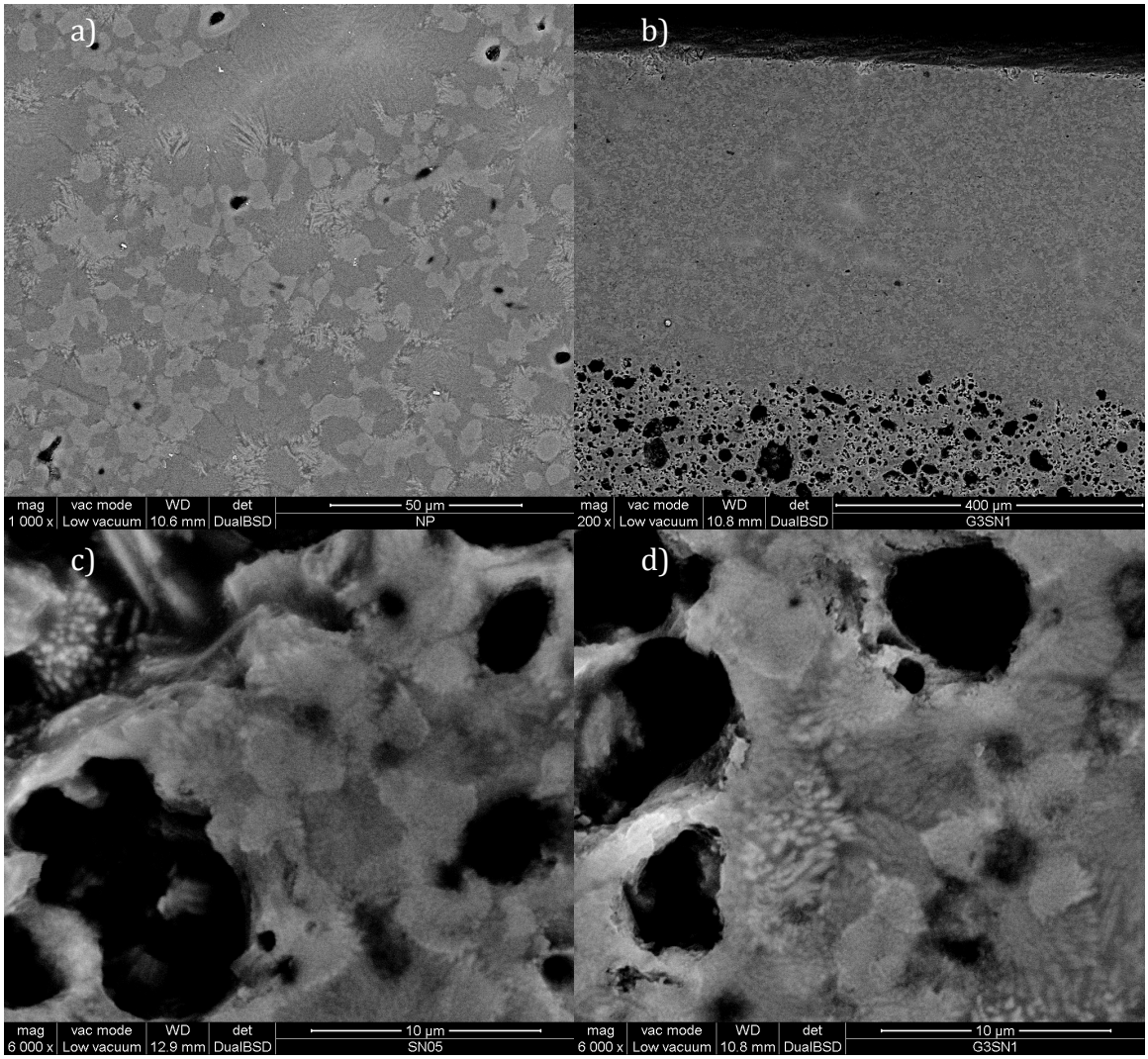

Fig. 39 – BEI of the dense glass ceramics. a) Dense glass ceramic. b) Cross section of the glaze applied to a foamed substrate (sample G_3SN_1). c) Detail of the microstructure of sample SN; b) Detail of the microstructure of a foamed sample using (sample G_3SN_1).

Differently from pure glass foams, the studied cellular glass ceramics present a low sphericity of the cells, as observed in the SEM images and in the graphical representations of the outlines of the cells reported in **Fig. 40**. The equivalent cell-size (diameter) distribution was evaluated by fitting the processed data with Lorentzian curves by means of image analysis, as reported in **Fig. 40c** and **f**. The Lorentzian curves peak at 4.3 and 4.0 µm for the samples foamed using different foaming agents (samples SN and G_3SN_1, respectively), indicating that the cell size distributions of the samples were nearly equivalent. However, sample G_3SN_1 possessed a

lower porosity resulting in a density of 1.94 g/cm^3, higher than that of sample SN that had a density of 1.85 g/cm^3. The difference in the density values reported in **Tab. 16** and **Tab. 17** was originated by the different heating treatment applied. In fact, the samples reported in **Tab. 16** were produced by directly inserting them in the kiln, whereas the samples of **Tab. 17** were obtained by applying a heating rate of 10°C/min. The heating rate affected both density and water absorption, in fact differently to samples G_3SN_1, sample SN had a water absorption value higher than 2 wt%, thus indicating that the application of a glaze should be considered for both the mixtures to protect the porous substrate.

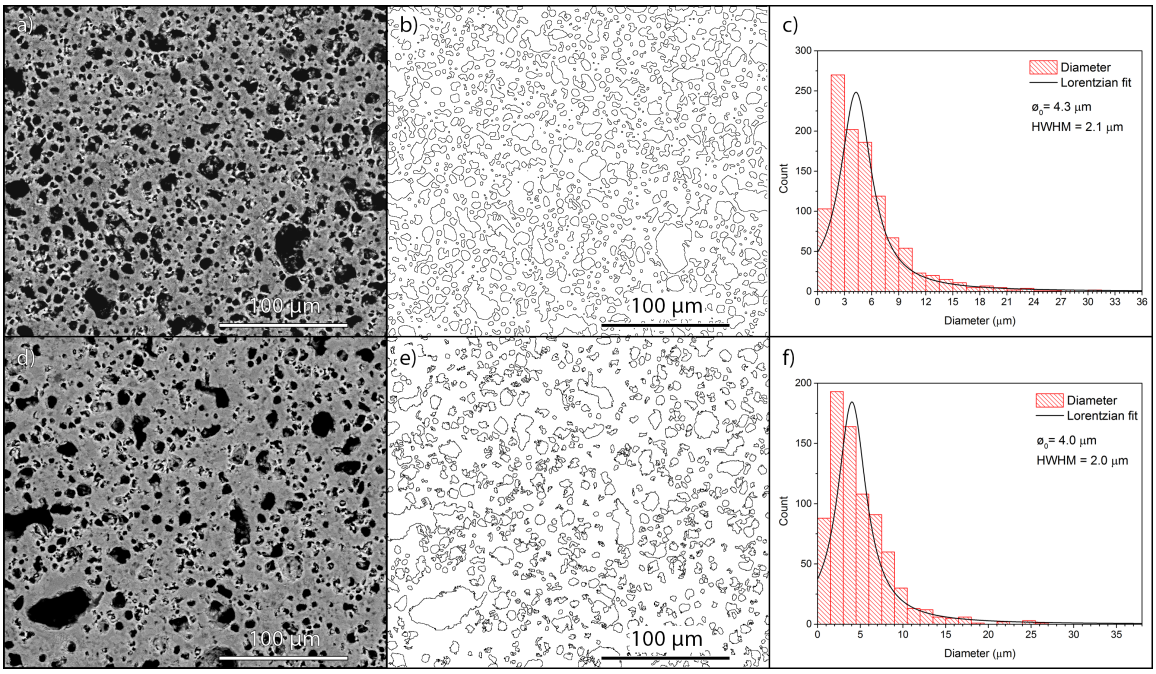

Fig. 40 – a-d) BEI at low magnification used to evaluate the cell size distribution of SN and G_3SN_1 porous samples. b-e) Outlines of the cells after image processing. c-f) Histogram plot of the cell size and Lorentzian fit to evaluate the cell size distribution.

Tab. 17 – Bulk density (ρ_b), elastic modulus E, bending strength (σ) and hardness (HV) of dense and porous glass ceramic tiles. Samples heated at 10°C/min to 950°C, 3h at 950°C.

Sample	ρ_b (g/cm^3)	E (GPa)	σ (MPa)	HV (GPa)	Wab (wt%)
NP	2.56 ± 0.04	80 ± 3	97 ± 8	6.7 ± 0.3	<0.2
SN	1.85 ± 0.05	39 ± 2	58 ± 6	-	3.1
G_3SN_1*	1.94 ± 0.02	49 ± 2	61 ± 6	-	1.9

*glazed

Although the bending strength of bars cut from the tiles of the dense samples was considerably higher, the porous glass ceramics possessed mechanical properties similar to those of dense commercial sinter-crystallized glass ceramics of similar composition, and compare favorably with the typical properties of traditional ceramics. [21] In particular, the porous samples had a high strength associated with a density decreased by about 25-28% with respect to the dense samples, and we can posit that the glazed side prevents the water absorption considering the negligible absorption displayed by the dense sample. For the dense samples, the total residual porosity, evaluated by gas pycnometry, was of 4.5 vol%.

The thermal conductivity measured at 25°C for an almost dense NP glass is 1.38 $W \cdot m^{-1} \cdot K^{-1}$. This value, which is consistent for a glass is the same as literature data reported for Neoparies (1.4 $W \cdot m^{-1} \cdot K^{-1}$) [22]. The values for porous samples SN and G3SN1 are respectively 0.64 and 0.61 $W \cdot m^{-1} \cdot K^{-1}$. These values were compared with analytical predictions using the Hashin & Shtrikman upper bound and percolation theory. The Hashin & Shtrikman (HS) upper bound gives the highest limit for an isotropic two phase material by considering isolated inclusions placed in a continuous matrix. [23] The following expression is used for the calculation:

$$\lambda_{eff,upper\ limit} = \lambda_s + \frac{v_p}{\frac{1}{\lambda_p - \lambda_s} + \frac{v_s}{3\lambda_s}}$$

where λ_s and λ_p are the thermal conductivities of, respectively, the solid phase and the pores, v_s and v_p are the corresponding volume fraction of these phases. The HS upper bound describes well a material with a closed porosity. In the percolation theory the continuous nature of each phase is taken into account, depending on its volume fraction. Landauer's expression was used for the calculation given by:

$$\lambda_{eff} = \frac{1}{4}\left[\lambda_p(3v_p - 1) + \lambda_s(2 - 3v_p) + \left(\left[\lambda_p(3v_p - 1) + \lambda_s(2 - 3v_p)\right]^2 + 8\lambda_s\lambda_p\right)^{1/2}\right]$$

This model describes well a material with an open porosity and a non organized solid skeleton, up to 70%. [24] It has been shown that the thermal conductivity of porous materials with an organized solid skeleton, like foams, is better described with the upper limit of the HS expressions [25, 26].

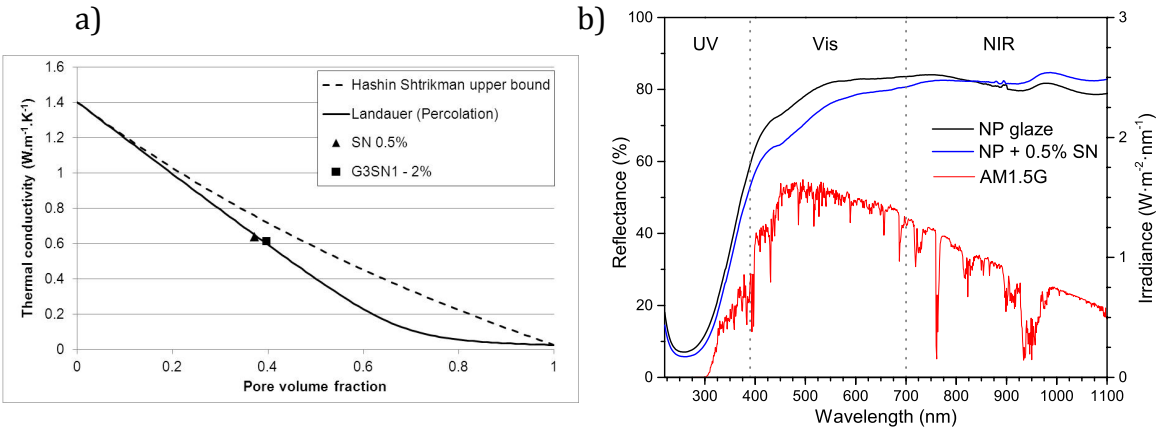

Fig. 41 – a) Thermal conductivity at room temperature as a function of the pore volume fraction. Comparison with the values calculated with the Hashin–Shtrikman upper bound and Landauer expressions; b) UV-Vis-NIR spectra for dense and foamed SN samples, and AM 1.5 Global solar irradiance according to the ASTM G173 standard.

Experimental results for porous SN and G3SN1 samples were compared with predictions with the analytical models in **Fig. 41a**, using a solid phase thermal conductivity of 1.38 $W \cdot m^{-1} \cdot K^{-1}$, which is the value measured for the dense NP glass. A good agreement is obtained between experimental data and predictions with Landauer's relation. For G3SN1 sample, which exhibits 29% of open porosity (and 40% of total porosity) this agreement is not surprising since the percolation theory describes well a material with an open porosity. For the porous SN sample, this agreement is more surprising, since the major part of the porosity is closed (35% of closed pores for a total porosity of 37%). Indeed if we extrapolate using the HS upper bound, this yields a value of 1.2 $W \cdot m^{-1} \cdot K^{-1}$ for fully dense material. We can assume that variation in composition may affect this end point value. The solid phase conductivity of the porous samples should be found between 1.2 and 1.4 $W \cdot m^{-1} \cdot K^{-1}$.

The Standard Reference Spectra ASTM Global reported in **Fig. 41b** displays the simulated spectral irradiance AM 1.5 Global of sun light for a 37° tilted surface, and is herewith used to show the wavelengths interval where the sun light is the most intense. In fact to reduce the heat absorption from the sunlight, it is of fundamental importance to reduce both the absorption from the visible light range (390-700 nm) and from the near infrared (NIR 750–1400 nm). In **Fig. 41b** are also shown the reflectance values of a dense NP and a porous SN sample without the glaze layer applied. We can see that the porosity slightly decreases the reflectance as a result of

light scattering, and a clear absorption of the UV radiation is due to the small band gap of the non bridging oxygens present in the glass network and due to the modifiers introduced in the glass ceramic composition. [27] The reflectance was quite high in the visible and near infrared regions where the greatest fraction of the solar irradiance power is distributed.

The white color presented by the manufactured samples assures a high reflectance in the visible region, considering that the high density of scattering centers provided by the crystal phases limits the heat absorption from the incoming visible sun light producing a greater reflectance and a higher opacity. [28]

5.4 Conclusions

Dense glass ceramics were obtained sintering a frit powder at 950°C with a controlled precipitation of wollastonite and hardystonite crystals in order to obtain a highly reflective color with a limited absorption of the sunlight radiation. We obtained lightweight substrates foaming the starting frit, the induced porosity reduced the thermal conductivity from 1.38 to 0.61-0.64 $W \cdot m^{-1} \cdot K^{-1}$. The high reflectance coupled to the low thermal conductivity indicates that the developed porous glass ceramics are suitable to be employed as an advanced barrier to heat, providing an efficient thermal insulation for buildings.

The distribution and the amount of porosity can be tuned by using engineered amounts of Si_3N_4 and gypsum as foaming agents. The two components have a synergistic effect in defining a reduction/oxidation couple and have the fundamental advantage of not degrading the white color of the glass-ceramics.

The application of the glaze further improves the reflectance of the material, prevents the incorporation of dust and water thus favoring a longer durability. Furthermore, considering the lightweight and the high albedo, these porous tiles could be applied as cladding materials for improved building insulation, whereas considering their high strength described, these lightweight materials could also be used for paving. In the future, we can envision that engineered ceramic tiles with a low thermal conductivity could compete with wood for paving, providing an improved thermal insulation between the ground or different floors in a building and even for a higher comfort when walking barefoot. The higher thermal conductivity of the dense tiles limits the benefits for thermal insulation applications, however they

could be used for paving when strength requirements are more important than the thermal insulation properties.

Bibliography

1 H. Akbari, M. Pomerantz, H. Taha, Cool surfaces and shade trees to reduce energy use and improve air quality in urban areas, Solar Energy 70 (2001) 295-310.

2 H. Akbari, H.D. Matthews, Global cooling updates: reflective roofs and pavements, Energy and Buildings, 55 (2012) 2–6.

3 M. Santamouris, Cooling the cities—a review of reflective and green roof mitigation technologies to fight heat island and improve comfort in urban environments, Solar Energy, http://dx.doi.org/10.1016/j.solener.2012.07.003, in press.

4 C. Ferrarin, A. Libbra, A. Muscio, C. Siligardi, Design of ceramic tiles with high solar reflectance through the development of a functional engobe, Ceramics International 39 (2013) 9583–9590

5 A. Synnefa, M. Santamouris, I. Livada, A study of the thermal performance of reflective coatings for the urban environment, *Solar Energy*, 80 (2006) 968–981.

6 This figure was prepared by PhD Robert A. Rohde and the cruves were based on the American Society for Testing and Materials (ASTM) Terrestrial Reference Spectra.

7 W. Holand and G. Beall, Glass-Ceramic Technology, 2nd edition, Wiley, 2012.

8 Annual Book of ASTM Standards 2004, Section 8: Plastics: D2383 – D4322, vol. 8ASTM International, West Conshohocken (2004)

9 A. Degiovanni: Thermal diffusivity and flash method. Rev. Gen. Therm. 185, 420–441 (1977).

10 W.J. Parker, R.J. Jenkins, C.P. Butler, and G.L. Abbott: Flash method of determining thermal diffusivity, heat capacity, and thermal conductivity. J. Appl. Phys. 32(9), 1679–1684 (1961).

11 Richet, P. Heat capacity of silicate glasses. Chem. Geol., 1987, 62, 111-124.

12 E. Bernardo, M. De Lazzari, P. Colombo, and A. Saburit Llaudis F. J. Garcia. Lightweight Porcelain Stoneware by Engineered CeO_2 Addition, Adv. Eng. Mater., 12 (2010) 65-67.

13 A. Saburit Llaudis, M. José Orts Tari, F. J. García Ten, E. Bernardo, P. Colombo, Foaming of flat glass cullet using Si_3N_4 and MnO_2 powders, Ceramics International 35 (2009) 1953–1959.

14 G. Scarinci, G. Brusatin, E. Bernardo, Glass foams, in: M. Scheffler, P. Colombo (Eds.), Cellular Ceramics. Structure, Manufacturing, Properties and Applications, Wiley-VCH, Weinheim, Germany, 2005.

15 A. Karamanov: Granite like materials from hazardous wastes obtained by sintercrystallisation of glass frits. Adv. Appl. Ceram., 2009, 108, 14–21.

16 E. Bernardo: Fast sinter-crystallization of a glass from waste materials. J. Non-Cryst. Solids, 2008, 354, 3486–3490.

17 E. Bernardo, G. Scarinci, E. Edme, U. Michon, N. Planty, Fast-Sintered Gehlenite Glass–Ceramics from Plasma-Vitrified Municipal Solid Waste Incinerator Fly Ashes, J. Am. Ceram. Soc., 92 [2] 528–530 (2009).

18 Ullmann's Encyclopedia of Industrial Chemistriy, Calcium Sulfate, 2012 Wiley-VCH Verlag GmbH & Co. KGaA, Weinheim.

19 Julian R. Goldsmith, Some Melilite Solid Solutions, The Journal of Geology Vol. 56, No. 5 (Sep., 1948), pp. 437-447.
20 Matsubara, S., Miyawaki, R., Kato, A., Yokoyama, K., Okamoto, A., Okayamalite, $Ca_2B_2SiO_7$, a new mineral, boron analogue of gehlenite, Mineralogical Magazine Volume 62, Issue 5, October 1998, Pages 703-706.
21 E. Bernardo, M. Varrasso, F. Cadamuro, S. Hreglich, Vitrification of wastes and preparation of chemically stable sintered glass-ceramic products, Journal of Non-Crystalline Solids 352 (2006) 4017–4023.
22 Schneider, S. J. Engineered materials handbook. 4, Ceramics and glasses. ASM International, 1991.
23 Hashin, Z. & Shtrikman, S. A Variational approach to the theory of the effective magnetic permeability of multiphase materials. Journal of Applied Physics, 1962, 33, 3125-3131.
24 Naït-Ali, B.; Haberko, K.; Vesteghem, H.; Absi, J. & Smith, D. S. Thermal conductivity of highly porous zirconia. Journal of the European Ceramic Society, 2006, 26, 3567-3574.
25 Bourret, J.; Tessier-Doyen, N.; Nait-Ali, B.; Pennec, F.; Alzina, A.; Peyratout, C. S. & Smith, D. S. Effect of the pore volume fraction on the thermal conductivity and mechanical properties of kaolin-based foams. Journal of the European Ceramic Society, 2013, 33, 1487-1495.
26 Sciamanna, V.; Nait-Ali, B.; Gonon, M. Mechanical properties and thermal conductivity of porous alumina ceramics obtained from particle stabilized foams. Ceramics International, 2015, 41 (2), 2599-2606.
27 H. Scholze, Glass. Nature, Structure and Properties, Springer-Verlag, Berlin, 1991
28 V. Marghussian, Nano-Glass Ceramics: Processing, Properties and Applications, Elsevier, 1st Edition 2015 pp 63-64.

Chapter 6 – White Frits Mixed With Whitening Agents

6.1 Introduction

In the present chapter is described a method to realize a dense glass ceramic resembling the color of a natural stone from the Greek island of Thassos. The characteristic snow like white stones from Thassos are most frequently called Thassos marbles whereas the chemical composition is rich in Mg and it would be more appropriate to refer to a Thassos dolomite rather than marble. Thassos marble was used in the past to clad the most important mosques of the Islamic world in Mekka and Medina (Saudi Arabia). The quarries of the island of Thassos were recently closed for environmental and political choices made by the local administrations and a new need for commercial products resembling the same color of the natural stone mined in Thassos arose.

We investigated frits providing white colors starting from natural and pure raw materials resembling the color of Thassos marble and of a commercial product provided by IRIS. A systematic study of the effect of whitening agents mixed with frits is also provided.

6.2 Materials and Methods

The whiteness is strictly correlated to the reflectance of the surface and was then evaluated by means of a UV-Vis spectrophotometer 570 Jasco equipped with integrating sphere (ISN-470 and $BaSO_4$ white standard). For the colorimetric measurements, the color matching functions were chosen for the CIE 1964 standard observers. The spectral reflectances were measured at 10 nm intervals in the range 360-740 nm with a Minolta CM-2600 colorimeter at the Photometry and Light Engineering Laboratory of the University of Padova. The XYZ tristimulus values were computed using a MATLAB routine,[1] using the ASTM Table 5 color-matching functions from the ASTM standard (ASTM, 2001).

6.2.1 Neoparies™ like Compositions

In Chapter 5 was described a method to realize a both dense and porous glass ceramic starting from the composition of Neoparies™ [2] using natural materials from KSA and a limited amount of pure chemicals. The pure chemicals were introduced because the composition of Neoparies™, NP, requires ZnO, K_2O, and B_2O_3 that were not present in the raw materials supplied by KACST. Subsequently, the composition NP was changed to substitute ZnO and introduce another modifying oxide present in the raw materials supplied by KACST. We thus investigated the substitution of ZnO with MgO in molar ratio close to 1:1 in a typical Neoparies™ composition, and to keep the same molar ratio between network former, modifier and intermediate ions. The composition NP and its modified composition called White Marble, WM, are reported in **Tab. 18**. Successively MgO was introduced in higher percentages together with ZnO (composition WM2) in order to favor the controlled crystallization of Mg rich crystal phases. In composition WM2 the only pure chemical used is ZnO whereas K^+ was introduced using a Na-K rich feldspar.

Contrary to Neoparies™, it was chosen to not introduce BaO, to limit the use of pure chemicals, and to use large amounts of natural raw materials that are affected by a relatively high amount of Fe_2O_3 impurities. It is well known and widely discussed that iron ions afford to the glaze a yellowish coloration. For this reason, it was chosen to investigate also the use of a commercial frit produced by Endeka with pure starting materials. This frit is composed by SiO_2 (50–60 wt%), ZrO_2 (8–14 wt%) and fluxing elements such as Na_2O, K_2O, PbO and B_2O_3 (20–25 wt%) as major components and stabilizing elements such as ZnO, Al_2O_3, CaO, BaO, MgO as minor components (7–9 wt% maximum). The commercial frit shown precipitation of $ZrSiO_4$ which gives the so called “white of zirconium”, here called white opaque WO. [3]

Tab. 18 – Chemical composition of glasses NP, WM, WM2 and Neoparies™.

	NP		WM		Neoparies™	
Oxide	wt%	mol.%	wt%	mol.%	wt%	mol.%
Al_2O_3	7.7	4.8	7.1	4.3	7.0	4.4
B_2O_3	1.3	1.2	1.2	1.1	1.0	0.9
BaO	0.0	0.0	0.0	0.0	4.0	1.7
CaO	20.3	22.8	19.4	21.2	17.1	19.6
Fe_2O_3	0.4	0.1	0.4	0.1	0.0	0.0
K_2O	2.5	1.7	3.5	2.3	2.0	1.4
MgO	0.7	1.1	3.4	5.1	0.0	0.0
Na_2O	2.5	2.5	2.4	2.4	3.0	3.1
SiO_2	57.4	60.1	62.0	63.2	59.3	63.6
TiO_2	0.7	0.6	0.6	0.4	0.0	0.0
ZnO	6.5	5.0	0.0	0.0	6.5	5.2

	wt%	wt%
Clay-E	14.8	10.8
Cullet	9.9	9.0
Limestone	29.6	21.6
Silica sand	34.5	34.3
Dolomite	0.0	11.7
Feldspar	0.0	6.3
ZnO	5.4	0.0
Borax	3.0	2.7
K_2CO_3	3.0	3.6

ZrO_2 and $ZrSiO_4$ are materials of great value used by the glaze industry to manufacture white opaque frits. [3] However, it has been established that to observe opacity ZrO_2 and $ZrSiO_4$ have to be added above a threshold amount, thus requiring large amounts introductions to achieve an adequate opacity. [4] The resulting zircon crystals have a significantly higher refraction index (2.05–2.40) than the glassy matrix (1.50–1.70) and thus effectively scatter light. [5] Although the "white of zirconium" glazes form fine white glass ceramics, the cost of the starting materials is quite high and many researchers are focused in valuable alternatives. [6]

Vitrification – For the production of both NP, and WM 200 grams of the dry raw powder mixture was put in a crucible and heated at 900°C, to decompose the carbonates. Then the mixture was heated at 1400°C in a kyanite refractory crucible in air, and kept in temperature for 90 minutes. After achieving complete melting of the raw materials, the melt was poured into water to produce a glass

frit. The frit was then collected, dried at 80°C overnight and then ground and sieved to obtain particles with a size below 90 microns.

Samples preparation and characterization – The preliminary studies were performed on disks made with 1.5 g of the dry frit powder mixture, uniaxially cold pressed in a mold at a pressure of 40 MPa. The produced sample was then fired in air by inserting it directly into an oven preheated at selected temperatures for 30 or 60 minutes. After cooling, the samples were polished and analyzed thorough XRD, and examined visually.

The same procedure was used for whitened samples, where the NP and WM dry powders were mixed, **Tab. 19**, with different whitening agents: ZnO, CaF_2, TiO_2, $ZrSiO_4$ and Al_2O_3. The results of the white colors are described successively in the paragraph, dedicated to the spectrophotometer analysis.

Tab. 19 – List of the frits fired at selected temperatures mixed with different whitening agents: ZnO, CaF_2, TiO_2, $ZrSiO_4$ and Al_2O_3.

Label	Frit	ZnO wt%	CaF_2 wt%	TiO_2 wt%	$ZrSiO_4$ wt%	Heating	t (min)	T (°C)
WM-1ZnO-DF-60min	WM	1				DF	60	1000
WM-2.5ZnO-DF-60min	WM	2.5				DF	60	1000
WM-5ZnO-DF-60min	WM	5				DF	60	1000
WM-1ZnO-1CaF_2-DF-60min	WM	1	1			DF	60	1000
WM-2.5ZnO-1CaF_2-DF-60min	WM	2.5	1			DF	60	1000
WM-5ZnO-1CaF_2-DF-60min	WM	5	1			DF	60	1000
WM-1TiO_2-DF-60min	WM			1		DF	60	1000
WM-2.5TiO_2-DF-60min	WM			2.5		DF	60	1000
WM-5TiO_2-DF-60min	WM			5		DF	60	1000
WM-1 $ZrSiO_4$-DF-60min	WM				1	DF	60	1000
WM-2.5 $ZrSiO_4$-DF-60min	WM				2.5	DF	60	1000
WM-5 $ZrSiO_4$-DF-60min	WM				5	DF	60	1000
WM-20 $ZrSiO_4$-DF-1050°C	WM				20	DF	60	1050
WM-20 $ZrSiO_4$-DF-1100°C	WM				20	DF	30	1100
WM-10°C-min-30min	WM					10°C/min	30	1000
WM-10°C-min-60min	WM					10°C/min	60	1000
NP-1TiO_2-DF-60min	NP			1		DF	30	950
NP-2.5TiO_2-DF-60min	NP			2.5		DF	30	950
NP-5TiO_2-DF-60min	NP			5		DF	30	950

6.2.2 Frits from pure chemicals

Composition WM was reproduced using pure starting materials, WMP, in order to drastically reduce the chromophore ions content. According to Torres et. al.,[7], we also investigated the production of a spinel-based glass ceramic material from a glass with composition in the system ZnO–MgO–B_2O_3–Al_2O_3–SiO_2 (composition SP). Spinel crystals are characterized by a high hardness (7.5-8

Mohs) and high refractive index (1.7), and are therefore of great potential interest for the realization of white opaque glass ceramics. The compositions WMP and SP, are reported in **Tab. 20**.

Vitrification – For the production of both WMP and SP compositions, 200 grams of the dry raw powder mixture was put in a crucible and heated at 900°C, to decompose the carbonates. The mixtures were then heated in a kyanite refractory crucible in air, and kept at temperature for 90 minutes. Mixture WMP was melted at 1400°C, while SP was melted at 1450°C. After achieving complete melting of the raw materials, the melt was poured into water to produce a glass frit. The frit was then collected, dried at 80°C overnight and then ground and sieved to obtain particles with a size below 90 microns.

Samples preparation and characterization – The preliminary studies were performed on disks made with 1.5 g of the dry frit powder mixture, uniaxially cold pressed in a mold at a pressure of 40 MPa. The produced sample was then fired in air by inserting it directly into an oven preheated at selected temperatures or by applying a 10°C/min heating. The samples were fired at selected temperatures in the range 950-1100°C, for 30, 60 or 120 min. The same procedure was used for whitened samples, where the WM and WMP dry powders were mixed using different whitening agents: ZnO, CaF_2, $ZrSiO_4$, MgO and Al_2O_3. The whitening SP-mix is a mixture of δ-Al_2O_3 and MgO, formulated in order to reproduce the composition of $MgAl_2O_4$ spinel.

A large size ceramic tile (e.g. 150×80 cm^2) may be fast fired, but certainly with a heating rate much lower than what was used for a direct firing in laboratory conditions. However, both direct firing and progressive heating treatments are useful to map how the color is modified by the thermal treatment.

Tab. 20- Chemical composition of glasses WMP and SP

	WMP		SP	
Oxide	wt%	mol.%	wt%	mol.%
Al_2O_3	7.1	4.3	22.5	14.4
B_2O_3	1.0	0.9	8.1	7.6
CaO	19.6	21.3	1.0	1.2
Fe_2O_3	0.02	0.01	0.01	0.01
K_2O	3.6	2.3	3.5	2.4
MgO	3.6	5.4	9.5	15.3
Na_2O	2.4	2.3	3.0	3.2
SiO_2	62.5	63.3	49.0	53.2
TiO_2	0.2	0.2	0.1	0.1
ZnO	0.0	0.0	3.4	2.7

	wt%	wt%
Kaolin*	19.8	57.5
Cullet**	11.0	5.7
$CaCO_3$*	25.3	-
Silica sand**	35.2	11.5
MgO*	2.4	6.9
ZnO*	-	2.3
Borax*	2.2	8.0
K_2CO_3*	4.1	3.4
Boric Acid*	-	4.6

* reagent grade
** KSA materials

6.3 Results and Discussion

6.3.1 Reflectance Analysis on Glass Ceramics Without Additives

In **Fig. 42a** are reported the reflectances recorded on samples WM showing the effect of the heating rate and firing temperature. All the spectra are characterized by an intense reflectance decrease peaked at about 455 nm corresponding to the absorption of the wavelengths of blue light that result in the perception of a slightly yellowish coloration at the human eye. At wavelengths lower than 550 nm the reflectance forms a plateau that continues in the NIR (near infrared).

It is clearly observed (**Fig. 42a**) the effect of the heating rate and firing temperature on samples WM. More specifically glass ceramics with a limited gloss were obtained directly heating samples WM at 900°C for 60 min, in fact the low reflectance (plateau ~77%) is probably an effect of both light absorption and

transmission resulting from the low density of scattering centers, i.e. crystal phases. After directly firing at 950°C, the plateau of the reflectance increases at ~82.5% whereas when directly firing at 1000°C a global increment (~2%) of the reflectance was observed. Although the difference between the samples fired at 950 and 1000°C is limited, from this preliminary experiments it is concluded that to obtain an optimized white opaque color, samples should be fired at a temperature of 1000°C. Moreover to design the thermal treatment providing the highest whiteness and opacity the effect of the heating rate was investigated applying a rates of 5, 10 and 20°C/min. It was then observed that the lower the heating rate the higher the reflectance, however the effect of the rate is much smaller compared to the influence of the firing temperature, in other words samples WM are suitable for both fast and slow firing when sintered at ~1000°C.

Considering the highest purity of the raw materials used, samples WMP were expected to show a reflectance (**Fig. 42b**) comparably higher than samples WM. The main difference between the two sets of samples was the removal of the absorption in the blue region and to a reflectance showing a broader flat curve. Moreover the reflectance of sample WMP fired at 1000°C is even lower than for sample WM. This might be explained considering that by using pure starting the amount of impurities was obviously lower and is well known that purities and defects in general are preferential sites for the nucleation of crystallites.

Samples SP (**Fig. 42c**) showed the absorption in the blue region already observed for samples WM given by the impurities embedded in the sample however the effect of the heating rate was totally different. In fact by applying a progressive heating rate of 10°C/min the overall reflectance values were lower comparing with samples directly fired at the same final temperature of 1000°C.

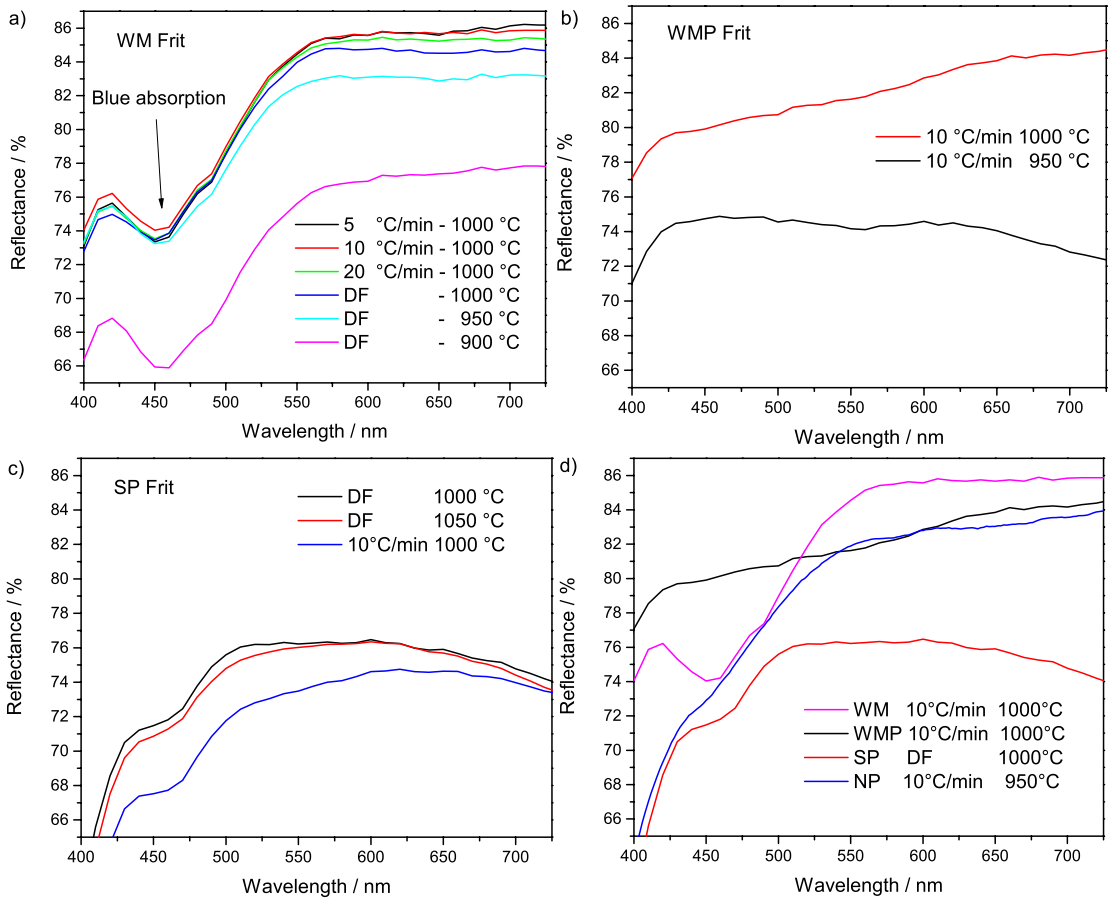

Fig. 42 – UV reflectance samples fired applying different heating rates and firing temperatures. a) Samples WM. b) Samples WMP. c) samples SP. d) comparison among samples WM, WMP, SP and NP.

The correlation between reflectance and thermal treatment is not straightforward and requires some specification. As reported many times in this work, to obtain a white color, a high density of scattering centers provided by the crystal phases is required. The crystallization of a glass frit in the CAS (calcium-aluminosilicate) system was found more effective for fast thermal treatments [8]. In fact crystallization could be somewhat enhanced by the availability of a remarkable amount of free glass surfaces when the sample is directly fired. On the contrary, a sample heated at 10°C/min, could experience some sintering before starting to crystallize; consequently, the reduction of the specific surface inhibits the nucleation of crystal phases. This explanation is valid for the frit SP whereas for samples WM and WMP the nucleation and growth is probably less affected by the loss of free glass surface during fast treatments.

In **Fig. 42d** are reported the reflectances of the samples WM, WMP, SP and NP that provided the most promising results. Samples SP presented the lowest reflectance compared to the other frits employed. WMP and NP presented similar values at high wavelength however WMP samples were not affected by the light absorption at low wavelengths. Importantly sample NP presented a reflectance well below WM, thus justifying the efforts in the design of the new composition.

6.3.2 Mineralogical analysis on glass ceramics without additives

In the present work the mineralogical analysis description is in support of the previous paragraph were the reflectances were described. However the intensity of the XRD patterns were often not high enough to provide sufficient information or to allow a reliable quantitative analysis, thus the following descriptions are mere qualitative comments about the crystal phases formed.

In **Fig. 43** are reported the diffractograms of samples WM and WMP directly fired at 950-1000°C for 60 minutes. The samples devitrified forming wollastonite ($CaSiO_3$) and diopside ($CaMgSi_2O_6$) crystals. The samples WM and WMP fired at 950°C presented a very similar pattern whereas sample WM fired at 1000°C showed a higher intensity of the peaks attributed to the diopside crystals. The precipitation of wollastonite as main crystal phase and diopside as secondary crystal phase was expected considering the chemical composition of the parent glass.

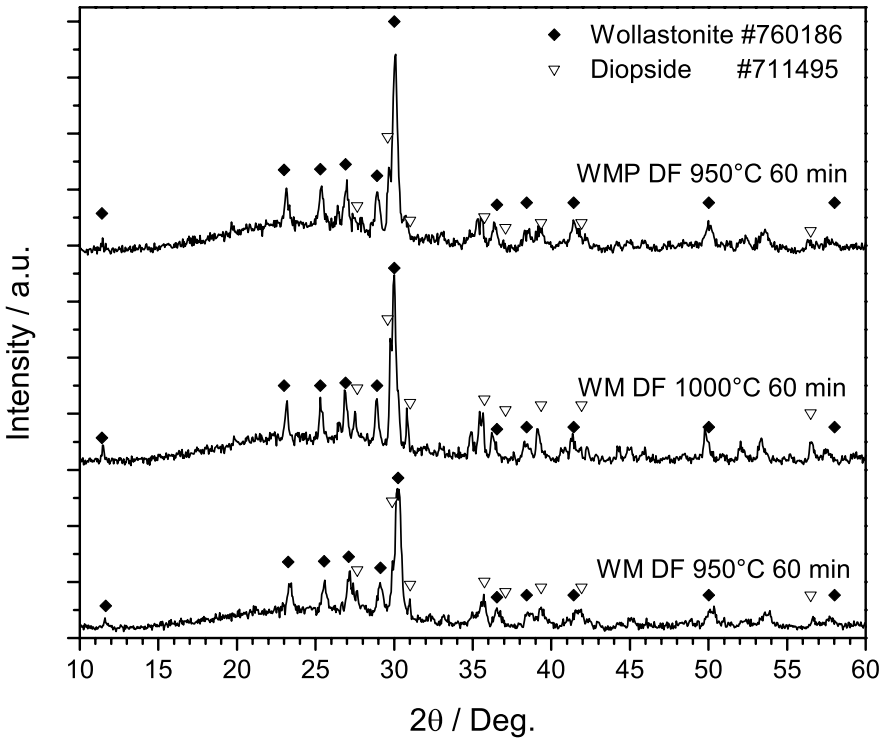

Fig. 43 – XRD analysis of samples from direct firing at 950 and 1000°C (60 min) for samples WM and 950°C (60 min) for sample WMP.

As predicted from the Mg rich and peraluminous composition of samples SP, coriderite ($Mg_2Al_4Si_5O_{18}$) and spinel ($MgAl_2O_4$) formation occurred at 1000°C, however comparing the diffraction peaks intensities lower precipitation of crystal phases was identified in the sample fired at 1050°C. The controlled precipitation of spinel and cordierite crystals could be enhanced increasing the Mg and Al content in the parent glass, however according to preliminary investigations the compositional change requires a melting temperature higher than 1450°C. In our research a great attention was spent in the limitation of the overall costs for a possible application, it was then preferred to choose glass compositions that are easily melted at 1400°C or below. In other words to produce a spinel rich glass ceramic the silica content should be reduced in sake of alumina content resulting in an undesired high melting temperature.

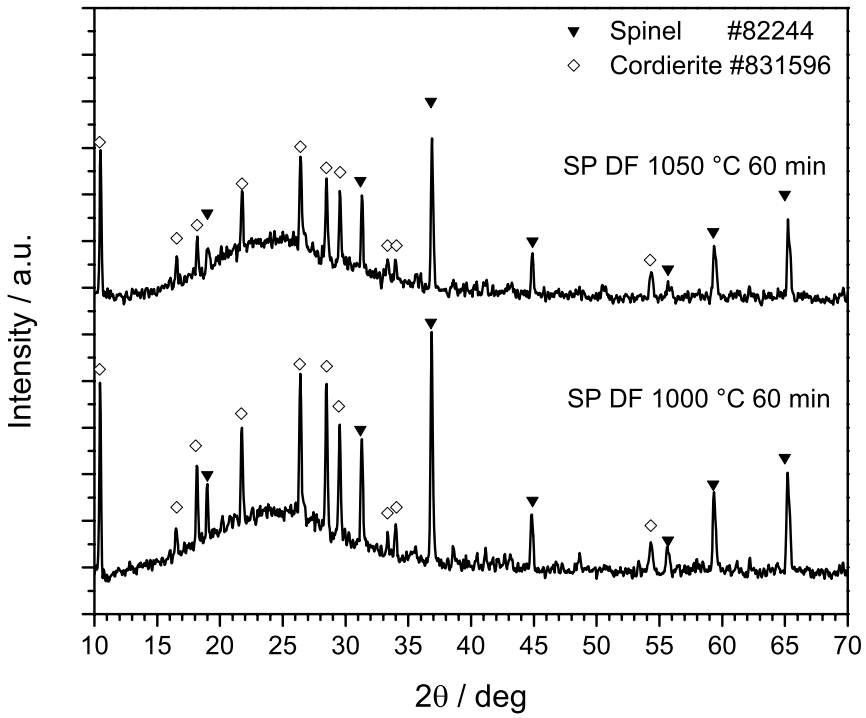

Fig. 44 – XRD analysis of samples from direct firing at 1000 and 1050°C (60 min) for samples SP.

6.3.3 Reflectance analysis on glass ceramics with additives

Although the main focus of this research was to identify a sample with a bright white color, a more general interpretation of the optical properties in the UV-NIR region is described in this paragraph.

All the samples of composition WM here discussed were directly sintered at 1000°C for 60 minutes if not differently described (

Tab. 19). For the sake of brevity, the reflectance spectra of samples NP were not reported because the results achieved with composition WM were more promising. Probably, the better quality of samples WM is that the raw materials employed were slightly less polluted by chromophore ions.

In **Fig. 45a** are represented the reflectance measurements for the samples of composition WM mixed with ZnO and CaF_2. In particular, the best results were achieved for composition WM mixed with 5 wt% of ZnO and 1 wt% CaF_2. The highest reflectance value achieved by the samples shown in **Fig. 45a** was about 90%, but the absorption around 400 nm was still present.

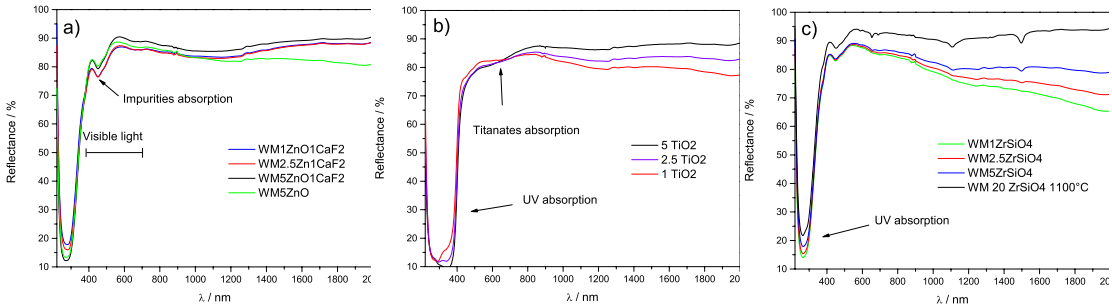

Fig. 45 – a) reflectance of specimens WM mixed with ZnO and CaF_2; b) reflectance of specimens WM mixed with TiO_2; d) reflectance of specimens WM mixed with $ZrSiO_4$.

Frit WM mixed with TiO_2, **Fig. 45b**, one of the most common whitening agents, was expected to give the whitest samples; in fact the refractive index of TiO_2 goes from 2.49 for anatase to 2.61 for rutile. The higher the difference between the refractive index of the matrix and that of the crystals, the better the scattering of light. The intense decrease of reflectance observed for this samples was probably due to the formation of iron titanates, which are used as brown pigments. Another important feature of TiO_2 was an undesired high of the UV light. In general the wavelength of the edge is believed to be due to the transition of a valance electron of a network anion to an excited state. Conversion of a network anion from the bridging state to a non-bridging state will lower the energy required for the electronic excitation, and shift the ultraviolet edge to lower frequencies. The addition of alkali oxides to silica, therefore, results in a shift of the ultraviolet edge toward the visible region of the spectrum [9] and in our experiments TiO_2 particularly increases the UV absorption.

The reflectance measurements of **Fig. 45c** show that with the increasing of zircon from 1 to 20 wt% the reflectance in the NIR was strongly enhanced. Furthermore, 1 wt% of zircon was a more effective whitening agent in comparison to the sample WM having 5 wt% of ZnO and 1 wt% of CaF_2.

6.3.4 Colorimetric Analysis – Comparisons With Thassos Marble

In **Tab. 21** are reported the tristimulus values (X,Y and Z) and CIELAB coordinates (L^*, a^* and b^*) calculated from the spectral reflectances acquired on the white sintered glass ceramics. From a colorimetric point of view, Thassos is a

white, slightly yellow-green, marble.[10-11] Comparing the CIELAB coordinates of the fired samples and of Thassos marble, some important understanding and conclusion can be made.

As easily observed from **Tab. 21** and **Fig. 47**, most of the WMP specimens displayed a higher lightness then Thassos marble. The achievement of a sample with high lightness is the most difficult issue to solve. To match the color of Thassos marble, we might reduce the iron content of composition WM going closer to composition WMP.

Directly sintering at 1000°C for 60 minutes composition WM mixed with 2.5 and 5 wt% of ZnO produced specimens with both L* and a* close to the characteristics of Thassos marble. By halving the iron content and introducing ZnO in composition WM, we might indeed go very close to the realization of a glass ceramic resembling the color of Thassos marble.

Probably, the successful results achieved using the SP-mix was related to its reactivity. Indeed, preliminary XRD analysis showed an improvement of the crystallization when using the SP-mix. However, we did not report here an XRD analysis due to the very preliminary stage reached by this study. This result simply suggests that future compositions should be modified in order to further improve the crystallization.

The whiteness of the WMP glass ceramic was proved to increase when using boric acid. Boric acid may have reduced the refractive index of the amorphous phase thus increasing the difference between the refractive indexes of the amorphous and crystal phases.

Composition SP should be modified to improve the devitrification upon firing, in fact the produced samples were translucent and considering the promising results achieved for composition WM and WMP, this composition may be dropped in further research efforts.

The commercial Thassos-like (**Fig. 46**) white stoneware produced by IRIS was found to be very close to the color of Thassos marble, but the a* (green) and b* (yellow) values are unbalanced. Then a future target may be the development of a modified WM composition which provides L* between 93.0 / 93.5 and b* < 3 using some inorganic pigment to adjust a* if required.

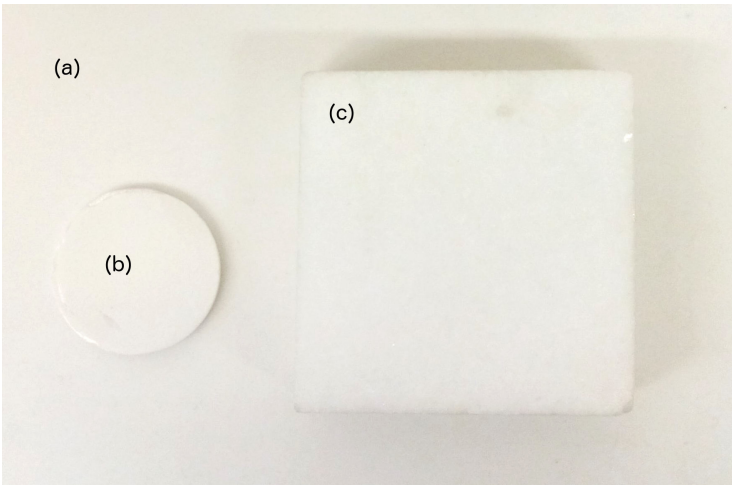

Fig. 46 – a) Commercial Thassos-like glass ceramic tile. b) WM2 glass ceramic sintered at 1000 °C for 60 min. c) Thassos marble. Note: the color of the samples is actually whiter, but it is difficult to capture this using a camera.

The possibility of reducing b* should be investigated further, knowing that Fe^{2+} ions provide in glasses red/yellow colors 3 times stronger than Fe^{3+} ions. By adding Mn^{3+} ions to the glass ceramic iron oxidize according to the reaction: $Fe^{2+} + Mn^{3+} \rightarrow Fe^{3+} + Mn^{2+}$. However the reaction may be affected by solarization problems. We might explore the use of the decolorizing agents, such as selenium oxide or other compounds of selenium (e.g. zinc selenite or calcium selenite).

In conclusion, we may state that glass ceramics with color characteristics reasonably similar to that of Thassos marble have been produced. However, further work is required in order to confirm and improve the results and adapt the composition of the glass ceramics to the requirements of industrial production and the use of natural (not laboratory) raw materials.

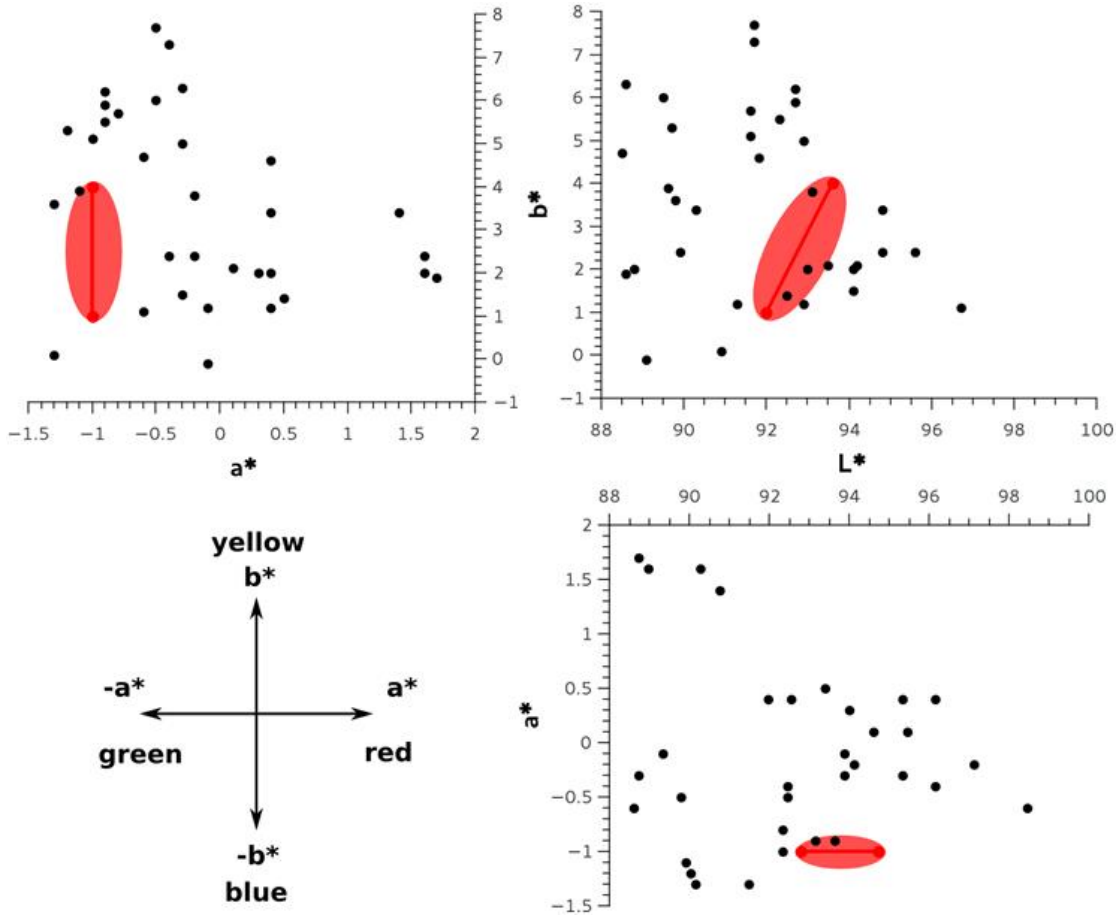

Fig. 47 – CIELAB coordinates representation for all the samples reported in **Tab. 21**. The red spots refer to the CIELAB coordinates interval given for Thassos marble [10] whereas the red ellipses describe the set of points which approximately resemble the typical colors of Thassos marbles.

Tab. 21 – White glass ceramic tristimulus values (X,Y and Z) and CIELAB coordinates (L^*, a^* and b^*). The color matching functions were chosen for the CIE 1964 standard observers and D65 light source was used.

Composition	Whitening wt%	type	Heating	T °C	t min	X	Y	Z	L*	a*	b*
Thassos*									**92.0-93.6**	**-1**	**1-4**
Thassos**									**92.9**	**-0.8**	**2.9**
IRIS (ceramic Thassos)						78.8	83.2	83.9	**93.1**	**-0.2**	**3.8**
Milk glass						73.5	78.2	83.8	90.9	-1.3	0.1
WO (Endeka)	10	Al_2O_3	10°C/min	1100	60	86.7	91.8	96.8	96.7	-0.6	1.1
WM			10°C/min	1000	30	71.2	75.7	74.3	89.7	-1.2	5.3
WM			10°C/min	1000	60	75.1	79.8	78.8	91.6	-1.0	5.1
WM			10°C/min	950	60	76.7	81.3	79.8	92.3	-0.9	5.5
WM	1	ZnO	DF	1000	60	75.4	79.9	78.0	91.6	-0.8	5.7
WM	2.5	ZnO	DF	1000	60	77.6	82.3	80.2	**92.7**	**-0.9**	5.9
WM	5	ZnO	DF	1000	60	77.5	82.2	79.8	**92.7**	**-0.9**	6.2
WM	1-1	ZnO-CaF_2	DF	1000	60	75.8	80.1	76.3	91.7	-0.4	7.3
WM	2.5-1	ZnO-CaF_2	DF	1000	60	75.5	79.9	75.5	91.7	-0.5	7.7
WM	1	$ZrSiO_4$	DF	1000	60	71.1	75.3	73.0	89.5	-0.5	6.0
WM	2.5	$ZrSiO_4$	DF	1000	60	69.5	73.4	70.8	88.6	-0.3	6.3
WM	5	$ZrSiO_4$	DF	1000	60	78.3	82.8	81.9	**92.9**	**-0.3**	5.0
WMP			10°C/min	950	120	70.5	74.4	80.0	89.1	-0.1	-0.1
WMP			10°C/min	1000	60	77.8	81.8	85.8	**92.5**	0.5	**1.4**
WMP	2.5	MgO	10°C/min	950	120	70.7	73.7	76.5	88.8	1.6	2.0
WMP	5	MgO	10°C/min	950	120	72.9	76.0	78.4	89.9	1.6	2.4
WMP	7.5	MgO	10°C/min	950	120	73.6	76.9	78.0	90.3	1.4	3.4
WMP	2.5	H_3BO_3	10°C/min	950	120	75.3	79.2	83.4	91.3	0.4	1.2
WMP	5	H_3BO_3	10°C/min	950	120	78.4	82.7	87.0	**92.9**	**-0.1**	**1.2**
WMP	7.5	H_3BO_3	10°C/min	950	120	81.0	85.6	89.6	**94.1**	**-0.3**	**1.5**
WMP	5	SP-mix	10°C/min	1000	120	78.9	83.1	86.3	**93.0**	0.3	**2.0**
WMP	10	SP-mix	10°C/min	1000	120	81.2	85.4	88.8	**94.1**	0.4	**2.0**
WMP	20	SP-mix	10°C/min	1000	120	82.8	87.1	88.6	**94.8**	0.4	**3.4**
WMP	5	SP-mix	10°C/min	1050	120	79.8	84.1	87.3	**93.5**	0.1	**2.1**
WMP	10	SP-mix	10°C/min	1050	120	81.4	85.8	89.0	**94.2**	0.1	**2.1**
WMP	5	SP-mix	10°C/min	1100	120	76.3	80.3	80.0	**91.8**	**0.4**	**4.6**
WMP	10	SP-mix	10°C/min	1100	120	82.4	87.2	90.0	**94.8**	**-0.4**	**2.4**
WMP	20	SP-mix	10°C/min	1100	120	84.3	89.0	92.0	**95.6**	**-0.2**	**2.4**
SP			DF	1000	60	71.3	75.9	76.7	89.8	-1.3	3.6
SP			DF	1050	60	71.1	75.5	76.0	89.6	-1.1	3.9
SP			10°C/min	1000	60	69.1	73.1	72.5	88.5	-0.6	4.7

* Ref [10]
** Ref [11]

6.4 Conclusions

The choice of the starting materials is fundamental to achieve a highly white color; when the starting materials are polluted by heavy metal no white colors are possible. The target is the production of a colorless frit, which then can crystallize producing crystals giving a white color. Zircon was proved to be an effective whitening agent, especially in high amounts and the same was for mixtures of ZnO and CaF_2. Contrarily to what expected TiO_2 lowered the whiteness enhancing a yellowish color.

Coloration of glasses by 3d transition metals ions ($Fe^{2+/3+}$, $Cr^{3+/6+}$) is due to electronic transitions between normally degenerate energy levels of d-electrons. The anions coordinating the transition metals influence the energy level of these electronic transitions (described by the crystal field theory) affecting the coloration of the glass matrix and crystal phases. To further reduce the coloring effect of the transition metals a systematic study of the chemical composition of glass using analytic techniques should be added to the UV spectroscopy, furthermore decoloring agents (Se, Mn, As) could be introduced to neutralize the effect of the impurities present in the starting materials.

Bibliography

1 Stephen Westland and Caterina Ripamonti, Computational Colour Science using MATLAB, John Wiley & Sons Ltd, 2004.

2 W. Holand and G. Beall, Glass ceramic Technology, 2nd edition, Wiley, 2012.

3 R. Casasola, J. M. Rincón, M. Romero. Glass–ceramic glazes for ceramic tiles: a review, Journal of Material Science (2012) 47:553–582.

4 Jacobs CWF (1954) J Am Ceram Soc 37:216. doi:10.1111/ j.1151-2916.1954.tb14026.x

5 Matthes WE (1995) Vidriados cera´micos. Omega, Barcelona

6 K. Pekkan, B. Karasu. Zircon-free frits suitable for single fast-firing opaque wall tile glazes and their industrial productions, Journal of the European Ceramic Society 29 (2009) 1571–1578

7 F.J. Torres et al. / Journal of Non-Crystalline Solids 351 (2005) 2453–2461.

8 M. Marangoni, I. Ponsot, R. Kuusik and E. Bernardo, Strong and chemically inert sinter crystallized glass ceramics based on Estonian oil shale ash, *Advances in Applied Ceramics*, 113 (2014) 120-128.

9 J. E. Shelby Introduction to Glass Science and Technology 2nd edition, The Royal Society of Chemistry 2005.

10 Zezza U., Massa V., Palazzi S., whiteness index characterization for Greek marbles ASMOSIA proceedings (1995) 191-195.

11 Zezza U., Non-destructive colour parameters applied to provenance studies of archeological Mediterrean white marbles, ASMOSIA proceedings (1995) 185-190.

List of Publications

Published in Journals

1. M. Marangoni, I. Ponsot, R. Kuusik, E. Bernardo. Strong and chemically inert sinter crystallised glass ceramics based on Estonian oil shale ash. Advances in applied ceramics, 2014, 113; p. 120-128.
2. M. A. Binhussain, M. Marangoni, E. Bernardo, P. Colombo. Sintered and glazed glass-ceramics from natural and waste raw materials. Ceramics international, 2014, 40, 3543-3551.
3. M. Marangoni, M. Secco, M. Parisatto, G. Artioli, E. Bernardo, P. Colombo, H. Altlasi, M. Binmajed, M. A. Binhussain. Cellular glass-ceramics from a self foaming mixture of glass and basalt scoria. Journal of non-crystalline solids, 2014.
4. S. Cetin, M. Marangoni, E. Bernardo. Lightweight glass–ceramic tiles from the sintering of mining tailings, Ceramics International 41 (2015) 5294–5300.
5. M. Marangoni, L. Arnout, L. Machiels, L. Pandelaers, E. Bernardo, P. Colombo, Y. Pontikes. Porous, sintered glass-ceramics from inorganic polymers based on fayalite slag, Journal of The American Ceramic Society. Accepted under revision.

Awards

Pfeil Award - IOM3 AWARDS 2015 for published work of particular merit in the field of ceramics “M. Marangoni, I. Ponsot, R. Kuusik, E. Bernardo. Strong and chemically inert sinter crystallised glass ceramics based on Estonian oil shale ash. Advances in applied ceramics, 2014, 113; p. 120-128”.

Patents

Approved

M. Binhussain, P. Colombo, E. Bernardo, M. Binmajed, M. Marangoni, H. H. Altalsi, A. M. Alajimi and A. Altamimi, Method for manufacturing glass-ceramic composite, EP 2752394, US 2014191448, Filed 4 March 2013.

Submitted

1. M. Binhussain, P. Colombo, E. Bernardo, M. Binmajed, M. Marangoni, H. H. Altalsi, A. M. Alajimi and A. Altamimi, A porous glass ceramic composition and method for manufacturing the same, EP 2752395 A1, Patent Application No. 13162767.1 - 1354, Filed 8 April 2013.
2. M. Binhussain, P. Colombo, E. Bernardo, M. Binmajed, M. Marangoni, H. H. Altalsi, A. M. Alajimi and A. Altamimi, A glaze composition, method for manufacturing glaze composition and methods of glazing, EP 2749544 A1, Patent Application No. 13162770.5 - 1354, Filed 8 April 2013.
3. M. Binhussain, P. Colombo, E. Bernardo, M. Binmajed, M. Marangoni, H. H. Altalsi, A. M. Alajimi and A. Altamimi, A glass-ceramic composition and method

for manufacturing the same, EP 2746239 A1, Patent Application No. 13157607.6 - 1354, Filed 4 April 2013.

Conferences

Oral presentations

1. M. Marangoni, A. B. Mohammed, E. Bernardo, P. Colombo, Glass and Glass-ceramics from Natural andWaste Raw Materials, 13th International Conference of the European Ceramic Society, June 27 2013.
2. M. Marangoni, I. Ponsot, E. Bernardo, P. Colombo, H. Altlasi, M. Binmajed, M. Binhussain. Glass and Glass-ceramics from Natural and Waste Raw Materials, CIMTEC 13th Ceramics Congress, June 2014.
3. M. Marangoni, M. Secco, M. Parisatto, G. Artioli, E. Bernardo, P. Colombo, H. Altlasi, M. Binmajed, M. Binhussain, Cellular glass-ceramics from a self foaming mixture of glass and basalt scoria. European Society of Glass, September 2014.

Proceedings

1. E. Bernardo, M. Marangoni, I. Ponsot. Reuse of inorganic waste in monolithic and cellular glass based materials for structural and functional applications, 2015, 4th International Slag Valorization Symposium.
2. R. Kuusik, M. Marangoni, E. Bernardo. Estonian oli shale ash as raw material for manufacturing glass ceramics, 2015, 4th International Slag Valorization Symposium.

Papers Submitted

1. Marangoni M., Ponsot I., Cicek B., Bernardo E., Double Layer Waste-derived Glass-Ceramics Prepared by Low Temperature Sintering/Sintercrystallization. Advances in Applied Ceramics, 2015.
2. Rincon A., Marangoni M., Cetin S., Bernardo E., Recycle of inorganic waste in monolithic and cellular glass-based materials for structural and functional applications, Journal of Chemical Technology & Biotechnology, 2015.
3. M. Marangoni, B. Nait-Ali, D. Smith, M. Binhussain, E. Bernardo, P. Colombo, White sintered glass-ceramic tiles with improved thermal insulation properties for building applications, Journal of The European Ceramic Society

Ringraziamenti

Desidero ringraziare i proff. Colombo e Bernardo che mi hanno accompagnato durante il dottorato con sapienza, affetto ed entusiasmo e i cui esempi e consigli hanno fortemente irrobustito la mia formazione tecnica e metodologica.

Ringrazio il prof. Binhussain per le stimolanti discussioni e il KACST per aver sostenuto economicamente questo progetto di ricerca.

Vorrei poi ringraziare tutti i tecnici e colleghi che mi hanno assistito pazientemente nel raccogliere le innumerevoli misure descritte nel lavoro di tesi; in particolar modo rivolgo un ringraziamento al dott. Gobbin, figura portante nei nostri laboratori sempre disponibile durante le sue intense giornate lavorative.

Un ringraziamento va anche ai colleghi di Padova e ai numerosi colleghi provenienti da ogni angolo di mondo che ho incontrato in questi anni.

Infine un pensiero in particolare va alla mia famiglia e a tutti i miei più cari amici che hanno saputo sopportarmi e sostenermi in questi anni.